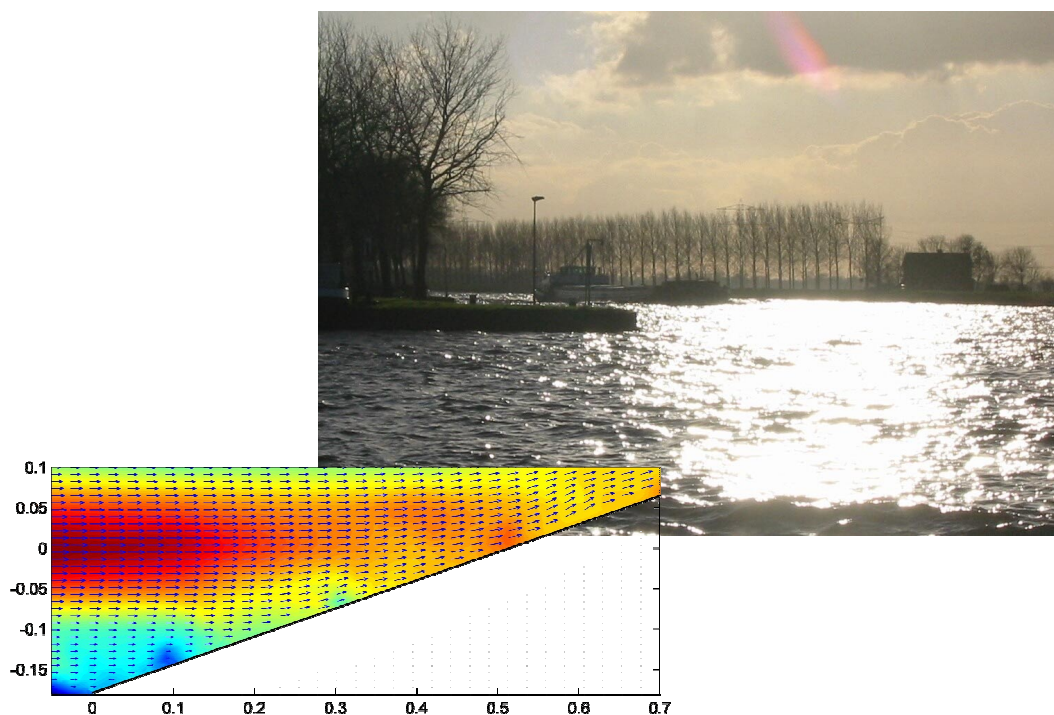


# Bowthruster-induced Damage



This report was established as a Master of Science thesis for Delft University of Technology, under the supervision of the following committee:

prof.dr.ir. M.J.F. Stive  
dr.ir. H.L. Fontijn  
ir. P.C. Janssen (RWS-DWW)  
ir. J. Olthof  
ir. H.J. Verhagen

Author: L.A. Schokking

Ministerie van Verkeer en Waterstaat

## Directoraat-Generaal Rijkswaterstaat

Dienst Weg- en Waterbouwkunde

# **Bowthruster-induced Damage**

3-6-2002

---



---

# Preface

As conclusion of my study at the Faculty of Civil Engineering of Delft University of Technology I wrote this Master of Science thesis. It was carried out at the Road and Hydraulic Engineering Division of the Directorate-General of Public Works and Water Management. The experiments were conducted at the Fluid Mechanics Laboratory of Delft University of Technology.

I express my gratitude towards Pieter Janssen for his daily support and critical review of my work. Also, I would like to thank Harry Fontijn for making sure the conducting of the experiments went as smooth as it did. For the support and guidance of the Faculty of Civil Engineering I wish to thank Henk Jan Verhagen, Jelle Olthof and Marcel Stive.

For supplying necessary data and being very helpful in answering all of my questions I would like to thank the Operation and Maintenance Division of the Amsterdam-Rijnkanaal.

Laurens Schokking,  
June, 2002.

---

---

# Abstract

Due to the increasing size and use of bowthrusters installed in vessels, Delft University of Technology carries out research to investigate the possible effects of this rather unknown phenomenon. In cooperation with the Ministry of Transport, Public Works and Water Management this research includes experimental tests as well as field research.

For this thesis, two different investigations have been carried out:

- The stability of stones in propeller-induced jet wash on a slope was investigated using an experimental model. This was done at Delft University of Technology.
- The scour effects of bow- and mainthrusters in Dutch inland waterways were investigated in a case study in the Amsterdam-Rijnkanaal, a 70 kilometre long channel leading from Amsterdam to Tiel.

Firstly, the experimental model was used to derive insight in the influence of the duct of a bowthruuster. To that end, velocity measurements in a jet induced by a free propeller were carried out and compared to similar measurements taken in a jet induced by a ducted propeller. The results show that the velocity in a free propeller jet decreases faster than the velocity in a ducted propeller jet, although both jets diverge at a similar angle. The reason for this faster velocity decrease is the fact that the relative turbulence intensity is larger for a free-propeller jet than for a ducted-propeller jet. Concerning the stability of stones, it was found that due to this difference in velocity decrease, the damage on the slope is considerably larger for a ducted propeller jet than for a free propeller jet when using a similar rotation rate, i.e. a similar initial velocity in this case.

Secondly, the model was used to investigate the damage pattern caused by the ducted-propeller jet. It was found that the maximum damage occurs at the toe of the slope, whilst the jet axis, carrying the largest velocities, hits the slope much higher. To investigate the reason for this discrepancy, velocity measurements were performed close to the slope, i.e. 0.025 [m] and 0.050 [m] above the slope. The results show that the average velocities are indeed highest at the location where the jet axis intersects with the slope. However, the largest peak velocities occur lower on the slope, but not as low as the location of maximum damage (the toe of the slope). Due to small velocities at the toe of the slope a convective acceleration of the water along the slope exists, which stops at the location of the largest peak velocities. Following Bernoulli's theorem, this acceleration induces a dominant upward pressure gradient along the lower part of the slope, resulting in a pressure force on a stone. It was found that the resulting force on a stone, which is a combination of this pressure force and shear force, is maximum at the toe of the slope, complying with the area of maximum damage. It was also found, that the direction of the stones' movement could be predicted from the same mechanisms.

---

The case study in the Amsterdam-Rijnkanaal focuses on berthing places only, since bowthrusters are mainly used at these locations. For a number of 15 locations along the Amsterdam-Rijnkanaal bathymetry maps have been analysed to find trends in scour and to relate these to the use of bow- and mainthrusters as far as possible. Based on these results, two different types of berthing places can be distinguished, uniform and non-uniform berthing places. A uniform berthing place is defined as a long berthing place ( $L > 300$  [m]) with no geometrical anomalies. A non-uniform berthing place is defined as a rather short berthing place ( $L < 300$  [m]) or a berthing place that contains distinct geometrical anomalies. At uniform berthing places, scour tends to be shallow and wide spread, usually not endangering the sheetpile construction. It is concluded that the irregularity in berthing (direction and location wise) combined with the time dependent character of scour development, is the reason for this. At non-uniform berthing places, scour tends to be more severe, since vessels berth in a more consistent manner, thereby creating scour at specific, concentrated spots. At these non-uniform berthing places it is possible to make a distinction between bowthruuster-induced scour and mainthruuster-induced scour. Based on the data available it is found that bowthruuster-induced scour may be of similar magnitude as mainthruuster-induced scour. For the Amsterdam-Rijnkanaal it was not found that the depth of bowthruuster-induced scourholes exceeds that of mainthruuster-induced scourholes.

The measured depth of some of the scourholes was compared to the calculated scourdepth for the location investigated. This comparison shows that there are calculation methods available (Römisch (1977) & Ducker and Miller (1996)) that produce results approximately similar to the measured results. However, these methods are only valid for non-uniform berthing places, since at uniform berthing places scour has no time to develop due to the irregularity of the berthing.

---

# Table of Contents

---

<b>PREFACE</b>	<b>5</b>
<b>ABSTRACT</b>	<b>7</b>
<b>1 INTRODUCTION</b>	<b>17</b>
<b>1.1 General</b>	<b>17</b>
<b>1.2 A bowthruster</b>	<b>18</b>
1.2.1 General	18
1.2.2 Physical representation of a bowthruster	18
1.2.3 Damage due to use of bowthrusters	18
<b>1.3 Aims</b>	<b>19</b>
<b>1.4 Thesis set-up</b>	<b>20</b>
<b>2 LITERATURE STUDY</b>	<b>21</b>
<b>2.1 Velocity field</b>	<b>21</b>
2.1.1 A jet	21
2.1.2 Calculating the initial velocity	21
2.1.3 The velocity distribution	25
<b>2.2 Stability and scour</b>	<b>28</b>
2.2.1 Critical velocity	28
2.2.1.1 Izbash (1930) and Shields (1936)	28
2.2.1.2 Correction factor for a slope	29
2.2.2 Vertical quay wall, stability and scour.	30
2.2.2.1 Blokland (1994)	30
2.2.2.2 Schmidt and Römisch (1993)	31
2.2.3 Scourdepth	33
2.2.3.1 Römisch (1977)	33
2.2.3.2 Westrich and Kobus (1974)	34
2.2.3.3 Rajaratnam and Beltaos (1977)	35
2.2.3.4 Hoffmans (1995)	36
<b>2.3 Evaluation</b>	<b>37</b>
2.3.1 Velocity field	37
2.3.2 Stability and scour	37
2.3.2.1 Stability	37
2.3.2.2 Stability and scour in front of a quay wall	37
<b>3 BACKGROUND OF THE EXPERIMENT</b>	<b>39</b>
<b>3.1 Prototype and experimental model dimensions</b>	<b>39</b>
3.1.1 Prototype dimensions	39

---

3.1.2	Scaling of the experimental model	39
3.1.3	Modelling turbulence, the Reynolds number	41
<b>3.2</b>	<b>Experimental model set-up</b>	<b>41</b>
3.2.1	General	41
3.2.2	Free propeller	42
3.2.2.1	General	42
3.2.2.2	Determining an upper limit for the diameter of the opening	42
3.2.3	The protection material	46
3.2.4	Conducting the tests	46
<b>4</b>	<b>INVESTIGATION OF THE FREE-PROPELLER JET</b>	<b>49</b>
<b>4.1</b>	<b>The velocity field</b>	<b>49</b>
4.1.1	Measuring	49
4.1.2	Initial velocity $U_0$ and flow contraction	50
4.1.3	Axial velocity	51
4.1.3.1	Entire velocity field	51
4.1.3.2	Flow establishment	52
4.1.4	Tangential velocity	53
4.1.5	Diverging of the jet and influence of bottom and free surface	54
4.1.6	Reproducibility	54
4.1.7	Circulation	55
4.1.7.1	Through the hole	55
4.1.7.2	Through the basin	56
4.1.8	Measurements and theory compared	56
4.1.9	Comparing the velocity fields	58
4.1.10	Conclusions on the velocity field	59
<b>4.2</b>	<b>Turbulence</b>	<b>59</b>
4.2.1	General	59
4.2.2	Relative turbulences in the jet	62
4.2.2.1	Axial relative turbulence	62
4.2.2.2	Tangential relative turbulence	64
4.2.3	Peak velocities	64
4.2.4	Comparing relative turbulences	66
4.2.5	Profile in height	67
4.2.6	Statistics of fluctuations	68
4.2.6.1	Jet axis	68
4.2.6.2	Above the jet axis	69
<b>4.3</b>	<b>Stability of materials</b>	<b>70</b>
4.3.1	Damage on the slope	70
4.3.2	Criterion of Izbash	70
4.3.3	Reynolds number	71
4.3.4	Comparing a ducted and a free propeller	72
4.3.5	Orientation of spreading	74
4.3.5.1	Direction	74
4.3.5.2	Intensity	75
4.3.6	Conclusions on the stability of materials	76
<b>4.4</b>	<b>Conclusions</b>	<b>76</b>

---

---

<b>5</b>	<b>DAMAGE LOCATION INVESTIGATION</b>	<b>77</b>
<b>5.1</b>	<b>General</b>	<b>77</b>
<b>5.2</b>	<b>The velocity field</b>	<b>79</b>
5.2.1	General	79
5.2.2	Velocities parallel to the slope	79
5.2.2.1	General	79
5.2.2.2	Type II measurements	80
5.2.2.3	Type I measurements	84
5.2.2.4	Type III (vertical) measurements	84
5.2.3	Vertical velocities	86
5.2.4	Horizontal velocities	88
5.2.5	Evaluation of the velocity field	90
5.2.6	Conclusions on the velocity field	91
<b>5.3</b>	<b>Damage location</b>	<b>91</b>
5.3.1	General	91
5.3.2	Peak velocities and turbulence	91
5.3.2.1	Values along the slope	91
5.3.2.2	Location of peak velocities	93
5.3.3	Frequency and energy analysis of vortices	95
5.3.4	Flow direction and slope	96
5.3.5	Shear velocity	96
5.3.6	Pressure gradient	98
5.3.7	Total force on a stone	100
5.3.8	Direction of movement	101
5.3.9	Conclusions on the damage location	104
<b>5.4</b>	<b>Conclusions</b>	<b>104</b>
<b>6</b>	<b>DAMAGE INVESTIGATION</b>	<b>105</b>
<b>6.1</b>	<b>General</b>	<b>105</b>
6.1.1	Approach	105
6.1.2	Data collection	105
6.1.3	Experience from practice	106
6.1.4	Selected waterway	108
<b>6.2</b>	<b>Background on berthing and scour</b>	<b>108</b>
<b>6.3</b>	<b>Uniform quays</b>	<b>109</b>
6.3.1	General	109
6.3.2	Examples of uniform quays	110
6.3.2.1	Maarsse	110
6.3.2.2	Other quays in the Amsterdam-Rijnkanaal	113
6.3.2.3	Douanekade Sas van Gent	113
6.3.3	Conclusions on uniform quays	114
<b>6.4</b>	<b>Non-uniform quays</b>	<b>114</b>
6.4.1	General	114
6.4.2	Examples of non-uniform quays	115
6.4.2.1	Roosenveltlaan	115
6.4.2.2	Location Plofsluis	115
6.4.2.3	Wijk bij Duurstede south side	119
6.4.2.4	Nigtevecht	120

---

---

6.4.2.5	Tiel	123
6.4.2.6	Wijk bij Duurstede north side	125
6.4.3	Conclusions on non-uniform quays	126
<b>6.5</b>	<b>Comparison with theory</b>	<b>126</b>
6.5.1	Governing vessel	126
6.5.2	Example: Plofsluis	127
6.5.2.1	Bottom velocity	127
6.5.2.2	Scourdepth at the Plofsluis	129
6.5.2.3	Evaluation and conclusions	131
6.5.3	Other examples: Maarsse and the Roosenveltlaan	132
<b>6.6</b>	<b>Conclusions and recommendations</b>	<b>133</b>
<b>7</b>	<b>CONCLUSIONS AND RECOMMENDATIONS</b>	<b>135</b>
<b>7.1</b>	<b>General</b>	<b>135</b>
<b>7.2</b>	<b>Model (aim 1a&amp;b)</b>	<b>135</b>
7.2.1	Free-propeller jet	135
7.2.2	Damage location on the slope	135
7.2.3	Recommendations in general	136
<b>7.3</b>	<b>Damage investigation in the Dutch inland waterways (aim 2)</b>	<b>137</b>
	<b>NOMENCLATURE</b>	<b>139</b>
	<b>REFERENCES</b>	<b>141</b>
	<b>APPENDICES</b>	
A.	Experimental model dimensions	A-1
B:	Pictures of the model	A-5
C:	Velocity profiles for ducted and free propeller	A-9
D:	Autocorrelation and Power Density Spectra of the jet	A-15
E:	PASCAL program 'diameter of opening in board'	A-23
F:	PASCAL program 'dataset analysis'	A-25
G:	Velocities and turbulences in the free-propeller jet	A-29
H:	Depth profile of the Amsterdam-Rijnkanaal at Houten	A-33
I:	Principle of operation of the EMS	A-35

---



# List of Figures

figure 1-1 Top view of the prototype situation (figure by Van Veldhoven (2001)).	18
figure 1-2 Side view of the prototype situation with a slope (figure by Van Veldhoven (2001)).	19
figure 1-3 Side view of the prototype situation with a vertical quay wall.	19
figure 2-1 Velocity distribution at exit from the propeller and in developed flow.	21
figure 2-2 Actuator disc.	22
figure 2-3 Flow establishment and established flow.	25
figure 2-4 Five zones in front of a quay wall, as defined by Schmidt and Römisch.	31
figure 2-5 Hole depth as a function of the stability parameter of Römisch (B).	34
figure 2-6 Two forms of scourholes.	34
figure 3-1 Side view of the prototype situation (figure by Van Veldhoven (2001)).	39
figure 3-2 Diverging of propeller jet and the entrainment zone.	43
figure 3-3 Velocity distribution in radial/tangential direction according to Giger, Dracos and Jirka (1991), measured (dots) and theoretical (line).	44
figure 3-4 Theoretical velocity distribution and the distinction between initial discharge and entrained discharge.	45
figure 3-5 Theoretical velocity distribution in the jet, just after the flow exits from the propeller at the point of maximum contraction.	45
figure 3-6 Close up of the probe of the EMS.	47
figure 4-1 Theoretical velocity distribution at exit and in developed flow.	49
figure 4-2 Measurement locations. For all points $y = 0$ .	49
figure 4-3 Axial velocity distribution at several points along the x-axis. The graphs present the values of $U_{x,z}/U_{0[-]}$ .	51
figure 4-4 Interpolated values for the axial velocity distribution in the free-propeller jet.	52
figure 4-5 Theoretical and measured velocity on the axis.	52
figure 4-6 Tangential velocity distribution.	53
figure 4-7 Initial measurements for $x = 0.6$ [m] and $0.7$ [m].	54
figure 4-8 Circulation through the hole.	55
figure 4-9 Top view of the model, showing the water flow and the cells that developed (on the left the inflow, on the right the outflow).	56
figure 4-10 Theoretical and measured velocity distribution at several distances from the propeller. Values represent $U_x/U_{max}$ .	57
figure 4-11 Difference in velocity development between ducted propeller and free propeller.	58
figure 4-12 Photographs of a starting free jet (Garside, J.E, from: Hinze, 1975, Turbulence).	61
figure 4-13 Axial relative turbulence.	62
figure 4-14 Vortices at boundary of a half-jet (Flugel, G, from: Hinze, 1975, Turbulence).	62
figure 4-15 Zone of flow establishment ( $x_0$ ).	63
figure 4-16 Tangential relative turbulence.	64
figure 4-17 Fluctuations in the jet at a random point, duration of 4.5 [s]. Peak velocity occurs at $t = 4.3$ [s].	64
figure 4-18 Relative axial turbulence of the ducted-propeller jet, free-propeller jet and a free water jet.	66
figure 4-19 Relative axial turbulence distribution over the height above the x-axis.	67
figure 4-20 Turbulences of free and ducted-propeller jet at $X/D = 6$ [-] and $X/D = 7$ [-] compared.	67
figure 4-21 Distribution of the fluctuations, measured and theoretical.	68
figure 4-22 Distributions of fluctuations at $x = 0.30$ [m], $y = 0$ , $z = 0.10$ [m].	69
figure 4-23 Damage at the slope related to the rpm of the propeller.	70
figure 4-24 Damages compared, related to the rpm of the propeller.	72
figure 4-25 Damages compared, related to the velocity at $x = 0.7$ [m].	73
figure 4-26 Net movements.	74
figure 4-27 Intensity of all movements, i.e. the total number of movements in the area considered.	75
figure 5-1 Location of maximum damage, visualized in the x-z plane.	77
figure 5-2 Location and direction of the damages visualized in the x'-y plane. Dark areas are areas with intense movement of stones. Every square equals 0.05 [m] by 0.05 [m].	77
figure 5-3 Different types of measuring.	79
figure 5-4 Measured points in the x'-y plane.	80
figure 5-5 The two heights at which the type II measurements were taken.	80
figure 5-6 The average velocities for $z' = 0.025$ [m] and $z' = 0.050$ [m].	81
figure 5-7 Below the x-axis the velocity increases with increased height above the slope.	81
figure 5-8 Total average velocities and flow direction at $z' = 0.025$ [m].	83
figure 5-9 Total average velocities and flow direction at $z' = 0.050$ [m].	83
figure 5-10 Type I & II measurements at $y = 0$ .	84
figure 5-11 EMS probes on the slope, top- and side view.	84

figure 5-12 Average velocities at $z' = 0.025$ [m], $y = 0$ for two different types of measuring.	85
figure 5-13 The angle between the flow direction and the x-axis along the slope at $z' = 0.025$ [m].	86
figure 5-14 The locations of the measurements in vertical direction (type III).	86
figure 5-15 Vertical velocities for $z = 0.050$ [m].	87
figure 5-16 Velocities in the x-z plane for $y = 0$ , $-0.050$ [m] < $x < 0.7$ [m], $-0.18$ [m] < $z < 0.1$ [m].	87
figure 5-17 Locations of the horizontal measurements. Between every point is a space of $0.10$ [m]. Distances are in metres.	88
figure 5-18 Horizontal velocities for $z = 0$ , $0 < x < 0.60$ [m], $-0.3$ [m] < $y < 0.3$ [m].	88
figure 5-19 Copy of the most important velocity field figures (all showing average velocities).	90
figure 5-20 Turbulence intensities along the slope for $y = 0$ , $z' = 0.025$ [m] & $0.050$ [m].	91
figure 5-21 Peak velocities on the slope, $z' = 0.050$ [m].	93
figure 5-22 Peak velocities along the slope at $y = 0$ , $z' = 0.050$ [m].	93
figure 5-23 Turbulence intensities ' $r_x$ ' in the ducted-propeller jet for different distances from the propeller.	94
figure 5-24 The forces acting on a stone in a body of flowing water with a constant average velocity in time and space.	96
figure 5-25 Shear force for $y = 0$ at the slope.	97
figure 5-26 Pressure difference over a stone in an accelerating body of water.	98
figure 5-27 Pressure force along the slope for $y = 0$ .	99
figure 5-28 Total upward force on the stone.	100
figure 5-29 Location of maximum movements and their direction. Every square equals $0.05$ [m] by $0.05$ [m].	101
figure 5-30 Average velocity along the slope for $z' = 0.025$ [m] and $y = 0$ .	102
figure 5-31 Acting forces on stone lifted from its bed.	102
figure 5-32 Acting forces on stone lifted from its bed, point at $x = 0.10$ [m] is neglected.	103
figure 6-1 The Amsterdam-Rijnkanaal with the main towns situated next to it.	108
figure 6-2 Berthing place at Maarsssen.	110
figure 6-3 Bathymetry at Maarsssen. All values are in metres. Reference level for depth profile ( $5$ [m] outside the quay) is NAP.	111
figure 6-4 Bathymetry at Maarsssen. All values are in metres. Reference level for depth profile ( $5$ [m] outside the quay) is NAP.	112
figure 6-5 Bathymetry at Sas van Gent. All depths are in metres. Reference level is NAP.	113
figure 6-6 Berthing places in the vicinity of Nieuwegein and Houten.	115
figure 6-7 Aerial photograph of the area shown in figure (6-6).	116
figure 6-8 Bathymetry at the Plofsluis, east side. All values are in metres. Reference level for the depth profile ( $5$ [m] outside the quay) is NAP.	117
figure 6-9 Bathymetry at the Plofsluis with the believed location and direction of most ships berthing here.	118
figure 6-10 Situation at Wijk bij Duurstede.	119
figure 6-11 Bathymetry at Wijk bij Duurstede. All values are in metres. Reference level for the depth profile ( $8$ [m] outside the quay) is NAP.	120
figure 6-12 Aerial photograph of the situation at Nigtevecht.	120
figure 6-13 Bathymetry at Nigtevecht. All values are in metres. Reference level for the depth profile ( $8$ [m] outside the quay) is NAP.	121
figure 6-14 Aerial photograph of the situation at Tiel.	123
figure 6-15 Bathymetry at Tiel. All values are in metres. Reference level is NAP.	124
figure 6-16 Bathymetry at Wijk bij Duurstede north side. All values are in metres. Reference level for the depth profile ( $10$ [m] outside the quay) is NAP.	125
figure 6-17 Situation at the Plofsluis when a large Rhine vessel is unberthing.	127
figure 6-18 Situation at the Plofsluis when a large Rhine vessel is unberthing.	128

---

# List of Tables

table 3-1 Prototype dimensions.	39
table 3-2 Model dimensions.	40
table 4-1 Value of ' $\bar{a}$ ' at $x/D$ from 1 [-] to 7 [-].	65
table 6-1 Characteristics of a large Rhine vessel.	126
table 6-2 Results of maximum scour from different formulas compared to the measured values at the Plofsluis.	131
table 6-3 Results of maximum scour from different formulas compared to the measured values at Maarsse.	132
table 6-4 Results of maximum scour from different formulas compared to the measured values at the Roosenveltlaan.	132



---

# 1 Introduction

## 1.1 General

The size of bowthruster and the engine powers installed in ships are increasing continuously over the past years. Present calculation methods on stability of stones in propeller-induced jet wash are thought to be inaccurate. Also, the effect of bowthrusters compared to the effect of mainthrusters is uncertain.

This is why Delft University of Technology has started a research program to find out what effects bowthrusters have on stability of (protection) materials.

Part of this program is therefore the conduction of experimental model tests, to gain insight into the mechanisms playing a role in propeller-induced jet wash and into the stability of stones in this jet wash. Eventually this should lead to more accurate equations concerning the relationship between this stability and the use of bowthrusters.

Consequently, another part of the program is to gain more insight in the actual influence of bowthrusters and the role they play next to mainthrusters. Rijkswaterstaat<sup>1</sup> concerns itself with the subject since it maintains large parts of the Dutch inland waterways.

Together, these two parts are the subject for this graduation thesis.

The two subjects mentioned above deal with different types of damage or erosion. In the Dutch inland waterways many quays are protected by sheetpiles. Possible erosion therefore occurs at the toe of this sheetpile.

A slope, however, is usually protected by loose stones and the damage therefore occurs at the slope itself (see figure (1-2) & (1-3)).

The report is divided into two sections:

The first part deals with the jet wash on a slope. For that part of the study an experimental model is used to get the necessary insight in the processes that occur in the water. It focuses on velocity distributions, turbulences and stability.

The second part describes a similar process, only on a larger scale: it deals with the question whether erosion near berthing facilities in the inland waterways can be related to the use of bowthrusters. It focuses on scourdepth and the possibility to separate bowthruster-induced scour from mainthruster-induced scour.

---

<sup>1</sup> Rijkswaterstaat is part of the Ministry of Transport, Public Works and Water Management in The Netherlands.

---

## 1.2 A bowthruster

### 1.2.1 General

A bowthruster is basically a propeller located in a duct in the bow of a ship. Its direction is horizontal and perpendicular to the longitudinal axis of the ship. When used, it initiates a force perpendicular to this axis, which makes the ship turn (see figure (1-1)).

The disadvantage of a bowthruster is that the jet wash can inflict damage to quays and to the bottoms and banks of waterways.

### 1.2.2 Physical representation of a bowthruster

There are basically three different ways to physically model a jet coming from a bowthruster:

- a free jet through a round orifice, induced by water pressure.
- a rotating propeller in a duct in a body of water.
- a rotating propeller without a duct in a body of water.

An earlier investigation by Van Veldhoven (2001) already proved that the first two models produce very different results concerning the stability of stones on a slope.

The third way of modelling a bowthruster, the free propeller, will be described in this report and the results concerning velocity distributions and the stability of protection materials will be compared to results derived from the first two models. They will also be compared to present calculation methods for the velocity distribution induced by bowthrusters, which are described in the accompanying literature study in chapter 2.

### 1.2.3 Damage due to use of bowthrusters

As already briefly mentioned in section 1.1, there are in general two ways in which erosion at a quay can occur:

- Erosion on a slope (figure (1-2)).
- Erosion at the toe of a vertical wall (figure (1-3)).

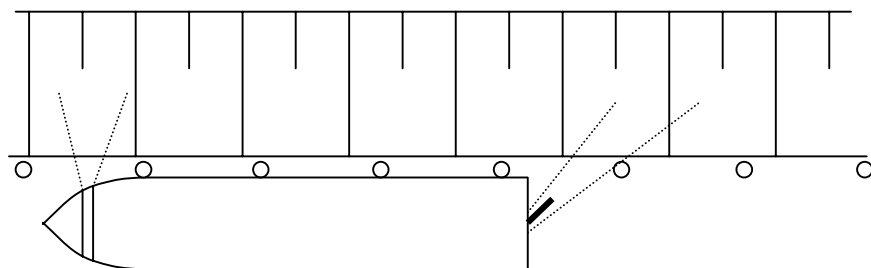


figure 1-1 Top view of the prototype situation (figure by Van Veldhoven (2001)).

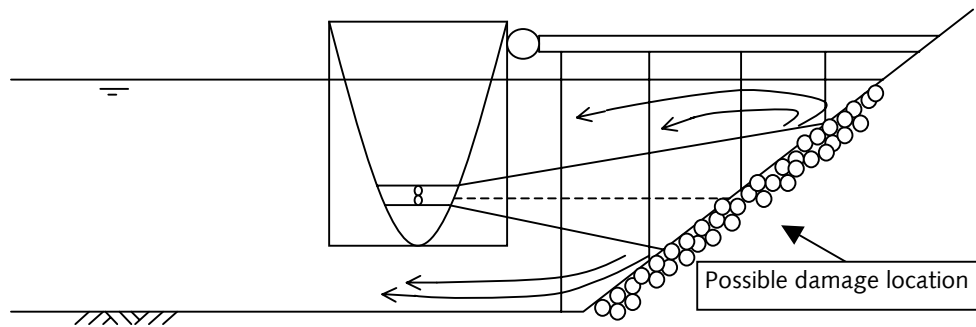


figure 1-2 Side view of the prototype situation with a slope (figure by Van Veldhoven (2001)).

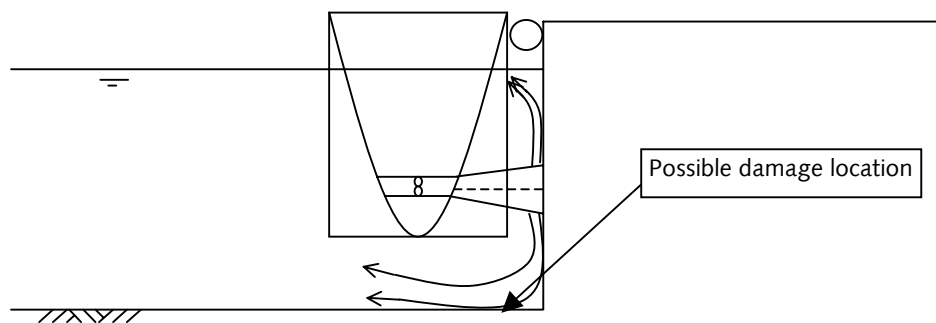


figure 1-3 Side view of the prototype situation with a vertical quay wall.

In the first case (figure (1-2)) the bowthruster is directly aimed at the protection material and if this material is not stable enough, erosion will occur.

In the second case (figure (1-3)) the jet coming from the bowthruster is deflected by the vertical wall (sheetpiles for instance) and hits the bottom. There, a scourhole can develop.

This latter case is the main concern of Rijkswaterstaat, since they mainly deal with inland waterway transport. In inland navigation canals the use of vertical walls to protect the quays is most common.

### 1.3 Aims

The aim of this thesis is twofold:

- 1a) To determine the correct way of modelling a bowthruster. As mentioned in section 1.2.2 there are three ways in which a bowthruster can be modelled. In this report, it will be determined whether a free-propeller jet gives similar results, concerning stability of stones and the distribution of the velocity as a ducted propeller<sup>2</sup>.
- 1b) Following from this, to explain the location of the damage on the slope, induced by a ducted-propeller jet.

<sup>2</sup> Van Veldhoven (2001) already concluded that a free jet should not be used for modeling a bowthruster and this type is therefore neglected here.

- 
- 2) To determine the relationship between erosion along quay walls in the Dutch inland waterways and the use of bowthrusters.

#### **1.4 Thesis set-up**

The conclusions that need to be drawn, based on the aims mentioned in section 1.3, are derived in the following manner:

Chapter 2 describes present calculation methods. They concern velocity distributions, stability of materials and scour depths. Approaches of different authors are given on the same subject. Eventually a comparison is made, and it is decided which equations are suitable for this study.

Chapter 3 describes the set-up of the experimental model as it was built in the Fluid Mechanics Laboratory of Delft University of Technology.

It deals with the set-up of the model of the ducted-propeller jet and of the free-propeller jet.

Chapter 4 and 5 deal with the results of the experimental model investigations. Chapter 4 describes the results for the free-propeller jet and chapter 5 deals with the investigation of the damage location on the slope, for the ducted-propeller jet. These chapters show the results concerning velocity distributions, turbulences, and stability.

Chapter 6 describes the damage investigation in the Dutch inland waterways. Approximately 15 berthing places were investigated and elaboration is given on some of the characteristic ones.

Each of the chapters 4, 5 and 6 ends with conclusions. Chapter 7 summarises these conclusions, which are supplemented by recommendations concerning all subjects mentioned.



---

## 2 Literature Study

This chapter deals with the theory behind jets on quay walls. Quite some research has been carried out on modelling jets and deriving calculation methods for such jets.

In this chapter the present theories are described on

- how to calculate the velocities in a jet.
- how to determine the stability of sediment in general.
- how to determine the stability of sediment next to a quay wall.

### 2.1 Velocity field

#### 2.1.1 A jet

The jets that are the subject of this report are initiated by a propeller. In general the propeller accelerates water particles. This gives the particles a velocity in axial, radial and tangential direction. The jet diverges as it passes through the surrounding water which usually has a lower velocity.

Present theories of modelling jets are based on the idea that a jet has an equal velocity distribution when it exits at the propeller. After that, the velocity distribution is assumed to have the shape of a normally distributed profile (see figure (2-1)).

The next figure enlightens the parameters that are used most in the following sections.

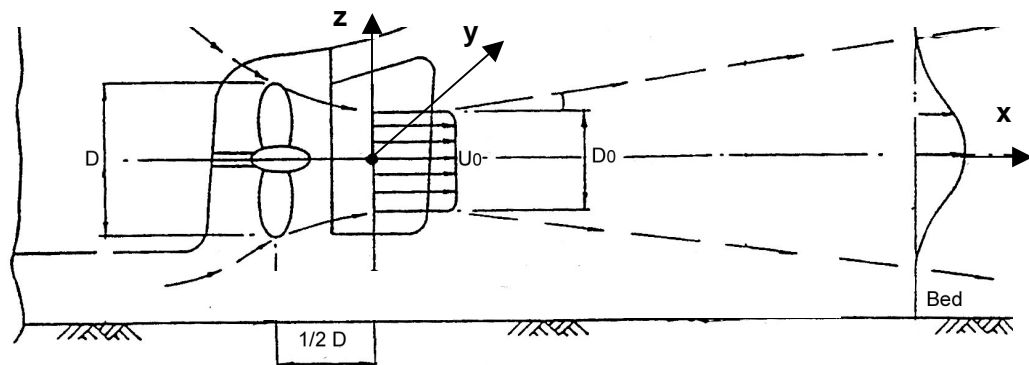


figure 2-1 Velocity distribution at exit from the propeller and in developed flow.

#### 2.1.2 Calculating the initial velocity

Most available theories use the initial velocity behind the propeller (in this thesis defined as either  $U_2$  or  $U_0$ ) to calculate the velocities in any given place in the jet.

To calculate this initial velocity the description of Blaauw & Van de Kaa (1978) on the momentum theory is used in this thesis.

In this theory the propeller is schematised into an actuator disc as follows:

- The propeller has an infinite number of blades.

- The propeller is rotating with an infinite velocity.
- The load of every blade is constant over the radius.
- The delivered thrust equals the propeller thrust.

Further more this theory only deals with the mean axial velocities. In reality however tangential and radial water velocities will also occur, initiated by the tangential velocity of the propeller.

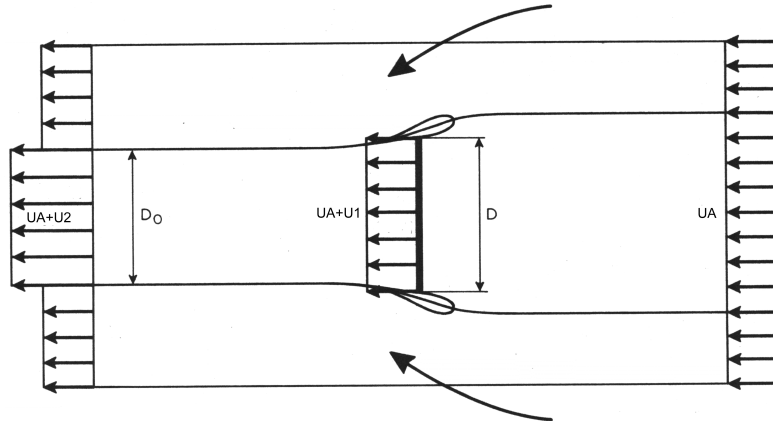


figure 2-2 Actuator disc.

The thrust of a ducted actuator disc ( $T_{(dps)}$  [N]) follows from the equation of motion:

$$T_{(dps)} = \frac{dU}{dt} \cdot \rho_w \cdot V \text{ [N]} \quad (2-1)$$

where

- U: velocity [m/s]
- $\rho$ : density of water [kg/m<sup>3</sup>]
- V: volume [m<sup>3</sup>]

The volume V that passes per unit of time 'dt' (and is accelerated with a velocity dU) is calculated at the ducted actuator disc, resulting in the following equation:

$$V_{(dps)} = \Delta t \cdot (U_A + U_1) \cdot \frac{1}{4} \pi \cdot D^2 \text{ [m}^3\text{]} \quad (2-2)$$

where

- t: time [s]
- D: diameter of propeller [m]
- $U_A$ : velocity of the surrounding water relative to (moving) actuator disc [m/s]
- $U_1$ : velocity increment in the disc [m/s]
- $U_2$ : resulting velocity increment [m/s]

dU is defined as the difference in velocity measured over the entire influence length of the disc and as can be seen in figure (2-2) is equal to  $U_2$ .

This results in the thrust of the disc:

$$T_{(dps)} = \rho_w \cdot (U_A + U_1) \cdot U_2 \cdot \frac{1}{4} \pi \cdot D^2 \quad [\text{N}] \quad (2-3)$$

If the influence of the duct is taken away we can calculate the thrust of the propeller alone by applying Bernoulli's theorem<sup>3</sup> that

$$U_1 = \frac{U_2}{2} \quad [\text{m/s}]$$

Equation (2-3) then results in:

$$T_{(prop)} = \rho_w \cdot \left( U_A + \frac{U_2}{2} \right) \cdot U_2 \cdot \frac{1}{4} \pi \cdot D^2 \quad [\text{N}] \quad (2-4)$$

With the aid of the condition of conservation of mass it follows that:

$$\frac{1}{4} \pi \cdot D^2 \cdot \rho_w (U_A + U_1) = \frac{1}{4} \pi \cdot D_0^2 \cdot \rho_w (U_A + U_2) \quad (2-5)$$

which leads to the contraction coefficient  $\varphi'$  [-]:

$$\varphi' = \frac{D_0^2}{D^2} = \frac{U_A + U_1}{U_A + U_2} \quad [-] \quad (2-6)$$

where

$D_0$ : Diameter of the jet at the maximum contraction [m]

This coefficient  $\varphi'$  gives the ratio between the area of the jet at the disc and at its maximum contraction.

For known values of  $T_{(dps)}$ ,  $T_{(prop)}$ ,  $U_{(A)}$  and  $D$  the contraction and the velocity increments  $U_1$  and  $U_2$  can be calculated.

Since a propeller can be characterized by a thrust coefficient it is usually easier to use this coefficient to determine the velocities.

The thrust coefficient  $K_T$  [-] for the disc is defined as:

$$K_{T(dps)} = \frac{T_{(dps)}}{\rho \cdot n^2 \cdot D^4} \quad [-] \quad (2-7)$$

for a ducted disc and for the propeller inside:

---

<sup>3</sup> Bernoulli states that on a streamline  $\frac{U^2}{2g} + \frac{p}{\rho g} + z = \text{constant}$ .

$$K_{T(prop)} = \frac{T_{(prop)}}{\rho \cdot n^2 \cdot D^4} \quad [-] \quad (2-8)$$

where

n: number of revolutions per second [ $s^{-1}$ ]

This coefficient lies between the 0.25 [-] and 0.50 [-]. This value can be seen as an expression of the efficiency of the propeller used.

Substituting the equations found for T in (2-7) and (2-8) leads to the following equations:

$$K_{T(dps)} = \frac{\rho \cdot \frac{1}{4} \pi \cdot D^2 \cdot (U_A + U_1) \cdot U_2}{\rho \cdot n^2 \cdot D^4} \quad [-] \quad (2-9)$$

$$K_{T(prop)} = \frac{\rho \cdot \frac{1}{4} \pi \cdot D^2 \cdot \left( U_A + \frac{U_2}{2} \right) \cdot U_2}{\rho \cdot n^2 \cdot D^4} \quad [-] \quad (2-10)$$

rewriting this and assuming  $U_A = 0$  (bollard pull condition and no current) the following results:

$$U_1 = \frac{K_{T(dps)} \cdot 4n^2 \cdot D^2}{U_2 \cdot \pi} \quad [m/s] \quad (2-11)$$

$$U_2 = \sqrt{\frac{8n^2 D^2}{\pi} \cdot K_{T(prop)}} \approx 1.60 \cdot n \cdot D \cdot \sqrt{K_{T(prop)}} \quad [m/s] \quad (2-12)$$

According to Römisch (1975) if  $K_T$  is unknown it is possible to use an average number of 0.35 (empirically found)<sup>4</sup>. This leads to:

$$U_2 = 0.95 \cdot n \cdot D \quad [m/s] \quad (2-13)$$

Since  $U_A = 0$  the velocity just behind the propeller is equal to  $U_2$ , which is also defined as the initial velocity  $U_0$ .

Substituting (2-11) and (2-12) in (2-6), results in

$$\varphi' = \frac{K_{t(dps)}}{2K_{t(prop)}} = \frac{D_0^2}{D^2} \quad [-] \quad (2-14)$$

For a non ducted propeller ( $T_{(prop)} = T_{(dps)}$  and  $U_1 = \frac{1}{2} U_2$  and  $U_A = 0$ ) it follows that:

<sup>4</sup> In case the value of  $K_T$  is not known, Blaauw and Van de Kaa give a different (empirical) method than Römisch and give a formula for  $U_0$  based on the installed engine power P (watts):

$$U_0 = 1.15 \cdot \left( \frac{P}{\rho \cdot D_0^2} \right)^{\frac{1}{3}} \quad [m/s]$$

$$\phi' = 0.5 \text{ [-]}$$

and for a ducted propeller ( $T_{(\text{prop})} = \frac{1}{2} T_{(\text{dps})}$ )

$$\phi' = 1 \text{ [-]}$$

When values of  $K_{T(\text{prop})}$ ,  $K_{T(\text{dps})}$ ,  $D$  and  $n$  are known it is possible to calculate the velocities of the jet behind the propeller.

Equation (2-14) and the found values also indicate that in case of a ducted propeller

$$D_0 = D \text{ [m]}$$

and in case of a non-ducted propeller

$$D_0 = \sqrt{0.5} \cdot D = 0.71 \cdot D \text{ [m]}$$

### 2.1.3 The velocity distribution

So far only the mean axial velocities at the outflow at the propeller have been treated. In this section the theory of Albertson et al. (from Blaauw & Van de Kaa (1978)) will be discussed. He derived a theory to estimate the velocity  $U_{x,z}$  at any location in the jet, making the following assumptions:

- The pressure is distributed hydrostatically throughout the flow.
- The diffusion process is dynamically similar under all conditions.
- The longitudinal component of velocity within the diffusion region varies according to the normal probability function at each cross-section.

The theory states that two zones can be distinguished, one of flow establishment and one of established flow.

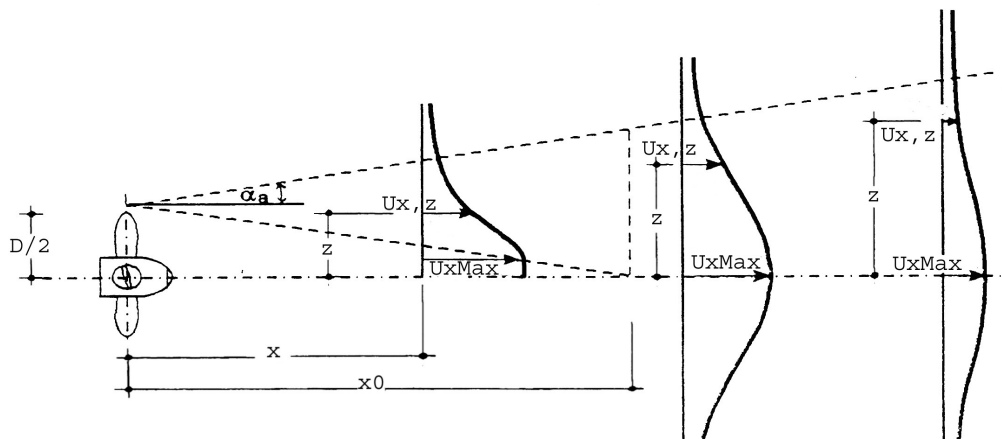


figure 2-3 Flow establishment and established flow.

In the first zone ( $x \leq x_0$ ) the jet is still developing. As can be seen in figure (2-3) the influence of the outer part of the propeller is not yet noticed along the x-axis. As soon as it is, the transition to established flow takes place.

In the first zone the velocity distribution is written as:

$$\frac{U_{x,z}}{U_0} = \exp\left[-\frac{(z + cx - D_0/2)^2}{2 \cdot (cx)^2}\right] \quad [-] \quad (2-15)$$

where

x: distance from propeller [m]  
 $U_{x,z}$ : velocity at point z,r [m/s]  
 z: radial distance from x-axis [m]  
 c: constant [-]

The maximum velocity, occurring at the x-axis, is however constant in the zone of flow establishment ( $x \leq x_0$ ):

$$\frac{U_{\max}}{U_0} = 1 \quad [-] \quad \text{for } x < x_0 \quad (2-16)$$

For the zone of established flow ( $x > x_0$ ) the velocity distribution in the jet can be determined in two steps. First the velocity along the x-axis  $U_{\max}(z = 0)$  is calculated as a function of x:

$$\frac{U_{\max}}{U_0} = \frac{1}{2 \cdot c_1} \cdot \left(\frac{x}{D_0}\right)^{-1} \quad [-] \quad (2-17)$$

Next the velocity at a certain radial distance from the x-axis ( $U_{x,z}$ ) is calculated as a function of the found  $U_{\max}$  at that location:

$$\frac{U_{x,z}}{U_{\max}} = \exp\left[-\frac{1}{2 \cdot c_2^2} \cdot \frac{z^2}{x^2}\right] \quad [-] \quad (2-18)$$

For the value of  $c_1$  Römisch and Fuehrer (1981) found empirically that for a jet initiated by a non ducted propeller

$$c_1 = 0.192 \quad [-]$$

and

$$c_2 = 0.15 \quad [-]$$

when  $D_0$  is substituted by D.

Substituting these values in (2-17) and (2-18) leads to the following equations:

---

$$\frac{U_{\max}}{U_0} = 2.6 \cdot \left(\frac{x}{D}\right)^{-1} \quad [-] \quad (2-19)$$

$$\frac{U_{x,z}}{U_{\max}} = \exp\left[-22.2 \cdot \frac{z^2}{x^2}\right] \quad [-] \quad (2-20)$$

Equations (2-19) and (2-20) are valid for the zone of established flow and for a undisturbed propeller jet. In the following section it will become clear that in case of a ducted propeller the distribution is different.

It is noted that others found different values.  
For instance Blaauw & Van de Kaa (1978) found:

$$c_1 = c_2 = 0.18 \quad [-]$$

which leads to the following formulas:

$$\frac{U_{\max}}{U_0} = 2.8 \cdot \left(\frac{x}{D_0}\right)^{-1} \quad [-] \quad (2-21)$$

$$\frac{U_{x,z}}{U_{\max}} = \exp\left[-15.4 \cdot \frac{z^2}{x^2}\right] \quad [-] \quad (2-22)$$

---

## 2.2 Stability and scour

The theories of Izbash (1930) and Shields (1936) on critical velocities related to stability are explained here. They both defined their own stability parameter. It will depend on the conditions which method to follow.

Since this thesis also deals with the practical aspect of jets causing scour in the inland waterways of the Netherlands some theory on this aspect is also mentioned. Several methods are explained and it is pointed out what limitations they have.

### 2.2.1 Critical velocity

#### 2.2.1.1 Izbash (1930) and Shields (1936)

There is a relationship between the load on a particle and its strength to withstand this load. The load is expressed as the square of the velocity and the strength is expressed as the submerged weight of the particle:

$$U_{cr}^2 \propto \left( \frac{\rho_s - \rho_w}{\rho_w} \right) \cdot g \cdot d \quad (2-23)$$

**Izbash** (1930) defined this relationship as:

$$\beta_{iz} = \frac{2 \cdot g \cdot \Delta \cdot d}{U_{cr}^2} \quad [-] \quad (2-24)$$

where

$\beta_{iz}$ :	parameter of Izbash [-]
$U_{cr}$ :	critical velocity [m/s]
$\Delta$ :	relative density $\left( \frac{\rho_s - \rho_w}{\rho_w} \right)$ [-]
$g$ :	gravitational constant [m/s <sup>2</sup> ]
$d$ :	particle diameter [m]
$\rho_s$ :	density of the sediment [kg/m <sup>3</sup> ]
$\rho_w$ :	density of the water [kg/m <sup>3</sup> ]

Izbash then determined in an empirical way that this parameter  $\beta_{iz}$  should be 0.7 [-] for a stable situation:

$$U_{cr} = 1.2 \sqrt{2 \cdot \Delta \cdot g \cdot d} \quad [m/s] \quad (2-25)$$

Izbash does not take the influence of the water depth into account and does not define the location of the critical velocity. These shortcomings however make it an easy to use formula and in the case of submerged jets it is practically applicable.

**Shields** (1936) introduced a well known criterion for stability analysis. He uses more parameters than Izbash does, introducing the shear stress, bottom roughness and water depth.



According to him the following relationship for the start of movement of sediment holds:

$$\frac{\tau}{(\rho_s - \rho_w) \cdot g \cdot d} = f\left(\frac{u^* \cdot d}{\nu}\right) = f(\text{Re}^*) = \psi \quad [-] \quad (2-26)$$

where

$$\begin{aligned} \tau: & \text{shear stress [N/m}^2\text{]} \\ u^* & = U \cdot \frac{\sqrt{g}}{C} \text{ shear velocity [m/s]} \\ C: & \text{Chezy value for bottom roughness [m}^{1/2}\text{/s]} \\ \psi: & \text{Shields parameter [-]} \\ \nu: & \text{kinematical viscosity [m}^2\text{/s]} \end{aligned} \quad (2-27)$$

It is noted however that considering the background of this formula<sup>5</sup>, this formula does not really apply to the movement of sediment caused by jets.

### 2.2.1.2 Correction factor for a slope

When the stones are situated on a slope, the stability will be influenced by this slope.

Therefore a correction factor  $K(\alpha)$  [-] is added to the stone diameter found.

This factor equals, for a flow running

up the slope:

$$K(\alpha) = \frac{\sin(\varphi + \alpha)}{\sin(\varphi)} \quad [-] \quad (2-28)$$

down the slope:

$$K(\alpha) = \frac{\sin(\varphi - \alpha)}{\sin(\varphi)} \quad [-] \quad (2-29)$$

along the slope:

$$K(\alpha) = \sqrt{\left(1 - \frac{\sin^2 \alpha}{\sin^2 \varphi}\right)} \quad [-] \quad (2-30)$$

where

$$\begin{aligned} K(\alpha): & \text{correction factor [-]} \\ \alpha: & \text{angle of slope [degrees]} \end{aligned}$$

<sup>5</sup> Shields uses the relationship between a free stationary flow on a sloping bed and the counteracting of the shear stresses of the water and the sediment. A jet however cannot be considered to be 'free flowing' nor is the energy dissipation caused by the mentioned shear stresses alone. Turbulence plays a very important role in the energy dissipation of the jet.

---

$\phi$ : angle of internal stability of the stones [degrees]

The found  $d_{50}$  of the critical stone diameter for a horizontal bed is divided by  $K(\alpha)$  which then leads to the  $d_{50}$  for the sloping bed.

### 2.2.2 Vertical quay wall, stability and scour.

Theories on stability and scour next to quay walls of *Blokland* (1994), *Römisch* (1993) and *Rajaratnam* (1977) are explained here.

#### 2.2.2.1 *Blokland* (1994)

*Blokland* calculates the maximum velocity at the bottom  $U_{\max, bot}$  caused by a jet perpendicular to a wall by:

$$U_{\max, bot} = 2.8 \cdot \frac{U_o \cdot D_0}{L + z} \quad [\text{m/s}] \quad \text{for} \quad \frac{L}{z} \geq 1.8 \quad [-] \quad (2-31)$$

$$U_{\max, bot} = 1.0 \cdot \frac{U_o \cdot D_0}{z} \quad [\text{m/s}] \quad \text{for} \quad \frac{L}{z} < 1.8 \quad [-] \quad (2-32)$$

where

L: distance from propeller to quay wall [m]

He determines the stability of bottom material using the parameter of Shields ( $\psi_{cr}$ ) and of Izbash ( $\beta_{iz}$ ) for the critical water velocity.

$$\psi_{cr} = \frac{\tau}{(\rho_s - \rho_w) \cdot g \cdot d} \quad [-] \quad (2-33)$$

and

$$\beta_{iz} = \frac{2 \cdot g \cdot \Delta \cdot d}{U_{\max, bot}^2} \quad [-] \quad (2-34)$$

where

$\Delta$ : relative density [-]

Using

$$\tau = c_f \cdot \frac{1}{2} \cdot \rho \cdot U_{\max, bot}^2 \quad [\text{N/m}^2] \quad (2-35)$$

the relation between the two parameters follows:

$$\beta_{iz} = \frac{c_f}{\psi} \quad [-] \quad (2-36)$$

where

$c_f$ : friction coefficient (equals  $\frac{g}{C^2}$ ) [-]

As critical value Blokland suggests to make use of either Römisch' findings on the parameter of Izbash, or Verhey's findings on the parameter of Shields:

$\beta_{iz,cr} \geq 2.5$  to 1.3 then the sediment is stable (Römisch, 1993)

or

$\psi_{cr} < 0.03$  (no movement) to 0.04 (some movement) then the sediment is stable (Verheij, 1983)

### 2.2.2.2 Schmidt and Römisch (1993)

When a bowthruster (assumed to be a ducted propeller) is directed onto a quay wall Schmidt and Römisch distinguish 5 zones, see figure (2-4):

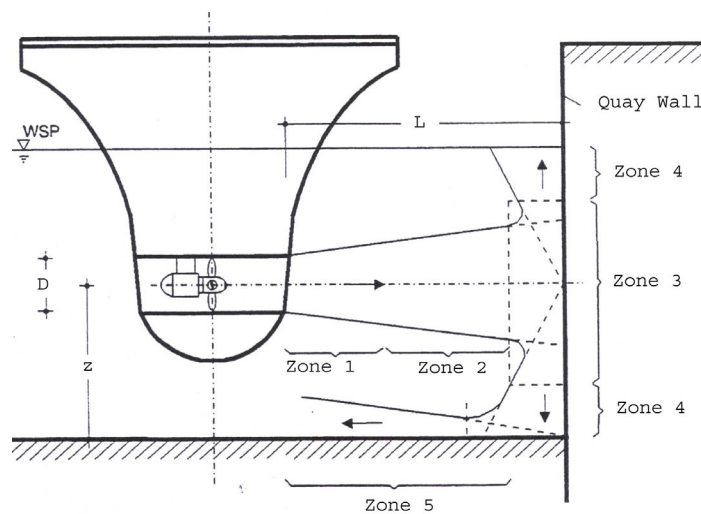


figure 2-4 Five zones in front of a quay wall, as defined by Schmidt and Römisch.

### Zones 1 and 2, Flow establishment and established flow.

Römisch states that the velocity field is dependent on the ratio between the distance from the propeller ( $x$ ) and the diameter ( $D$ ):

$$\frac{U_{x,max}}{U_o} = f\left(\frac{x}{D}\right) \quad (2-37)$$

From experiments Schmidt (1998) derived that the solution to this yields (valid for a bowthruster):

$$\frac{U_{x,\max}}{U_o} = 2.0 \cdot \left(\frac{x}{D}\right)^{-1.0} \quad (2-38)$$

Equation (2-38) is valid in the zone of established flow. In the entire zone of flow establishment it holds that  $U_{x,\max} = U_o$ .

Since there should be continuity at the border between zone 1 and 2, from equation (2-38) then follows that the zone of flow establishment has a length of  $x_0 = 2.0 \cdot D$ . This is considerably smaller than a jet initiated by a free propeller since from equation (2-19) follows:  $x_0 = 2.6 \cdot D$  [m].

### Zone 3, Pressure zone.

In this zone the jet hits the wall and a pressure zone is established. The kinetic energy of the flow is converted into pressure, which has a maximum where the velocity reaches zero. The decrease of velocity and increase of pressure starts at a distance of about  $0.3 \cdot L$  [m] (Kraatz, 1989<sup>6</sup>) in front of the quay wall, where  $L$  is the distance in metres between quay wall and thruster. This also indicates that the equation found in zone 2 is valid for  $x_0 < x \leq 0.7L$ .

### Zone 4, Radial wall jet zone.

After this the flow changes direction from a horizontal jet to a radial wall jet and pressure is converted into velocity (kinetic energy) again.

At the location  $z = 0.3 \cdot L$  [m] the pressure is minimum again and velocity reaches its maximum again (Kraatz, 1989). In this point the 'wall-jet' originates until it either reaches the bottom or the water surface. Since this study focuses on the effect of jets on bottom and bottom protection we are only interested in the bottom.

### Zone 5, Bottom.

According to Römisch (1975) the loss of velocity during the change of direction due to the wall is negligible. So the maximum velocity at the bottom equals the velocity just in front of the quay wall. Using equation (2-38) with  $x = L$ :

$$\frac{U_{\max,bot}}{U_o} = 2.0 \cdot \left(\frac{L}{D}\right)^{-1.0} \quad [-] \quad (2-39)$$

where

$L$ : distance from quay wall [m]

**Remark:** The theoretical foundation for his assumption seems very weak. Especially since the height of the propeller from the bottom must have its influence on the velocity decrease. However, in practice it may be useful.

Römisch defined a stability parameter  $B$  [-]:

---

<sup>6</sup> No background for this value is given.

---


$$B = \frac{U_{\max,bot}}{\sqrt{\frac{\rho_s - \rho_w}{\rho_w} \cdot g \cdot d}} \quad [-] \quad (2-40)$$

and when this parameter reaches  $B = B_{\text{crit}} = 1.25$  [-] erosion starts (by his definition).

### 2.2.3 Scourdepth

Apart from the stability, we will also look at scour depth:

#### 2.2.3.1 Römisch (1977)

Römisch and Fuehrer (1977) defined that the ratio of the depth of the hole and the diameter of the sediment can be written as a function of the stability parameter.

$$\frac{h_{\text{hole}}}{d} = f \left( \frac{U_{\max,bot}}{\sqrt{\frac{\rho_s - \rho_w}{\rho_w} \cdot g \cdot d}} \right) = f(B) \quad (2-41)$$

where

$h_{\text{hole}}$ : depth of the hole [m]

Römisch and Fuehrer defined that if  $\frac{h_{\text{hole}}}{d_{ch}} = 0.2$  [-] the erosion

process had started.

The solution to the equation (2-41) was empirically found to be:

$$\frac{h_{\text{hole}}}{d} = 0.025 \cdot B^{11} \quad \text{for} \quad \frac{h_{\text{hole}}}{d} < 10 \quad [-] \quad (2-42)$$

and

$$\frac{h_{\text{hole}}}{d} = 2.0 \cdot B^{2.8} \quad \text{for} \quad \frac{h_{\text{hole}}}{d} > 10 \quad [-] \quad (2-43)$$

See figure (2-5) for a graphical interpretation:

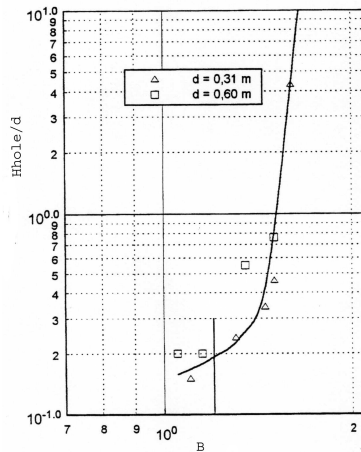


figure 2-5 Hole depth as a function of the stability parameter of Römisch ( $B$ ).

Since there is no time parameter in their equation, the scourdepth found with this equation should be regarded as an upper limit.

This formula was later slightly changed by Ducker and Miller (1996) to the following form:

$$\frac{h_{hole}}{d_{85}} = C_m \cdot 0.1 \cdot \left( \frac{B}{B_{crit}} \right)^{13} \quad \text{for } 1.0 < \left( \frac{B}{B_{crit}} \right) < 1.4 \quad [-] \quad (2-44)$$

$$\frac{h_{hole}}{d_{85}} = C_m \cdot 4.6 \cdot \left( \frac{B}{B_{crit}} \right)^{2.25} \quad \text{for } \left( \frac{B}{B_{crit}} \right) > 1.4 \quad [-] \quad (2-45)$$

where

$C_m$  : constant [-] (0.3 [-] for manoeuvring ships, 1.0 [-] for ships at rest)

### 2.2.3.2 Westrich and Kobus (1974)

Westrich and Kobus (1974) defined two different forms of erosion holes (figure (2-6)):

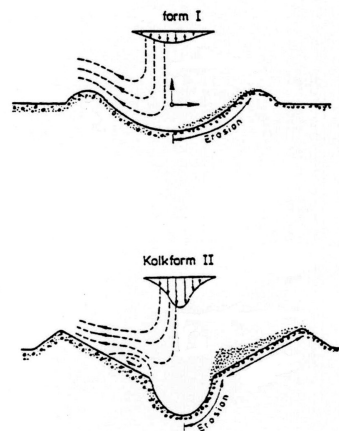


figure 2-6 Two forms of scourholes.

The form of the holes and the size are dependent on the following conditions:

- The quotient of the water velocity and the fall velocity of the particles ( $U_0/w$  [-]).
- The relative distance ( $z/D$  [-]).
- Impulse parameter ( $(I_0/\rho)/(w^2/z^2)$  [-]).
- Time parameter ( $(w \cdot t/z)$  [-]).

Furthermore,

- They found through experiments that when the parameter  $U_{x,l}/w = 1.5$  [-] the first form will appear. If this parameter reaches 2.9 [-] the second form will appear.
- $U_{x,z}/w > 1.0$  [-] to 1.2 [-] is the minimum value for erosion to appear at all.
- The relative distance determines the velocity reduction and the area of attack.
- The rate of erosion is a function of the impulse and time parameter.

### 2.2.3.3 Rajaratnam and Beltaos (1977)

Rajaratnam and Beltaos (1977) applied the theory of Westrich and Kobus (1974) on their own theory for horizontal jets and derived a relation between the depth of the hole and the densimetric Froude number which is dependent on the distance from the propeller to the bottom:

$$\frac{h_{hole}}{z} = f \left( \frac{Fr_0}{\frac{z}{D}} \right) \quad [-] \quad (2-46)$$

and also between the radius of the hole and the distance:

$$\frac{r}{z} = f \left( \frac{Fr_0}{\frac{z}{D}} \right) \quad [-] \quad (2-47)$$

where

$$Fr_0 : \text{ densimetric Froude number} = \frac{U_0}{\sqrt{g \cdot d \cdot \frac{\rho_s - \rho_w}{\rho_w}}} \quad [-] \quad (2-48)$$

r: radius of the hole [m]  
z: height of the propeller above the bottom [m]  
d: diameter of the sediment [m]

Rajaratnam and Aderibigbe (1996) defined an erosion parameter  $E_{cr}$  [-] using the this relationship between 'D' and 'z':

$$E_{cr} = \frac{U_0 \cdot \left(\frac{D}{z}\right)}{\sqrt{g \cdot d \cdot \left(\frac{\rho_s - \rho_w}{\rho_w}\right)}} \quad [-] \quad (2-49)$$

For  $0.12 [-] < E_{cr} \leq 0.35 [-]$  form number I appears, for  $E_{cr} > 0.35 [-]$  the transition to form II takes place.

**Remark:** Rajaratnam uses  $U_0$  as initial velocity of the vertical jet. When applying his theory to bowthrusters, the initial vertical velocity at the quay wall has to be calculated first. This can be done by for instance using the theory of Römisch.

#### 2.2.3.4 Hoffmans (1995)

Mainly because of the applicability of his scour formula the theory of Hoffmans (1995, from DWW 1997) is mentioned. Hoffmans defined a very easy to use formula for calculating the scour depth as a function of velocity and discharge only:

$$h_{hole} = c_{3H} \left(Q \cdot \frac{U_{max,bot}}{g}\right)^{\frac{1}{3}} \quad [m] \quad (2-50)$$

where

$c_{3H}$ : constant, equals 2.0 [-]  
 Q: discharge [ $m^3/s$ ]

The DWW (Road and Hydraulic Engineering Division of the Ministry of Transport, Public Works and Water Management in the Netherlands) uses it to calculate scour next to quay walls in the inland waterways of the Netherlands. It was originally developed for jets originating from culverts over a bed of sand, but may be applicable for propeller jets too.

Some remarks on the formula of Hoffmans:

- Since it holds very few parameters it is easy to use, but most likely to be less accurate than for instance the formulas of Römisch or Rajaratnam.
- It is questionable to what extent a horizontal jet coming from a culvert can be compared to a deflected vertical jet coming from a propeller.
- It is limited to calculations on sand.



---

## 2.3 Evaluation

### 2.3.1 Velocity field

It appears that there is a method to calculate the initial velocity of a jet and the distribution of the velocity in detail in axial and radial direction.

Measurements have proven that this method produces correct values (for instance: Van Veldhoven, 2001). However, different authors use different coefficients to match their measured results to the theoretical values.

Further more, these theories have limitations concerning the influence of turbulence and the influence of the propeller axis.

### 2.3.2 Stability and scour

#### 2.3.2.1 Stability

Two well-used relations for stability are available, the one of Shields and the one of Izbash. Shields criterion is based on a stationary flow with a developed boundary layer. Since little is known as to what the velocities at the slope are, and certainly jet induced flows are not expected to be stationary, it is not advised to use his theory.

It seems that Izbash is more appropriate here. It only deals with the relation between the particle diameter, particle weight and the velocity.

Schiereck (2000) specifically points out that the formula of Izbash should be used in cases where a velocity near a bottom is known but the relation with the water depth is not clear, like in a jet entering a body of water.

#### 2.3.2.2 Stability and scour in front of a quay wall

As pointed out above, several useful theories are available. It will depend on the conditions to determine which theory is most useful.

For making approximations on scour depth in the inland waterways it seems logical to use the theory of Hoffmans (1995), since few parameters need to be known and sand or sandy clay is the most common material on the bottom in the Dutch inland waterways (for which he derived his equation). Since Ducker and Miller (1996) adapted the equation of Römisch for manoeuvring ships, it seems interesting to use this equation as well and compare the results to the results of Hoffmans' equation.



## 3 Background of the experiment

### 3.1 Prototype and experimental model dimensions

In the model we are simulating a ship that is moored at a quay supported by a pile structure. Underneath the quay a slope is situated with an angle of 18 [degrees] (i.e. a slope of 1:3 [-], see figure (3-1)).

#### 3.1.1 Prototype dimensions

The model used for the tests is the same model that Van Veldhoven (2001) used for his tests.

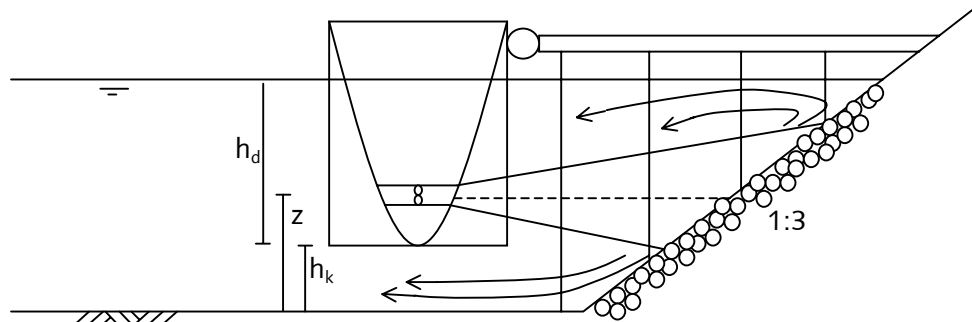


figure 3-1 Side view of the prototype situation (figure by Van Veldhoven (2001)).

Van Veldhoven used a large container vessel for the prototype situation. This led to the following prototype conditions (table (3-1)).

Variable	Symbol	Value
Water depth	$h_w$ [m]	12
Slope <sup>7</sup> ratio	$m$ [-]	1:3
Maximum beam of vessel	$W$ [m]	32
Draught of vessel	$h_d$ [m]	11
Keel clearance	$h_k$ [m]	1
Height of propeller axis above bottom	$z$ [m]	4
Length of duct	$L_d$ [m]	6
Distance from duct exit to slope	$L$ [m]	26
Diameter of propeller (bow)	$D$ [m]	2
Power of bowthruster	$P$ [kW]	1100
Number of blades on propeller	$n_b$ [-]	4
Rotation rate	$n$ [rpm]	300
Initial velocity	$U_o$ [m/s]	6.1
Minimum median stone diameter	$d_{50}$ [m]	0.22

table 3-1 Prototype dimensions.

#### 3.1.2 Scaling of the experimental model

The model was geometrically scaled at a scale of 1:25 [-], determined by the size of the available basin. This is valid for all

<sup>7</sup> Van Veldhoven (2001) states that the slope ratio varies in prototype situations from 1:1.33 [-] to 1:2.6 [-]. No reason is given for the use of the (less steep) slope of 1:3 [-].

characteristic lengths. For the velocities, the model was scaled using Froude's scaling law for dynamic similarity.

The Froude number is defined as:

$$Fr = \frac{U^2}{g \cdot L} \quad [-] \quad (3-1)$$

where

Fr: Froude number [-]  
 U: velocity [m/s]  
 L: characteristic length [m]

Dynamic similarity between model and prototype is achieved when

$$\frac{U_p^2}{U_m^2} = \frac{L_p}{L_m} \quad [-] \quad (3-2)$$

in which subscript 'p' denotes prototype and subscript 'm' denotes model.

Given the length scale of 1:25 [-] the velocities in the model are scaled at  $1:\sqrt{25}$  (following from equation (3-2)).

Furthermore, Van Veldhoven made some adjustments to the scale of the diameter of the propeller and to the length of the tunnel since he thought it questionable whether the stones on the slope would move at all when using a propeller scaled 1:25 [-]. Therefore he used a scale of 1:20 [-] for the propeller and for the duct.

This led to the following dimensions for the model in table (3-2):

Variable	Symbol	Value
Water depth	$h_w$ [m]	0.48
Slope ratio	$m$ [-]	1:3
Maximum beam of vessel	$W$ [m]	1.28
Draught of vessel	$h_d$ [m]	0.44
Keel clearance	$h_k$ [m]	0.04
Height of propeller axis above bottom	$z$ [m]	0.19
Length of duct	$L_d$ [m]	0.30
Distance from duct exit to slope	$L$ [m]	1.16
Diameter of propeller (bow)	$D$ [m]	0.10
Power of bowthruster	$P$ [kW]	30.7
Number of blades on propeller	$n_b$ [-]	4
Rotation rate	$n$ [rpm]	1342
Initial velocity	$U_0$ [m/s]	1.36
Minimum median stone diameter	$d_{50}$ [m]	0.009

table 3-2 Model dimensions.

**Remark:** The model is suitable to point out the differences between a ducted- and a free-propeller jet. Even though the model was

scaled from a prototype situation, the findings on stability of stones and occurring velocities cannot be scaled back to this prototype situation, since it is believed that the model has too many geometrical shortcomings when compared to a prototype situation. For instance, the hull of the ship is modelled by a board, with no keel clearance and no stern or bow in a basin with a limited width. The intention of the model is to derive insight into the mechanisms playing a role in bowthrustrer-induced jet wash.

### 3.1.3 Modelling turbulence, the Reynolds number

The flow in the prototype is turbulent. For a correct representation of the prototype situation in the model, this means that in the model the flow also needs to be turbulent. Otherwise the viscous effects of the water start to play an important role.

Therefore, when carrying out model tests the Reynolds number for the propeller as well as for the stones in the protection layer should be larger than  $3 \cdot 10^3$  [-]<sup>8</sup>. The Reynolds number of the propeller-induced jet is defined as:

$$\text{Re}_j = \frac{D \cdot U_0}{\nu} \quad [-] \quad (3-3)$$

Where

- Re<sub>j</sub>: Reynolds number of the propeller induced jet [-]
- D: diameter of propeller [m]
- U<sub>0</sub>: initial velocity [m/s]
- ν: kinematic viscosity (=1.33·10<sup>-6</sup>) [m<sup>2</sup>/s]

Depending on the rotation rate this criterion will be met. This has been checked when conducting the tests.

The Reynolds number for the protection material is defined in a similar way, only D is substituted by the d<sub>50</sub> of the grains and the local velocity (U) is used, leading to:

$$\text{Re}_g = \frac{d_{50} \cdot U}{\nu} \quad [-]$$

Depending on the velocity at the slope for which the stones start to move, scale effects have to be taken into account and therefore this has been checked too when conducting the tests.

## 3.2 Experimental model set-up

### 3.2.1 General

The model was built in the Fluid Mechanics Laboratory of the Faculty of Civil Engineering and Geosciences of Delft, University of Technology.

---

<sup>8</sup> Values used in literature vary from  $2.5 \cdot 10^3$  [-] to  $7 \cdot 10^4$  [-]. Here the value of Pearce (1966) is taken which equals  $3.0 \cdot 10^3$  [-].

---

In appendix A the reader can find the drawings and dimensions of the model, for both the ducted and the free propeller. An important feature of the model is the fact that the water flows away through outlets on the sides of the basin. This is done to (try to) minimise the circulation. If the water cannot flow away freely after reaching the slope it keeps circulating through the basin. The outflow is compensated by a constant inflow of water in the basin behind the propeller.

The basin used has a width of 2.0 [m]. This width was therefore governing for the maximum width of the slope. Since the jet spreads out when reaching the slope, the influence of the sidewalls is important when performing measurements. In the model the flow will be hindered by these walls and will either go upward/forward to the outlets, or flow backwards/downwards, creating circulation cells. In the prototype this will not be the case, since there are no walls. According to Van Veldhoven, using a theory by Beltaos (1976), when measuring no more than  $y = 0.3$  [m] outside the x-axis of the jet, the measurements do not contain an error caused by the influence of the walls.

Besides this, we are only making a comparison between two different ways of physical modelling, which both have the same limitations and errors, so the limited width of the basin does not pose much of a problem.

### **3.2.2 Free propeller**

#### *3.2.2.1 General*

The propeller jet is supposed to be free and undisturbed in the first test of this study, which uses a free propeller to make a comparison to a ducted-propeller jet. However, the propeller is situated in a board, which simulates the hull of the ship, preventing water from circulating.

To determine the correct diameter of the opening, we have to look at the following dilemma:

The jet will entrain water as it builds up. This water will have a certain velocity and will ultimately disappear over both sides of the basin. Since we keep the water level constant by the inflow on the backside of the propeller, this inflowing water will flow through the same opening as the one in which the propeller is situated. If we make the opening too large, circulation through the opening may occur, if we make it too small, the water supply is hindered and we are not dealing with a free-propeller jet any more.

In the next section, a founded assumption for the size of the hole is made.

#### *3.2.2.2 Determining an upper limit for the diameter of the opening*

The board should not disturb the flow around the propeller, including the entrainment. This means that the diameter of the opening in the board has to be equal to or larger than the diameter of the jet including the entrainment. Therefore, it is necessary to calculate the maximum entrained discharge and its velocity. The

division of these two values gives the extra area needed in the board to let the entrained water freely enter the basin. The maximum amount of entrained water will be entrained in the propeller wash above the slope (approximately 1 [m] from the origin of the jet).

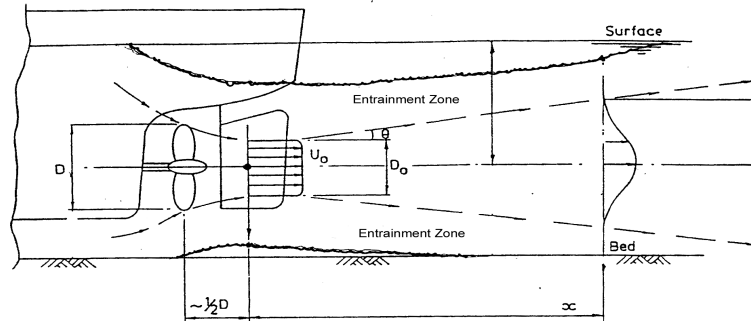


figure 3-2 Diverging of propeller jet and the entrainment zone.

Giger, Dracos and Jirka (1991) derived an equation for the velocity distribution in a jet including entrainment as a function of the width of the jet.

$$\frac{U}{U_{\max}} = \exp[-A\eta^2] - \exp[-A\eta_B^2] \cdot \frac{1}{\sqrt{2\pi} \cdot s_\gamma} \cdot \int_0^\eta \exp\left[-\frac{1}{2} \cdot \left(\frac{\eta - \eta_{\gamma=0.5}}{s_\gamma}\right)^2\right] d\eta \quad (3-4)$$

where

- U: velocity at point y [m/s]
- $U_{\max}$ : velocity at x-axis, which equals the maximum velocity at a certain distance from the propeller [m/s]
- A: constant (equals  $-\ln(0.5)$ ) [-]
- $\eta$ : y/b [-]
- $\eta_B$ : constant (equals 2.53) [-]
- $\eta_{\gamma=0.5}$ : constant (equals 1.68) [-]
- y: distance perpendicular to x-axis [m]
- b: radius of jet [m]
- $s_\gamma$ : standard deviation (equals 0.36) [-]
- $\gamma$ : intermittency factor<sup>9</sup> (equals 0.5) [-]

They verified this equation with experiments and found the formula to be valid for

$$1 < \frac{x}{h_w} < 38.5 \quad [-]$$

where

- x: distance from propeller [m]
- $h_w$ : water depth [m]

<sup>9</sup> This factor is defined as the period of time during which fluid carrying a certain property (turbulence or a scalar) passes by an observation station divided by the total time of the observation T. Giger, Dracos and Jirka (1991) found this factor to be 0.5 [-].

This quotient,  $\xi'$ , equals in our situation:

$$\xi' = \frac{x}{h_w} = \frac{1}{0.5} = 2 \text{ [-]} \text{ which makes equation (3-4) valid for this case.}$$

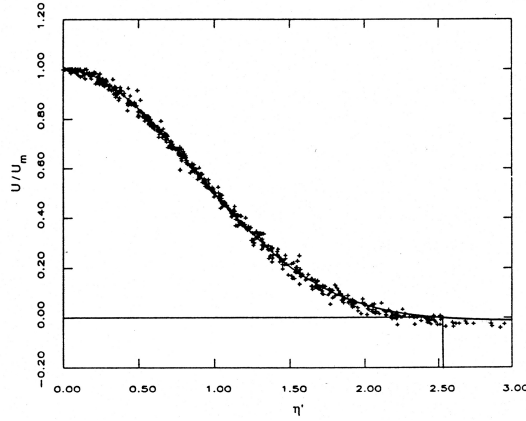


figure 3-3 Velocity distribution in radial/tangential direction according to Giger, Dracos and Jirka (1991), measured (dots) and theoretical (line).

Figure (3-3) and (4-4) show the graphical interpretation of equation (3-4).

The total area under the curve in figure (3-3) has a value of 1 [-] if we look at the initial discharge only<sup>10</sup> (this area represents  $U/U_{\max} \cdot y/b$  [-]).

This equation was numerically integrated over the entire area from  $\eta = 0$  to  $\eta_{U/U_{\max}=0} = 2.53$  [-] (see appendix E). By multiplying the area with the local velocity at each integration step the discharge as a function of  $U_{\max}$  and  $\eta$  results.

$$\frac{Q}{U_m} = \int_0^{\eta} \left( \exp[-A\eta^2] - \exp[-A\eta_b^2] \cdot \frac{1}{\sqrt{2\pi} \cdot s_\gamma} \cdot \int_0^{\eta} \exp\left[-\frac{1}{2} \cdot \left(\frac{\eta - \eta_{\gamma=0.5}}{s_\gamma}\right)^2\right] d\eta \right) \cdot (2\pi\eta) d\eta \quad (3-5)$$

The area underneath the curve equals 1 [-] when  $\eta$  reaches 1.60 [-] (see figure (3-4)).

$U/U_m = 0$  at  $\eta = 2.53$  [-]. The area between  $\eta = 1.60$  [-] and  $\eta = 2.53$  [-] is thus entrained water.

<sup>10</sup> This fact is best understood if the reader considers the theoretical outflow at the propeller, which is distributed evenly over the height.  $U/U_{\max} = 1$  [-] over the entire height and  $\eta_{\max}$  equals 1 [-] as well ( $y$  equals  $b$ ). The total area then equals 1 [-]. This area represents the discharge, normalized with the maximum velocity and the initial width, assuming radial symmetry. This profile changes shape ( $y$  increases, increasing  $\eta$  as well) when the distance from the propeller increases but applying the law of conservation of mass, the area that represents the initial discharge still equals 1 [-].



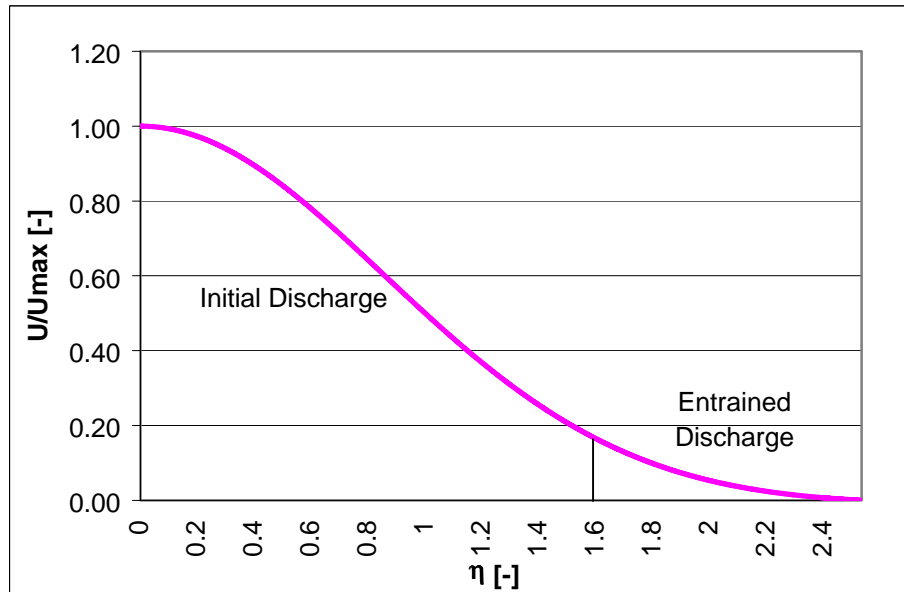


figure 3-4 Theoretical velocity distribution and the distinction between initial discharge and entrained discharge.

It is found that the discharge from  $\eta = 0$  to  $\eta = 2.53$  [-] is a factor 1.16 [-] greater than the (initial) discharge from  $\eta = 0$  to  $\eta = 1.60$  [-].

The initial discharge can be calculated using the assumption that just behind the propeller the velocity of the water is evenly distributed over the height.

The propeller used in the model combined with the attached electrically driven motor with a controlled rotational speed produces a maximum water velocity of approximately  $U = 1.5$  [m/s]. Taking into account that a contraction of approximately 70 [%] will occur<sup>11</sup> the diameter of the jet decreases to  $0.7 \cdot 0.10$  [m] = 0.07 [m] where the maximum velocity occurs.

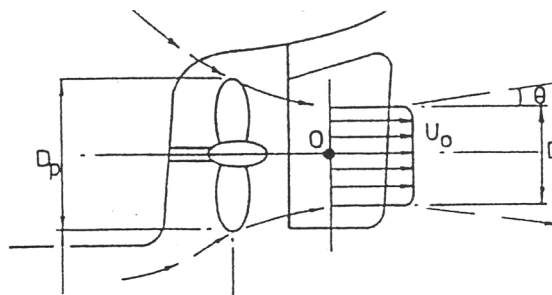


figure 3-5 Theoretical velocity distribution in the jet, just after the flow exits from the propeller at the point of maximum contraction.

This leads to a discharge of 5.8 [litres/s] ( $Q = U \cdot A \cdot 1000$  [litres/s]).

<sup>11</sup> According to Blaauw & Van de Kaa (1978). For more details the reader is referred to chapter 2, Literature study.

---

The discharge at the slope is then found to be  $1.16 \cdot 5.8$  [litres/s] = 6.7 [litres/s]. So the extra discharge initiated by the entrainment is 0.9 [litres/s].

Since there is only one opening in the board this extra discharge can only come through the same opening as the one in which the propeller is located.

To calculate the width of this jet, including entrained water we have to make an assumption on the mean velocity of the entrained water.

Giger, Dracos and Jirka (1991) found that entrained water usually has a velocity of around 0.05 times the jet's maximum velocity. Since the jet is relatively small at the location of the opening and the discharge is the same as at the location where the width of the jet is a lot larger, the influence of the jet on the entrained water is supposed to be smaller. It is believed that this influence will be substantially smaller than 0.05 times the jet's maximum velocity, but still significant. Since there appears to be no former study on the subject, an assumption has to be made. Since the value should be smaller than 0.05 [-] and larger than 0, we will use half of the value found by Giger, Dracos and Jirka (1991), 0.025 [-]. The mean velocity therefore results in  $0.025 \cdot 1.5$  [m/s] = 0.0375 [m/s]. This leads, combined with the discharge, to a diameter for the opening of 0.20 [m]<sup>12</sup>.

### 3.2.3 The protection material

Different colours of paint are used for the stones to create distinct areas of 5 [cm] by 5 [cm] on the slope. In this way it can be visually recorded when a stone has moved and in principle also where it originated. If a stone is moved outside its square, this is considered as damage.

As in Van Veldhoven's tests, only a small area of the slope is applied with these squares (approximately 3 layers thick) since the stones appeared to move only at the lower part of the slope (approximately in the first 0.5 [m] from the toe) and no further than approximately 0.3 [m] from the centreline of the slope.

In appendices A & B the reader can find drawings, dimensions and some pictures of the model set-up.

### 3.2.4 Conducting the tests

Basically the tests consisted of three aspects:

- First, the velocity field of the free-propeller jet has been measured at several locations in height and distance from the propeller. This has been done at a constant initial velocity, to which all measured velocities are normalised (in order to enable comparison with other tests). This initial velocity was measured just in front of the propeller at several heights. Theoretically the initial velocity is constant

---

<sup>12</sup> The use of the value of 0.05 times the maximum velocity in the jet results in a diameter for the hole of 0.15 [m], so the influence of the factor is significant. In section 4.1.7 it will be concluded whether the size was taken correctly.

---

over the height of the propeller but it has been verified first whether this is true.

- Next, the start of movement of protection material in the jet wash of a free-propeller jet has been investigated. The material used here has a  $d_{50}$  of 0.009 [m]. By increasing the initial velocity with small steps the point of initiation of movement can be determined. The total number of stones moved has been projected cumulatively against the initial velocity. The results have also been compared to results derived from tests done with a ducted propeller (Van Veldhoven, 2001).
- Eventually, velocity measurements close to the slope have been taken to derive insight in the velocities that occur close to the slope and in the mechanisms responsible for movement of the protection material.

The velocity measurements have been performed with an EMS (Electro Magnetic velocity Sensor).



*figure 3-6 Close up of the probe of the EMS.*

The EMS creates an electromagnetic field between the 'metal points', which is disturbed by the water flow, resulting in a signal. The characteristic length of the measuring volume is approximately 1 [cm] and the size of the disc itself is approximately 3 [cm] in diameter.

More details about the EMS are found in the next chapter and in appendix I.

The EMS is connected to an amplifier which sends a(n) (analogue) current to an analogue/digital converter. This converter converts the analogue signal into a digital signal, which is sent to the computer, where it is recorded and displayed using a software program called 'Daisy Lab'.

---

# 4 Investigation of the free-propeller jet

## 4.1 The velocity field

In this chapter the velocity distribution in the jet will be described. Theoretically, as mentioned in the literature study, the velocity field is supposed to be equally distributed over the height when exiting at the propeller. After that it starts diverging and develops to what has the shape of a normally distributed profile (figure (4-1)). There is a zone of flow establishment and a zone of established flow. In the first zone the velocity at the axis is supposed to be constant. In the second zone the velocity starts to decrease. In this chapter measurements of the velocity field will be described and compared to theoretical values.

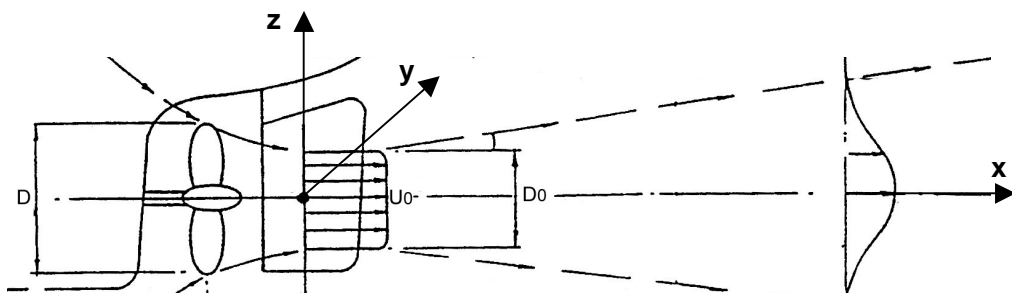


figure 4-1 Theoretical velocity distribution at exit and in developed flow.

### 4.1.1 Measuring

For determining the velocity distribution in the jet, the velocities are measured at approximately 100 locations with varying values of  $x$  and  $z$  ( $y = 0$ ,  $0.05 \text{ [m]} < x < 0.7 \text{ [m]}$ ,  $-0.16 \text{ [m]} < z < 0.2 \text{ [m]}$ , see figure (4-2)). In all cases the propeller was rotating with a rotation rate of  $1100 \text{ [rpm]}$ .

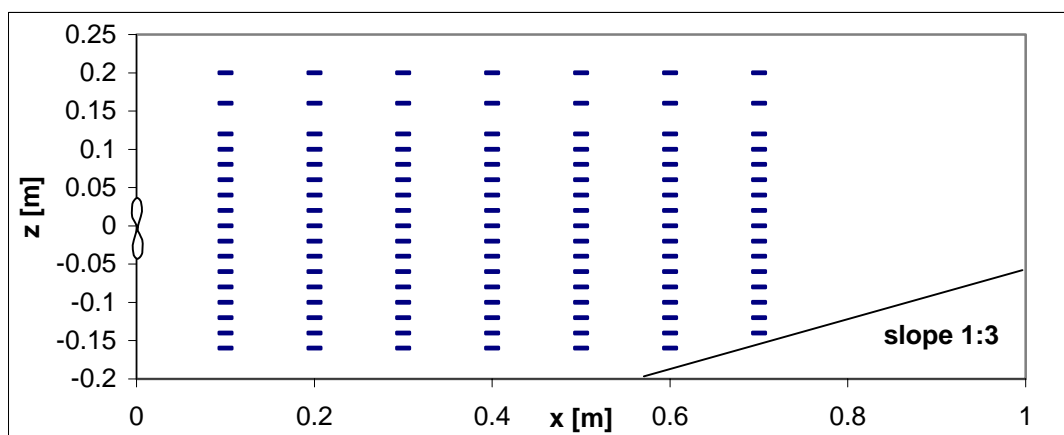


figure 4-2 Measurement locations. For all points  $y = 0$ .

As already briefly mentioned in the previous chapter, the instrument used here is an EMS, an instrument that uses electromagnetism to measure the flow velocity. This is done by a disc that has a diameter

of approximately 3 [cm] and therefore physically influences the flow. The smallest vortices that the device can measure are approximately 1 [cm] large, the smallest velocity it can measure is 1 [cm/s], which brings certain limitations to measuring with an EMS. The duration of a measurement at each point was taken at 6 [minutes] (or 360 [s]). Smaller intervals proved to give different mean values when measuring a certain point several times, which is caused by the turbulent character of the flow. For a time span of 6 [minutes] or more the mean value appeared to be stable.

At each point the velocity in tangential direction ( $U_y$ ) and in axial direction ( $U_x$ ) is recorded at a sample rate of 50 [Hz]. Apart from the locations mentioned above, at location  $x = 0.05$  [m] measurements were taken at every 0.005 [m] in radial direction ( $-0.1 < z < 0.1$  [m]) to determine the initial velocity at 1100 [rpm]. This point was chosen, since according to Blaauw & Van de Kaa (1978) the maximum contraction takes place at this point and this is also where (by their definition) the initial velocity  $U_0$  takes place.

#### 4.1.2 Initial velocity $U_0$ and flow contraction

To determine the initial velocity  $U_0$  at 1100 rpm, the total flow of momentum is calculated by integrating each measured velocity at  $x = 0.05$  [m] over its area concerned ( $\int \rho U^2 dA$ , assuming radial symmetry on the upper and lower half of the profile). This is then divided by the initial diameter of the jet and the mean velocity follows:

$$U_0 = \sqrt{\frac{I}{A \cdot \rho}} \quad [\text{m/s}] \quad (4-1)$$

where

- $U_0$ : mean initial velocity just behind the propeller [m/s]
- $I$ : flow of momentum ( $I = \int \rho U^2 dA$ ) [ $\text{kg m s}^{-2}$ ]
- $A$ : area concerned [ $\text{m}^2$ ]
- $\rho$ : density of the fluid ( $=1000$ ) [ $\text{kg/m}^3$ ]

When rotating the propeller with 1100 [rpm]  $I$  equals 15 [ $\text{kg m s}^{-2}$ ].

Blaauw & van de Kaa (1978) state that the contraction coefficient  $\phi^{(13)}$  for a free propeller equals 0.5 [-]. This leads to  $\frac{D_0}{D} = 0.7$  [-] which then leads to an initial diameter  $D_0$  of 0.07 [m]. This maximum contraction occurs at a distance from the propeller of  $0.5 \cdot D$  ( $= 0.05$  [m]), Blaauw & Van de Kaa (1978) .

Figure (4-3) shows that the jet is at its smallest at  $x/D = 0.5$  [-]. But it seems incorrect to take the diameter of the jet at 0.07 [m]. The

$$\phi^{(13)} = \frac{K_{t(dps)}}{2K_{t(prop)}} = \frac{D_0^2}{D^2}$$

maximum velocities occur around  $z = 0.03$  [m] and  $z = -0.03$  [m], but are still fairly large for  $z > 0.03$  [m] or  $z < -0.03$  [m]. Therefore it is not logical to call this the boundary of the jet already. As can be seen, the velocities drop rapidly between  $0.03$  [m]  $< z < 0.06$  [m] to  $0.07$  [m]. If we take the mean value of this, the jet would have a diameter of  $0.09$  [m] to  $0.10$  [m]. Since the test with the ducted propeller was performed with a  $D_0$  of  $0.10$  [m] for practical reasons we will also use this value for calculating the initial velocity.

This leads to a  $U_0$  of  $1.38$  [m/s] and for the thrust coefficient  $K_T$  to a value of  $0.23$  [-]<sup>14</sup>.

### 4.1.3 Axial velocity

#### 4.1.3.1 Entire velocity field

For the intervals between  $x = 0.05$  [m] and  $x = 0.7$  [m] ( $D = 0.10$  [m]) the velocities are plotted against the height above the  $x$ -axis of the jet in figure (4-3). The velocities are normalised with the initial velocity  $U_0$ .

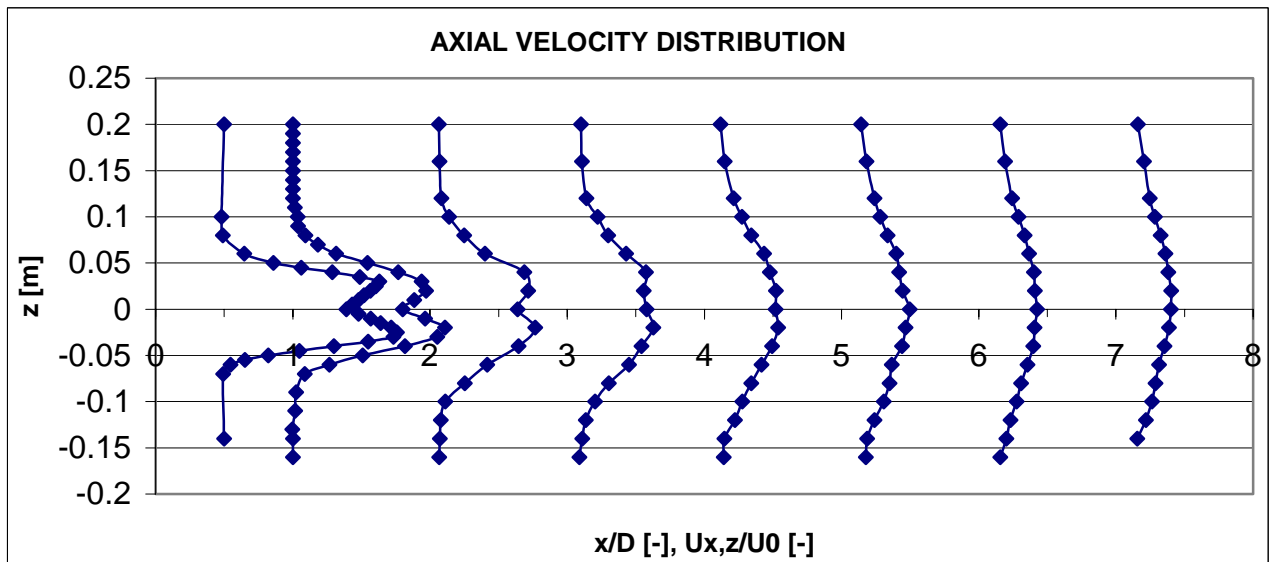


figure 4-3 Axial velocity distribution at several points along the  $x$ -axis. The graphs present the values of  $U_{x,z}/U_0$  [-].

In the first part of the jet the influence of the propeller axis is clearly visible, causing the indentation in the velocity profile. This slowly disappears when  $x$  reaches  $0.3$  [m] to  $0.4$  [m] ( $D = 0.1$  [m]). In addition, figure (4-3) shows that the highest velocities occur at the lower half of the profile, i.e. below the propeller axis. The reason for it is not known. Although it is an interesting phenomenon, it is beyond the scope of this thesis and will not be looked into closer.

<sup>14</sup>  $K_{T(prop)} = \left( \frac{U_0}{1.60 \cdot n \cdot D} \right)^2$  [-]. For an explanation on the meaning of the thrust coefficient, see section 2.1.2, Literature study.

Figure (4-4) shows the velocity distribution when the values are interpolated.

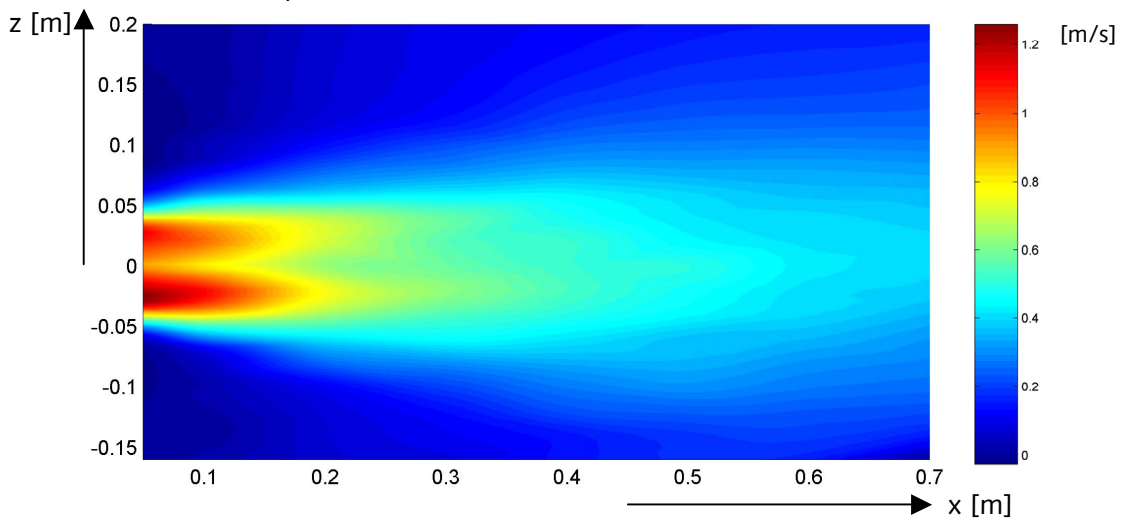


figure 4-4 Interpolated values for the axial velocity distribution in the free-propeller jet.

#### 4.1.3.2 Flow establishment

In several articles from several authors (Fuehrer, Römisch and Engelke (1981), Rajaratnam (1976), Blaauw & Van de Kaa (1978)) it is stated that there is a zone of flow establishment in which the velocity at the x-axis is constant and equal to the initial velocity  $U_0$ . The idea behind this is that in this zone the influence of the boundary region of the jet that develops when entering a body of water is not noticed on the x-axis (for more details the reader is referred to chapter 2, Literature study, and also section 4.2.2, Turbulence).

The measurements (figure (4-5)), however, show something different: There are two zones that can be distinguished. In the first zone, between  $x = 0$  and  $x = 0.2$  [m] ( $x/D = 2$  [-]) there is a rapid and almost linear decrease in velocity at the jet axis ( $z = 0$ ). After this, the velocity decrease is a lot less but also almost linear. So contradicting the theory, the velocity decreases fastest in the zone immediately in front of the propeller.

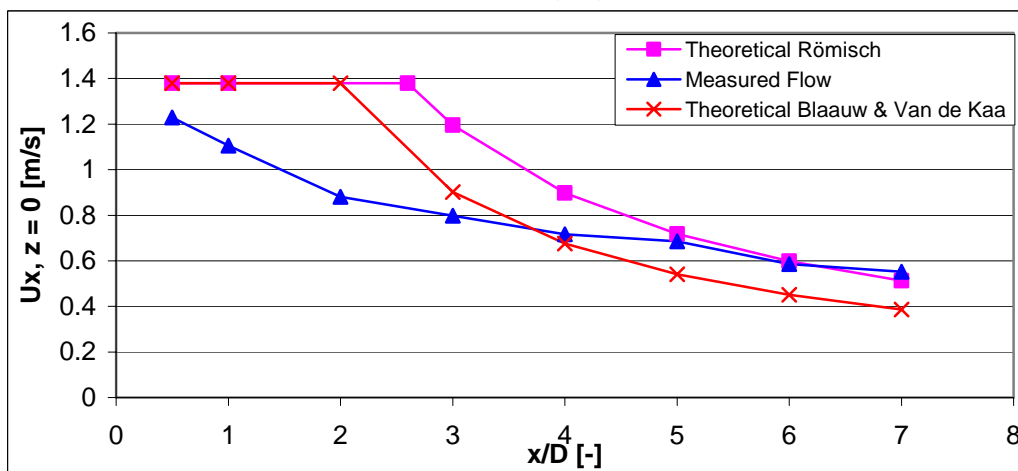


figure 4-5 Theoretical and measured velocity on the axis.



Römisch (1981) found that the length of the zone of flow establishment equals  $2.6 \cdot D$  (which is 0.26 [m] in this case), Blaauw & Van de Kaa (1978) say it equals  $2.8 \cdot D_0$  (which is 0.20 [m] in this case)<sup>15</sup>.

If we now call the first zone, with the rapid decrease, the zone of flow establishment<sup>16</sup>, its length is equal to the value found by Blaauw & Van de Kaa (1978). It seems that a linear relation between velocity and distance produces better results than the method suggested by either Römisch, or Blaauw & Van de Kaa.

**Remark:** The reader is referred to section 4.2 where turbulence in the jet is analysed and an explanation is given for the fact that in the first zone the velocities decrease instead of being constant (in that section it is concluded that high turbulence probably leads to the rapid decrease on the axis. The high turbulence is supposed to be initiated by the use of the propeller, something that the present theories do not deal with).

#### 4.1.4 Tangential velocity

The tangential velocities are also normalised with the initial velocity in axial direction in figure (4-6):

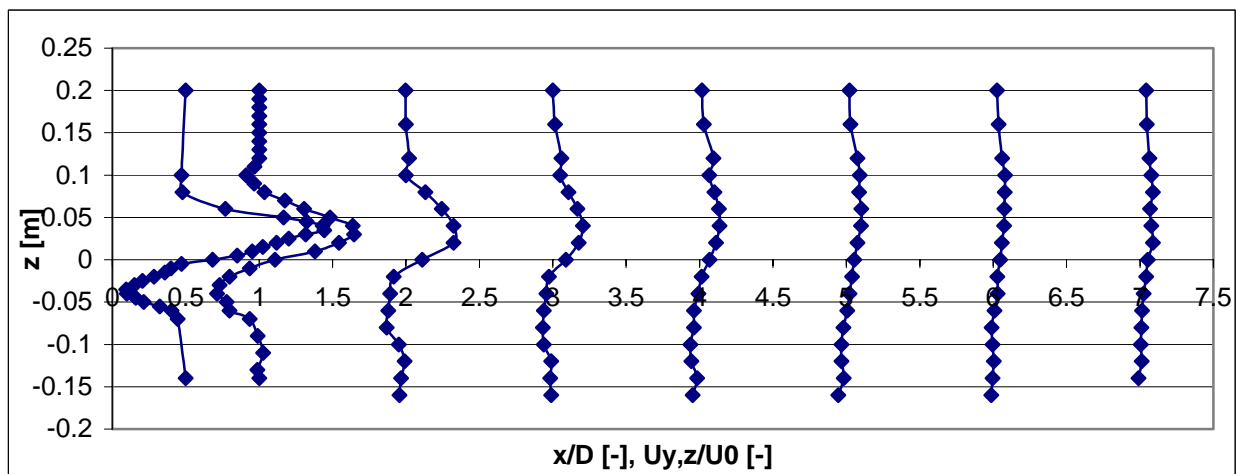


figure 4-6 Tangential velocity distribution.

It is interesting to see here, that the axial velocities are larger below the axis than above; in the case of tangential velocities it seems to be vice versa.

But also here, it will not be looked into any closer.

<sup>15</sup> Römisch uses  $D_0$  whereas Blaauw & Van de Kaa use  $D$ . In the case of a free propeller,  $D_0 = 0.7 D$ . (Blaauw & Van de Kaa 1975).

<sup>16</sup> By definition the flow in this zone does not notice the influence of the surrounding water at the  $x$ -axis. Even though it is not clear if the influence of the surrounding water is not noticed in this zone, it seems appropriate to maintain the division of the jet into those two zones since two zones are still distinguished.

The highest velocities (at  $x = 0.05$  [m]) occur at approximately 0.04 [m] above and below the axis.

This is almost the same location as what we defined to be the boundary of the jet (section 4.1.2). Apparently the highest tangential velocities occur in the boundary layer of the jet.

The figure also shows that the tangential velocities decrease a lot faster in space ( $x$ -direction) than the axial velocities. For instance at  $x/D = 4$  [-], 50 [%] of the initial axial velocity is left, but only 10 [%] of the initial tangential velocity. The possible reasons for it are treated in section 4.2.2.

#### 4.1.5 Diverging of the jet and influence of bottom and free surface

Since the jet diverges, it will reach the bottom and free water surface at a certain point. The angle of spreading in axial direction is assumed to be 1:6 [-] (Römisch, 1977), or around 10 [degrees]. The results confirm this: in the model the angle of spreading is about 1:6.25 [-]. For our model this means that the influence of the bottom is noticed when  $x$  reaches 0.7 [m] to 0.8 [m]. Since this is already on the slope it is assumed that the bottom does not influence the jet in the section in front of the slope.

#### 4.1.6 Reproducibility

When the velocity field was measured for the first time, the results showed some irregularities just in front of the slope. See figure (4-7):

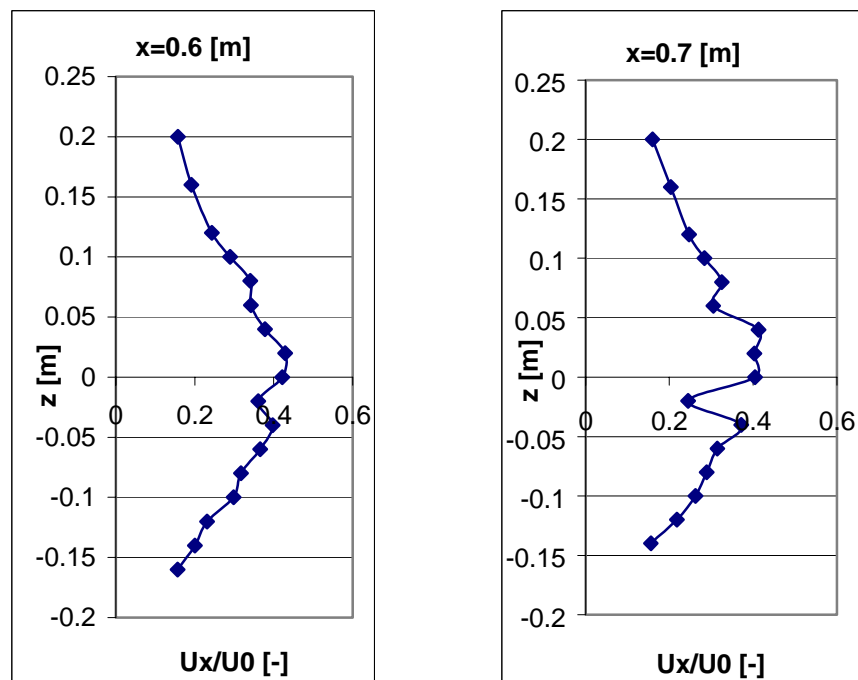


figure 4-7 Initial measurements for  $x = 0.6$  [m] and 0.7 [m].

At  $z = 0.06$  [m] and  $z = -0.02$  [m] a clear indentation is developing. It is highly unlikely that these points are caused by some sort of error in measuring since the points were successively measured in

---

height before moving to another location in x-direction. So, between the indents on  $x = 0.6$  [m] and  $x = 0.7$  [m], 16 other points were measured, which show no irregularities.

When the experiment was repeated, the indentations were not measured again. The reason for this might be the following: The first measurements were done after all prior horizontal measurements were taken. This means that the jet had caused a (small) scourhole in the slope. The second measurements were taken after the slope had been replenished with protection material. Since this was the only visible difference between the two situations, this probably caused the difference, by influencing the flow.

The locations were re-measured twice but it was not possible to reproduce the same results as the first time. Therefore it was decided to reject the initial data.

The reason for mentioning this, is that it implicates that small irregularities in the model may be of significant influence on the data derived.

#### 4.1.7 Circulation

##### 4.1.7.1 Through the hole

As described in the model set-up, the diameter of the hole was taken twice the size of the diameter of the propeller ( $D_{\text{hole}} = 0.20$  [m]). This was based on calculations of the entrainment by the jet (see section 3.2.2, model set-up).

Some measurements were done to see if the size of this hole (0.20 [m]) was taken correctly.

At  $x = 0.05$  [m]<sup>(17)</sup>,  $z = 0$  the velocities were measured in a horizontal plane, perpendicular to the axis of the jet.

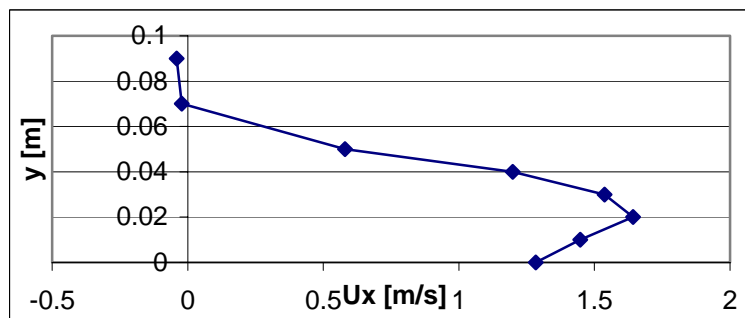


figure 4-8 Circulation through the hole.

As can be seen in figure (4-8), there is some water circulating through the hole. Since it has a small velocity of around 0.04 [m/s] it is not supposed to have any significant effect on the results. It is therefore concluded that the hole is a little too large, but certainly not too small, so there is no restricting effect of the board on the development of the jet.

---

<sup>(17)</sup> With the EMS is not possible to measure closer than 5 [cm] to a steel object. In this case the propeller would cause disturbances in the signal if measuring any closer.

#### 4.1.7.2 Through the basin

Twenty measurements were performed to determine the maximum velocities that occurred due to circulation. This was done by measuring outside the jet at  $0.1 \text{ [m]} < x < 0.7 \text{ [m]}$ ,  $0.2 \text{ [m]} < y < 0.8 \text{ [m]}$ ,  $-0.16 \text{ [m]} < z < 0.28 \text{ [m]}$ .

At the maximum initial velocity (1.4 [m/s]) the maximum circulation velocity equalled 0.15 [m/s]. This occurred in a large cell that developed on the free surface. Figure (4-9) below shows the locations of the cells in the model. Although this is non-negligible, it is not possible to decrease these circulation effects with the model used. For the comparison between the two models (ducted and non-ducted propeller) it poses no problems since both models contain these circulation effects.

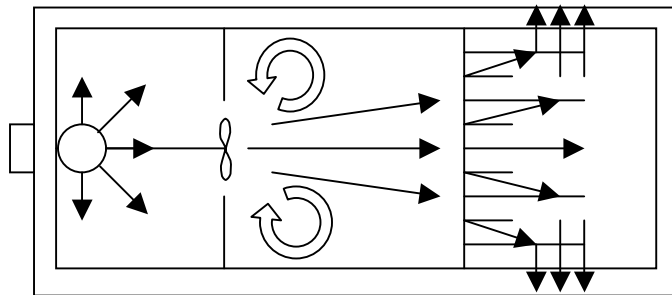


figure 4-9 Top view of the model, showing the water flow and the cells that developed (on the left the inflow, on the right the outflow).

#### 4.1.8 Measurements and theory compared

In the literature study the theory on the velocity distribution is given. Römisch (1981) and Blaauw & van de Kaa (1978) found different values for certain constants in the formula:

Blaauw & Van de Kaa:

$$\frac{U_{\max}}{U_0} = 2.8 \cdot \left( \frac{x}{D_0} \right)^{-1} \quad [-] \quad (4-2)$$

$$\frac{U_{x,z}}{U_{\max}} = \exp \left[ -15.4 \cdot \frac{z^2}{x^2} \right] \quad [-] \quad (4-3)$$

Römisch:

$$\frac{U_{\max}}{U_0} = 2.6 \cdot \left( \frac{x}{D} \right)^{-1} \quad [-] \quad (4-4)$$

$$\frac{U_{x,z}}{U_{\max}} = \exp \left[ -22.2 \cdot \frac{z^2}{x^2} \right] \quad [-] \quad (4-5)$$

These formulas were derived for the zone of established flow (see literature study, chapter 2). They are compared with the measured values for the zone of established flow in figure (4-10).

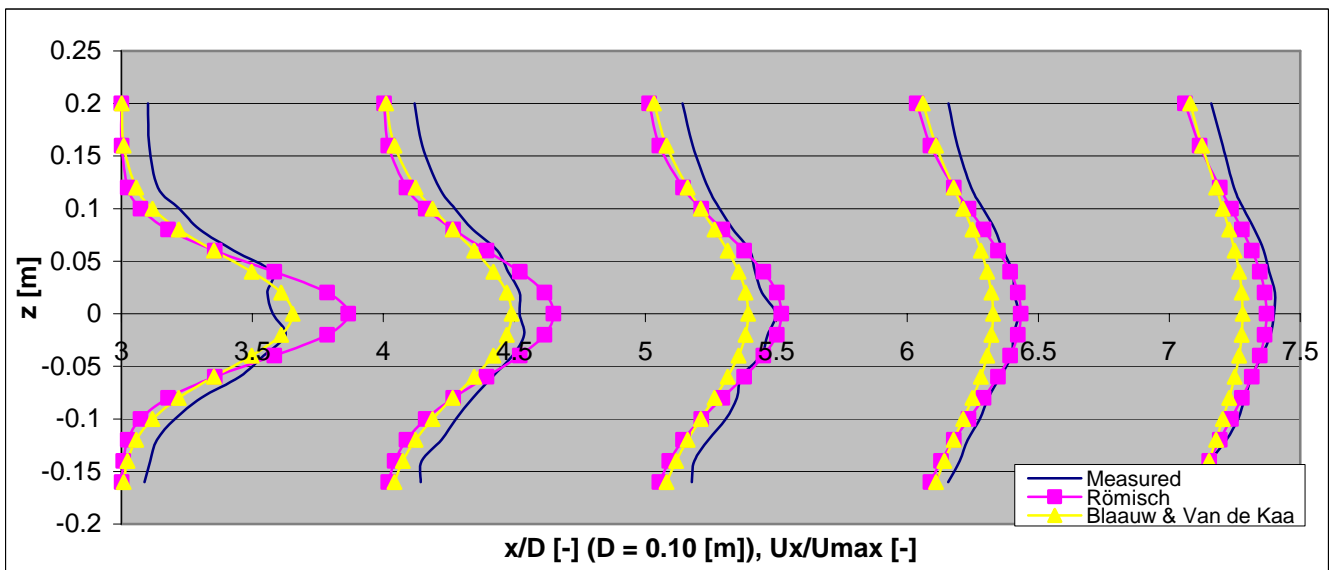


figure 4-10 Theoretical and measured velocity distribution at several distances from the propeller. Values represent  $U_x/U_{max}$ .

The values found match those for the equations of Blaauw & van de Kaa (equations (4-2) and (4-3)) quite well for  $x = 0.3$  [m] and  $0.4$  [m]. For  $x = 0.5$  [m],  $0.6$  [m] and  $0.7$  [m] it seems that Römisch (equations (4-4) and (4-5)) gives a better prediction. For the lower and upper part of the field ( $z < -0.1$  [m] and  $z > 0.1$  [m]) it seems that both theories predict slightly low values compared to the measurements (as much as  $0.18$  [m/s]). As already mentioned before, circulation may be the cause of this.

#### 4.1.9 Comparing the velocity fields

One of the objectives of this thesis is to make a comparison between a ducted-propeller jet and a free-propeller jet. In this chapter their velocity distributions will be compared.

As already mentioned before (section 4.1.2), the thrust coefficient of the free propeller was found to be 0.23 [-]. For the same propeller, but in the ducted situation, Van Veldhoven found a value of 0.22 [-]. This means that the initial velocities at a certain rotation rate are practically identical. At three distances from the propeller the velocities are compared (for the entire set of figures the reader is referred to the appendix C):

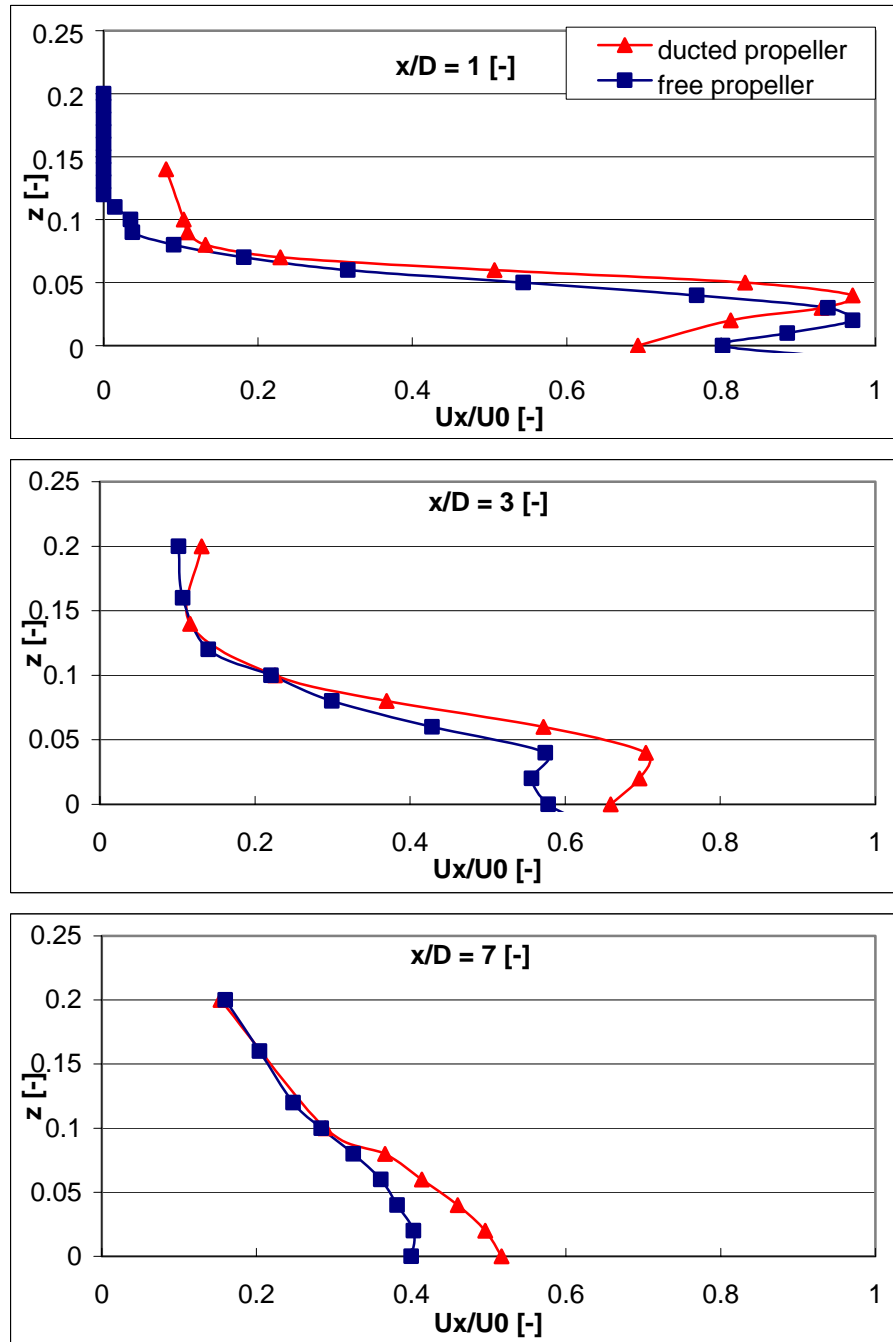


figure 4-11 Difference in velocity development between ducted propeller and free propeller.

---

Figure (4-11) shows that the initial profiles are quite similar at  $x/D = 1$  [-]. The free-propeller jet has a slightly smaller diameter than the ducted-propeller jet. This is explained by the fact that the free-propeller jet has a contraction coefficient of 0.5 [-] whereas a ducted-propeller jet has a contraction coefficient of 1.0 [-] (Blaauw & Van de Kaa, 1978).

Farther away from the propeller it is clear that the velocity along the axis ( $z = 0$ ) decreases more rapidly for the free propeller than it does for the ducted one. At  $x = 0.7$  [m] the difference has grown to 25 [%].

It is also noted, following from figure (4-11), that both jets diverge almost equally.

Since the initial profiles are practically similar, so is the initial discharge of both jets ( $Q = U \cdot A$  [ $m^3/s$ ]). Since at  $x/D = 7$  [-] the widths are still practically the same, but the velocities are not, the discharge of the free propeller has decreased considerably compared to the discharge of the ducted propeller.

It is assumed that greater turbulence causes the free-propeller jet to mix faster with the surrounding water and causes the velocities to die down quicker. In section 4.2 this is looked into closer.

#### **4.1.10 Conclusions on the velocity field**

When we look at the difference between the velocity fields of a jet initiated by a free propeller and the velocity field of a jet initiated by a ducted propeller we can draw the following conclusions:

- The jets diverge at almost the same angle.
- The mean axial velocity of the free-propeller jet decreases more rapidly than the mean axial velocity of the ducted-propeller jet.

## **4.2 Turbulence**

### **4.2.1 General**

The definition of turbulence can be given as: "Turbulent fluid motion is an irregular condition of flow in which the various quantities show a random variation with time and space coordinates, so that statistically distinct average values can be discerned" (Hinze, 1975).

Taylor and Von Kármán (1937) state that turbulence can be generated by friction forces at fixed walls or by the flow of layers of fluids with different velocities past or over one another. The first form is known as 'wall turbulence', the second form as 'free turbulence'.

When looking in the jet itself we are only dealing with free turbulence, when looking close to the slope (chapter 5) we will be dealing with both.

---

The velocity at a certain point and time can be written as:

$$U = \bar{U} + U' \quad [\text{m/s}] \quad (4-6)$$

in which  $\bar{U}$  indicates the average value of U and U' indicates the superimposed fluctuation. The root mean square method is used to obtain distinct values for the intensity of the fluctuations (a measure for the standard deviation):  $\sqrt{\overline{U'^2}}$  [m/s]

This is divided by the mean velocity resulting (by definition) in the relative turbulence r.

$$r = \frac{\sqrt{\overline{U'^2}}}{\bar{U}} \quad [-] \quad (4-7)$$

The measurements were taken in axial and tangential direction (x and y). Therefore we define the relative turbulence in these directions in a given point as:

$$r_x = \frac{\sqrt{\overline{U_x'^2}}}{\bar{U}_{x,z=0}} \quad [-] \quad (4-8)$$

and

$$r_y = \frac{\sqrt{\overline{U_y'^2}}}{\bar{U}_{y,z=0}} \quad [-] \quad (4-9)$$

The mean values on the x-axis are taken here, since the velocities can be very low when reaching the bottom or free surface. This would lead to very high relative turbulence numbers. In that way a point with a mean velocity of zero would have an infinite relative turbulence, which is unrealistic.

The physical meaning of 'r' is to give an indication of the intensity of the turbulent fluctuations compared to the velocity of the flow it occurs in. The mean velocity of this flow is said to occur on the x-axis ( $\bar{U}_{y,z=0}$  and  $\bar{U}_{x,z=0}$ ).

This also leads to a limitation of using this method. We are not only dealing here with turbulence initiated by a flow. It is expected that the propeller initiated a great deal of turbulence. Therefore it is questionable whether this is the right method to present the value of the turbulence. It gives however a good indication of the turbulent fluctuations and again, for making comparisons to the ducted-propeller jet it poses no problem.

The actual velocity is recorded 50 times per second. Subtracting the mean value of the entire dataset from each recorded velocity gives the fluctuation. Subsequently the relative turbulence for each measured point can be calculated.



---

As mentioned in section 4.1.1, the instrument used to measure the velocities has certain limitations. First of all, it disturbs the flow by its presence. Therefore it will influence the measurements. Secondly, it measures in two directions only. In this model measurements were done in axial and tangential direction.

But more important for measuring the turbulence is the minimum size of the vortices the EMS can detect. The diameter of the disc of the EMS itself is about 3 [cm] and it can detect vortices of about 1 [cm] large. This means that vortices smaller than approximately 1 [cm] are not taken into account.

The stones on the slope have a  $d_{50}$  of 0.9 [cm], practically the same size as the smallest vortices that can be measured.

Hofland (2001) and Booij (1992) found that the vortices that are most effective have a diameter of 1.5 respectively 2 times the diameter of the stone. Therefore it is believed that the most effective vortices are most likely taken into account, but smaller vortices will also contribute to the total turbulence intensities. If we believe that these are also of importance to the stability of the stones on the slope it is important to keep in mind that these are not measured.

Therefore it is doubtful to make any statements about the relation between stability and turbulence based on this model.

But looking at the goal of this model -to determine in which way to model a bowthruster- this shortcoming is of minor importance. Comparisons can be made on the measurable fluctuations.

To give an idea of the development of turbulence in a jet, figure (4-12) shows a top view of a starting free jet.

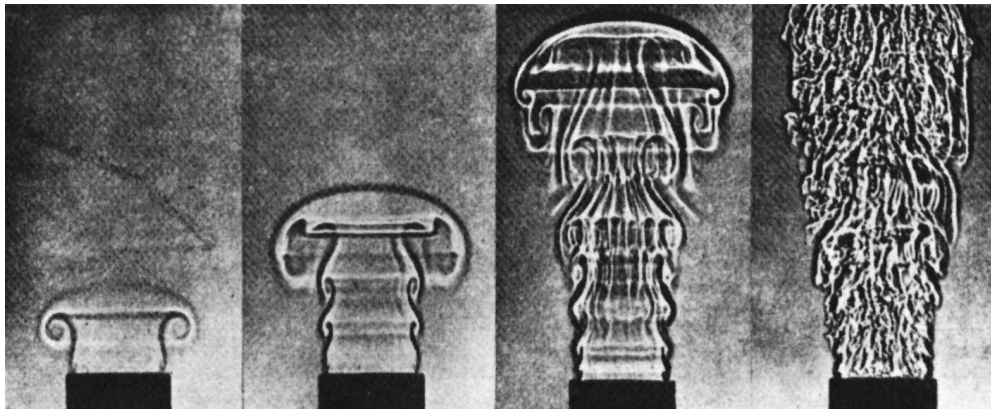


figure 4-12 Photographs of a starting free jet (Garside, J.E, from: Hinze, 1975, Turbulence).

Since in our case we deal with a propeller, the turbulence pattern will be different, but the above figure (4-12) gives a good indication.

---

## 4.2.2 Relative turbulences in the jet

### 4.2.2.1 Axial relative turbulence

If we plot the axial relative turbulence for all points measured on the axis of the jet we derive the following figure (4-13):

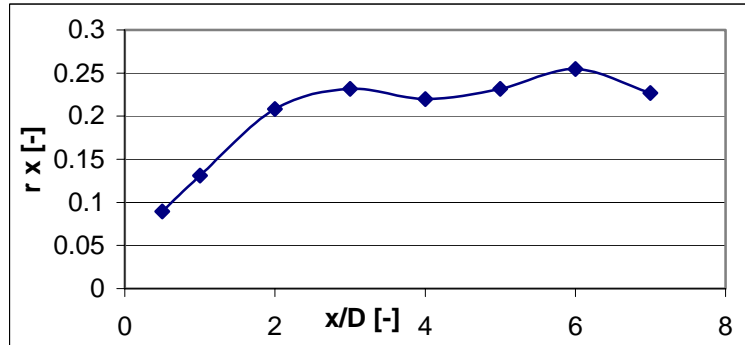


figure 4-13 Axial relative turbulence.

As can be seen the relative axial turbulence is low in the vicinity of the propeller and increases as the distance from the propeller increases.

At a distance of about two to three times the diameter of the propeller it seems to stabilize at a value of around 0.23 [-]. Blaauw & Van de Kaa (1978) predict a value of about 0.28 [-] at a distance of 8 times the diameter of the propeller. So the relative turbulence seems to stabilize sooner than that, but also at a (slightly) lower value.

Some elaboration on the subject might be necessary:

If we consider a jet penetrating in a body of water, the water at the axis of the jet will not notice the presence of the surrounding water at first. At the boundary of the jet a shear layer develops, causing turbulent vortices. This phenomenon always occurs when currents with different velocities interact (figure (4-14)).

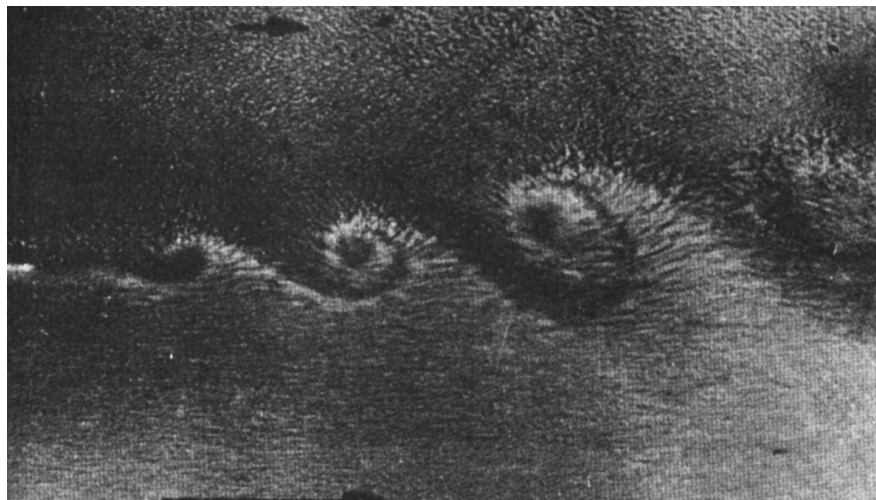


figure 4-14 Vortices at boundary of a half-jet (Flugel, G, from: Hinze, 1975, Turbulence).

This turbulence diverges outwards and inwards. It takes some time to reach the axis of the jet, and consequently (at a certain velocity) this also takes distance. This distance is defined as  $x_0$  (see chapter 2, literature study for details).

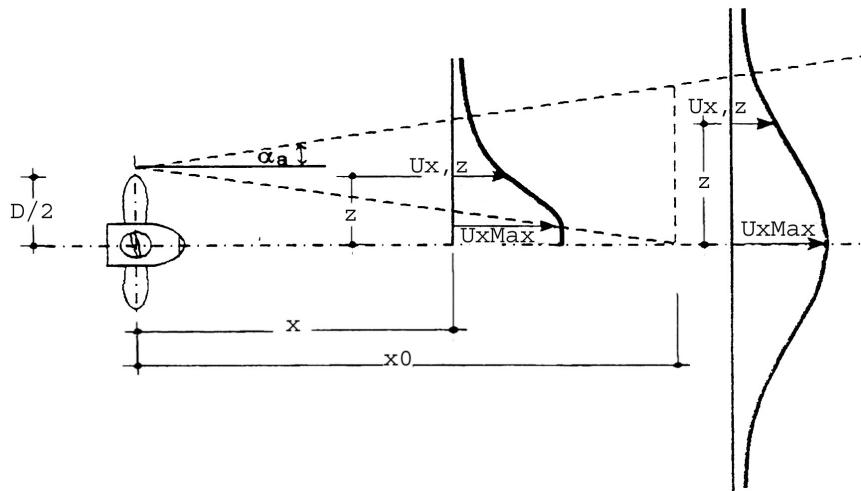


figure 4-15 Zone of flow establishment ( $x_0$ ).

As mentioned in section 4.1.3 the length of the zone of flow establishment equals 0.2 [m]. Here it is clear to see that the increase in turbulence is largest between 0.05 [m] and 0.2 [m] from the propeller (figure (4-13)). This is the same region in which the velocity at the axis decreases fastest (section 4.1.3).

It is therefore highly likely that the fast increase in turbulence on the axis leads to a fast decrease of flow velocity.

The fact that the turbulence at the axis seems to stabilize after  $x = 0.2$  [m] also supports the idea that this is the boundary of the zone of flow establishment.

As already concluded in section 4.1.3, the theories of Römisch and Blaauw & Van de Kaa (1978) did not match the experimental results for the zone of flow establishment. The reason for this could be the following:

Their theories are based on a free jet –which is not induced by a propeller- entering a body of water. In our model the jet is induced by a propeller. This propeller causes a lot of extra turbulence. A free jet only has an axial velocity, causing turbulence along the shear layer when it enters a body of water. A propeller however generates velocities in radial and tangential direction too, directly penetrating the surrounding water. This causes a great deal of extra turbulence and entrainment.

Another fact that may play a role, is the fact that the theories do not consider the propeller axis. As already seen in section 4.1.3, figure (4-3), there is an indentation just behind the axis. This velocity difference inside the jet will also lead to extra turbulence in the region of the axis.

It is therefore likely that both reasons mentioned above together result in the fast increase of turbulence on the axis, which leads to a fast decrease of velocity, explaining why the theories of Römisch and Blaauw & Van de Kaa cannot be used in the zone of flow establishment in the case of a free-propeller jet.

#### 4.2.2.2 Tangential relative turbulence

The same growth pattern is found for the tangential relative turbulences. They are, however, about 5 times larger than the axial relative turbulences and it is not clear at which value the relative tangential turbulences stabilise (if so at all).

It does, however, concur with the assumption that the velocities in tangential direction die down quicker because of the greater turbulence (compare figures (4-3) and (4-6)).

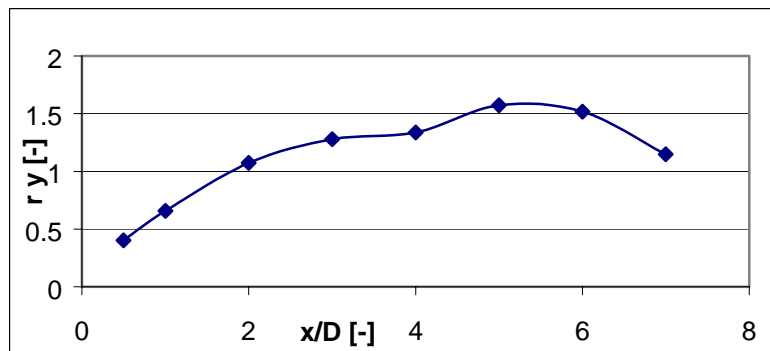


figure 4-16 Tangential relative turbulence.

#### 4.2.3 Peak velocities

Peak velocities are considered to be very important to the stability of the protection material on the slope. That is why it is interesting to compare the peak velocities found in the model to theoretical velocities.

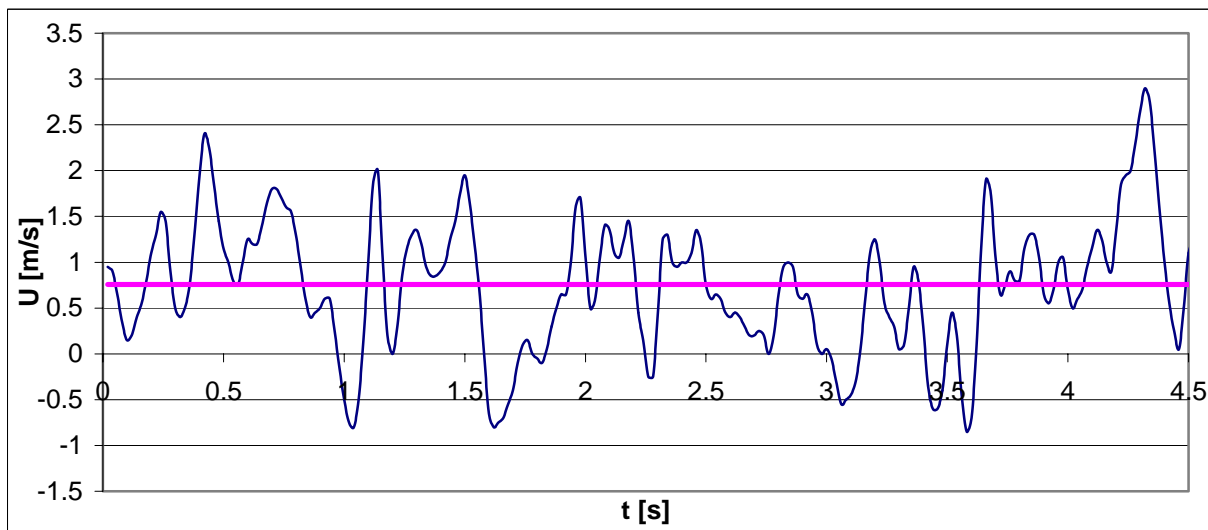


figure 4-17 Fluctuations in the jet at a random point, duration of 4.5 [s]. Peak velocity occurs at t = 4.3 [s].

Figure (4-17) shows the actual velocity and the average velocity for a random point,  $0 [s] < t < 4.5 [s]$ .

These peak velocities in any point are often described as (for instance Schiereck, 2000):

$$\tilde{U}_{\max} = \bar{U} + a \cdot \sqrt{\overline{U'^2}} \quad [m/s] \quad (4-10)$$

where

- $\tilde{U}_{\max}$  : peak velocity in the point considered [m/s]
- $\bar{U}$  : mean velocity in the point considered [m/s]
- $\sqrt{\overline{U'^2}}$  : turbulence intensity in the point considered [m/s]
- a: constant; often the value 3 [-] is found during experiments.

For all 119 points measured the values of 'a<sub>x</sub>' and 'a<sub>y</sub>' are calculated (in a given dataset all parameters except 'a' of equation (4-10) are known).

These two values are then averaged for each point resulting in 'a'.

$$a = \frac{a_x + a_y}{2} \quad [-] \quad (4-11)$$

For a certain distance from the propeller these values of 'a' are then averaged over the height resulting in ' $\bar{a}$ '. It appears that at several distances from the propeller they are practically identical:

x/D [-]	$\bar{a}$ [-]
1	3.57
2	3.62
3	3.48
4	3.38
5	3.33
6	3.20
7	3.51
<b>Total Mean</b>	<b>3.4</b>

table 4-1 Value of ' $\bar{a}$ ' at x/D from 1 [-] to 7 [-].

It appears that the found total mean value of 3.4 [-] is slightly higher than the usually found value of 3 [-]. The often-found value of 3 [-] is however based on a free jet, not on a propeller jet. This may cause the difference.

In addition to that, other experiments showed similar results as those found in our model:

The Engineering Consultants of Rotterdam Public Works did a prototype test in 1993. They used a tugboat and performed velocity measurements on one of the main propeller jets. Among other things, they measured the water velocity at several distances from

the propeller. With the equipment used they could also distinguish the turbulent fluctuations<sup>18</sup>. The duration of one measurement was 2 [minutes] and they found a mean value for 'a' of 3.4 [-]. So compared to this prototype measurement the value found for 'a' in our model is the same (but was derived with a longer measuring interval).

This supports the idea that the (peak) fluctuations were correctly measured in the model.

#### 4.2.4 Comparing relative turbulences

If we compare the relative turbulences found on the axis of a free-propeller jet with the results found by Van Veldhoven (2001) for a ducted-propeller jet, the following figure (4-18) results for the axial relative turbulence 'r<sub>x</sub>':

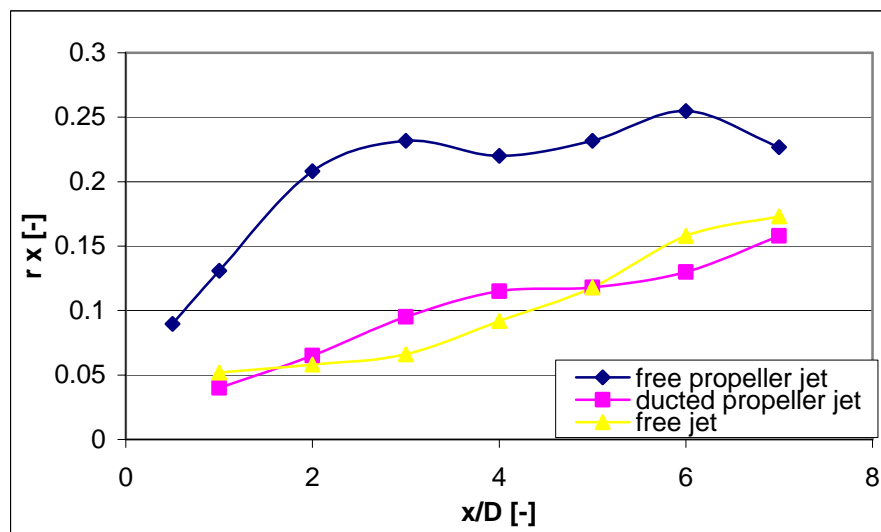


figure 4-18 Relative axial turbulence of the ducted-propeller jet, free-propeller jet and a free-water jet.

It is clear that the relative turbulences in the axis of the free propeller are much higher (as much as 100 [%] for some points) than those found when using a ducted propeller.

Assuming that this (measurable) turbulence is important to the movement of protection material, this fact may be very important when looking at damage on the slope.

Van Veldhoven (2001) found practically the same relative turbulence on the x-axis both for a free jet and for a ducted-propeller jet. Since the jet and the ducted-propeller jet both originate from a pipe, it is believed that this causes the difference in turbulence due to the fact that the duct has a restricting effect on the development of turbulence.

<sup>18</sup> The EMS they used was of the same brand and type that was used in our model.

In section 4.1.9 it was noted that the velocity fields for a ducted and free-propeller jet diverge at practically the same angle. The mean velocity however decreases more rapidly for the free propeller than for the ducted one. It was already suggested that the difference in discharge is caused by greater turbulence in the jet initiated by the free propeller. Because of this greater turbulence the jet will mix better with the surrounding water and its energy is dissipated faster. Figure (4-18) seems to justify this theory.

#### 4.2.5 Profile in height

The distribution of the relative turbulence in axial direction  $r_x$  over the height (figure (4-19)) shows that almost all relative turbulences have a value of around 0.25 [-] when  $z/x < 0.3$  [-]. For  $z/x > 3$  [-] the turbulences decrease quickly, except for  $x/D = 6$  [-] to  $7$  [-]. This is probably due to the influence of the slope, since a return current is expected there to cause extra turbulence.

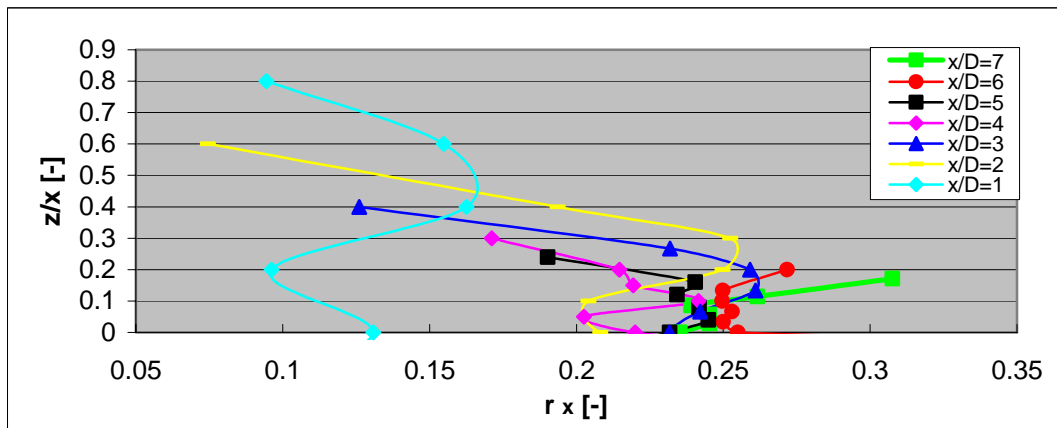


figure 4-19 Relative axial turbulence distribution over the height above the x-axis.

The results of van Veldhoven (2001) for a ducted propeller show a similar profile, except for the increments at  $x/D = 6$  [-] to  $7$  [-] (see figure (4-20)).

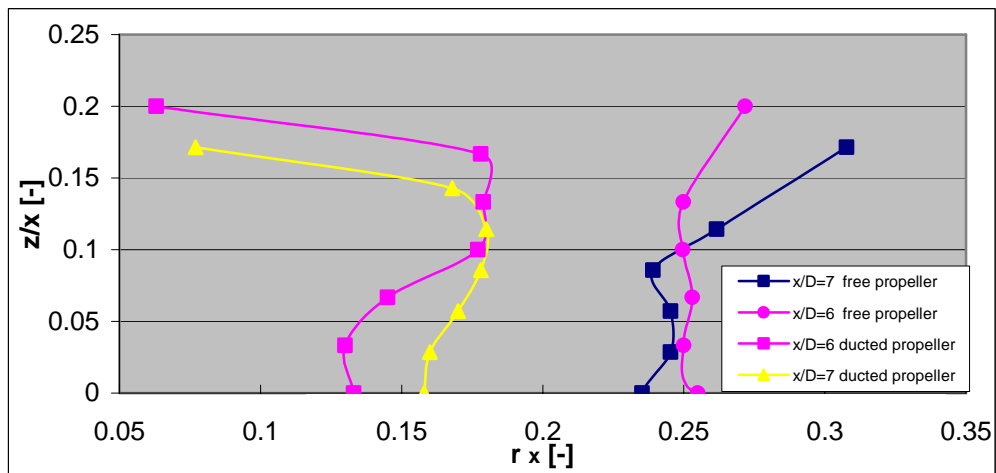


figure 4-20 Turbulences of free and ducted-propeller jet at  $X/D = 6$  [-] and  $X/D = 7$  [-] compared.

Van Veldhoven (2001) found a maximum value for  $r_x$  around 0.18 [-] compared to 0.26 [-] in our model (not taking the values for  $x/D = 6$  [-] and 7 [-] into account, since the influence of the slope is not considered here).

#### 4.2.6 Statistics of fluctuations

##### 4.2.6.1 Jet axis

The distribution of the velocities of the fluctuations in a given point is supposed to be according to a normal probability density function (Hinze, 1975). By calculating the standard deviation and the mean of a dataset one can project the theoretical distribution on the actual distribution. This is done for some points at the axis of the jet:

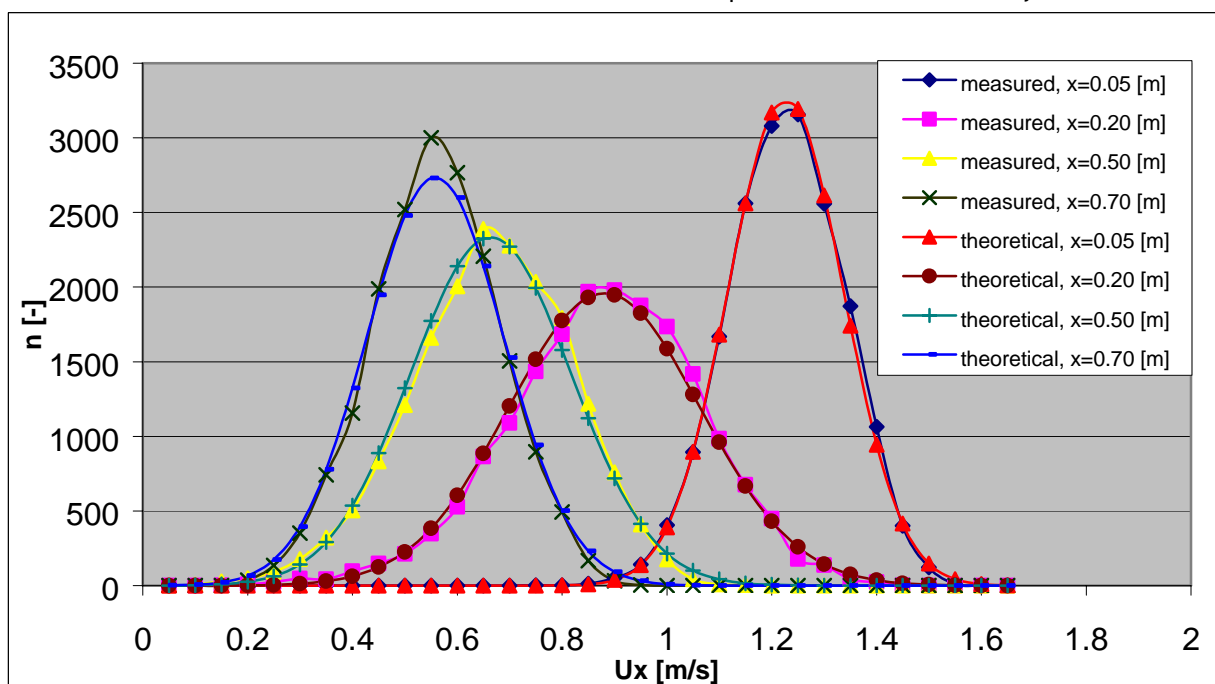


figure 4-21 Distribution of the fluctuations, measured and theoretical.

The measurements were done for 6 [minutes] per point. At 50 [Hz] this leads to 18000 recordings. In figure (4-21), 'n' represents the number of recordings of a certain velocity.

The interval of the velocity, plotted on the x-axis is 0.05 [m]<sup>19</sup>.

As can be seen, the distribution corresponds well to that of the theoretical distribution, which indicates that the turbulent fluctuations were probably measured properly.

<sup>19</sup> The digital converter of the EMS combined with the a range of 0 to 5 [m/s] leads to a maximum accuracy of 0.05 [m/s] which is therefore also the minimum velocity it can detect at this range.



---

#### 4.2.6.2 Above the jet axis

When looking above the x-axis, for instance at  $z = 0.010$  [m] it appears that the distribution of the fluctuations does not longer comply with a normal probability distribution function (see figure (4-22)).

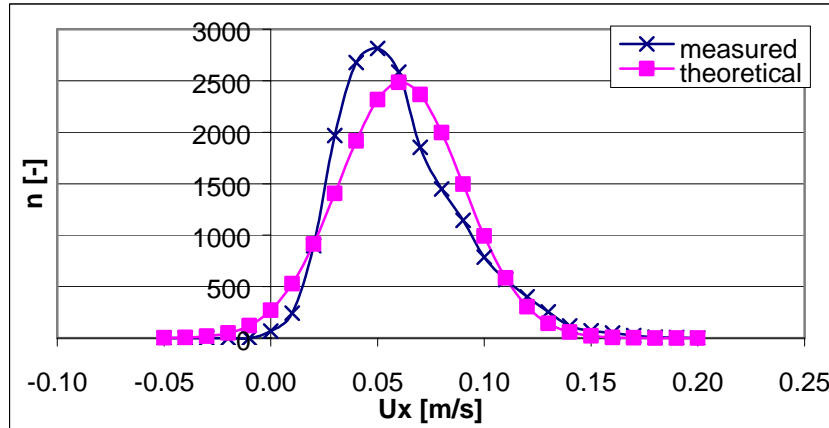


figure 4-22 Distributions of fluctuations at  $x = 0.30$  [m],  $y = 0$ ,  $z = 0.10$  [m].

The DWW (Oral information, Van der Wal, 2002) found that when currents with significant different velocities interact the distribution of the fluctuations becomes asymmetric. It appears that the same is valid here (location  $x = 0.30$  [m],  $z = 0.10$  [m],  $y = 0$  is considered to be in the boundary layer of the jet where layers with different velocities interact).

The phenomenon is just mentioned here and not looked into any closer since it does not contribute to the goals of this thesis.

---

### 4.3 Stability of materials

#### 4.3.1 Damage on the slope

The second part of the tests concerned the stability of the protection material on the slope.

The protection material used has a  $d_{50}$  of 0.009 [m]. The rotation rate, resulting in an initial velocity, was increased after each measurement after a stable situation had developed<sup>20</sup>. The starting velocity equalled 0.5 [m/s]. The velocity was increased with steps of around 0.1 [m/s] until it reached 1.1 [m/s].

After each interval it was recorded how many stones had moved and also in what direction.

The test was repeated ten times to get a representative mean value.

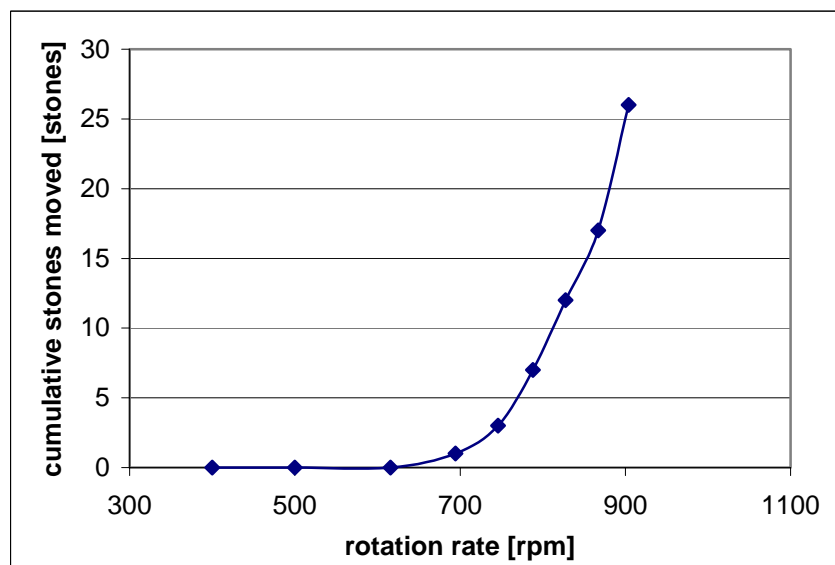


figure 4-23 Damage at the slope related to the rpm of the propeller.

As can be seen in figure (4-23), at a rotation rate of around 700 [rpm] the transition from rest to movement takes place. This is at an initial velocity of 0.9 [m/s]. In that case the average velocity just in front of the slope equals approximately 0.35 [m/s]<sup>21</sup>.

#### 4.3.2 Criterion of Izbash

Izbash defined his stability parameter as

$$\beta_{iz} = \frac{2 \cdot g \cdot \Delta \cdot d}{U^2} [-] \quad (4-12)$$

---

<sup>20</sup> A stable situation is defined as a situation in which no movement has taken place for 15 minutes.

<sup>21</sup> Measured value at  $x = 0.7$  [m]. When calculated according to the theory of Römisch, 0.32 [m/s] is found.

Since we are dealing with a slope, the used  $d_{50}$  here is equivalent to a  $d_{50} \cdot K(\alpha)$  on a horizontal bed.

Since the stability is smallest when the water runs down the slope, this situation is supposed to be the most unfavourable situation combined with the highest velocity found<sup>22</sup>.

$$K(\alpha) = \frac{\sin(\varphi - \alpha)}{\sin(\varphi)} \quad [-] \quad (4-13)$$

with  $\varphi = 40^\circ$  and  $\alpha = 18^\circ$ ,  $K(\alpha)$  becomes 0.58 [-].

The peak velocity was calculated in section 4.2.3 as:

$$\tilde{U}_{\max} = \bar{U} + a \cdot \sqrt{\bar{U}^2} \quad [\text{m/s}] \quad (4-10)$$

'a' was found to be 3.4 [-].

For  $\bar{U} = 0.35$  [m/s] (found in section 4.3.1 as the velocity at which the transition to movement takes place) and  $r = 0.23$  [-] it follows that  $\tilde{U}_{\max} = 0.62$  [m/s].

$\beta_{iz}$  then equals 4.3 [-].

The WL found (1985) that for a horizontal bed the parameter of Izbash should be between 6.5 [-] and 4 [-] depending how much movement is permitted. It seems that the found stability parameter (in combination with the peak velocities and the slope factor) complies with the range found by the WL.

### 4.3.3 Reynolds number

As mentioned in the model set-up, chapter 3, the Reynolds number of the jet should be larger than  $3.0 \cdot 10^3$  [-] to ensure that scale effects are negligible (Pearce, 1966).

$$\text{Re}_j = \frac{U_0 \cdot D}{\nu} \quad [-] \quad (4-14)$$

where :

$\text{Re}_j$ :	Reynolds number for the jet [-]
$U_0$ :	Initial velocity [m/s]
$D$ :	Diameter of the propeller [m]
$\nu$ :	kinematical viscosity [m <sup>2</sup> /s]

In the model the minimum value for  $\text{Re}_j$  was found to be  $3.75 \cdot 10^4$  [-].

<sup>22</sup> It is not known whether the maximum velocity found here is directed down the slope, but it is taken as an upper limit here.

So for the modelling of the jet and its velocity field the model shows no scale effects.

The Reynolds number for the stones:

$$\text{Re}_g = \frac{U \cdot d_{50}}{\nu} \quad [-] \quad (4-15)$$

For the velocity at which the transition to movement takes place, the Reynolds number equals  $2.4 \cdot 10^3$  [-] ( $U = 0.35$  [m/s]). This means that the criterion is not met and that scale effects are not negligible here. Therefore the prototype will behave (slightly) different.

Since this test was performed mainly to determine the difference between a free propeller and a ducted one -in which the same scale effects apply- this is of no consequence on the conclusions that need to be drawn.

**Remark:** The velocity used here to calculate the Reynolds number was measured at  $x = 0.7$  [m] and not at the slope. The actual velocity at the slope is thought to be a combined action of the velocities in all 3 directions, and therefore may be higher or lower around the actual particle considered leading to a different Reynolds number for the stones.

#### 4.3.4 Comparing a ducted and a free propeller

If we look at the ducted propeller the damage<sup>23</sup> done at an equal rotation rate is significantly higher than for the free propeller, as shown in figure (4-24).

The initial velocity is practically the same. The difference is that the velocity decrease for the ducted propeller is a lot smaller than for the free one (see figure (4-11)). So at the slope this results in a different velocity.

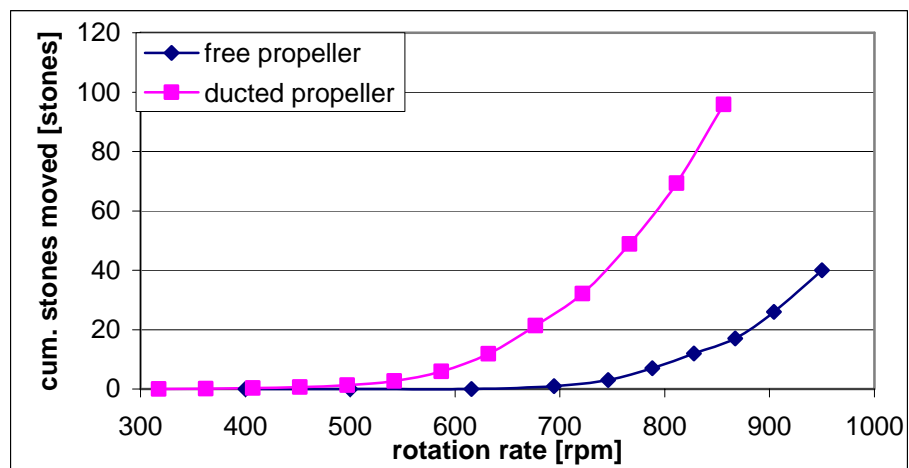


figure 4-24 Damages compared, related to the rpm of the propeller.

If we however do not relate the damage to the rotation rate but to the velocity at the slope ( $x = 0.7$  [m]), a different picture arises.

<sup>23</sup> Damage: Total number of stones moved.

---

With an equal velocity at the slope, the damages do not differ much.

Figure (4-25) shows that at a certain damage, the difference in the local velocity is less than 0.02 [m/s]. The fact that the free-propeller jet carries almost 40 [%] higher relative turbulence in front of the slope does not seem to influence the stability<sup>24</sup>.

Van Veldhoven (2001) came to a similar conclusion when comparing a free jet to a ducted-propeller jet. He found a significant difference in damages, but could not relate it to the turbulence.

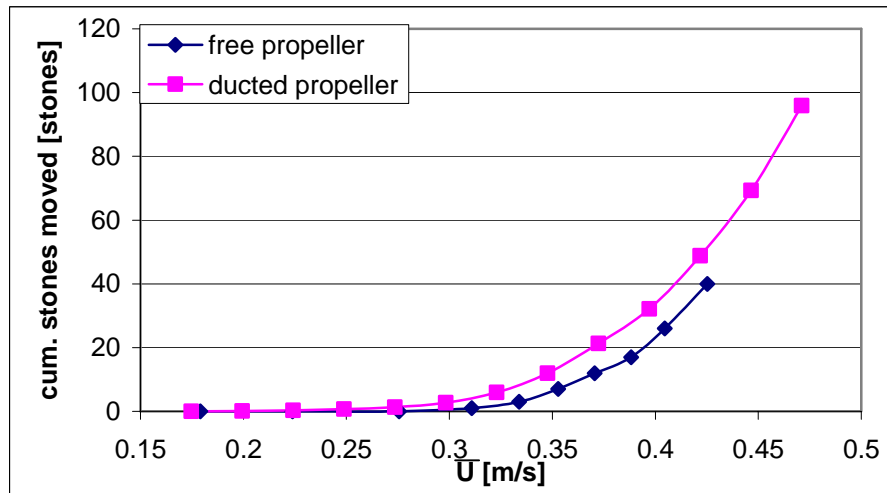


figure 4-25 Damages compared, related to the velocity at  $x = 0.7$  [m].

**Remark:** Since the velocities are not measured at the slope, mean values here are taken for  $x = 0.7$  [m],  $-0.1$  [m]  $< z < 0.1$  [m]. The figure presented above is therefore only an indication of local velocities related to damage. More measurements of velocities at the slope should be carried out to gain more insight into what the exact relations are.

---

<sup>24</sup> This does not imply that turbulence does not have any affect on the stability of the stones. No measurements were taken at the slope, so it is not possible here to indicate the influence of turbulence.

---

### 4.3.5 Orientation of spreading

#### 4.3.5.1 Direction

To obtain an idea of the orientation of the spreading of the stones we take all net movements (absolute (outgoing – incoming)) that occurred at least 2 times during the ten tests, see figure (4-26) (for a picture of the slope and stones, the reader is referred to appendix B).

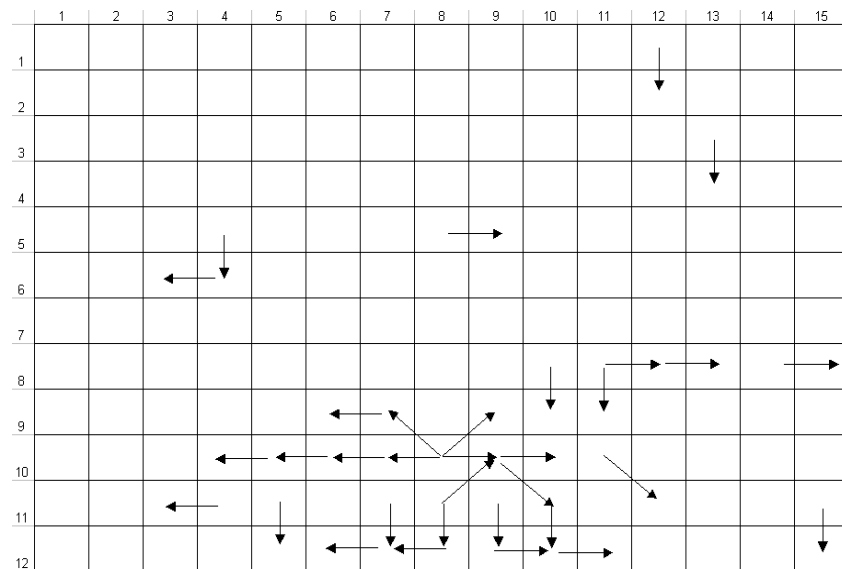


figure 4-26 Net movements.

Figure (4-26) shows that points (8,10) and (8,11) are the centre points of the spreading of the stones. It is expected that the current has an upward direction above and a downward direction below row 10/11, taking the protection material along. Higher on the slope the stones are moved downward, even though one would expect the current to be still directed upward. The flow is probably strong enough to lift a stone from its place, but not strong enough to carry it upward. The stone falls down along the slope and settles in a more stable position.

### 4.3.5.2 Intensity

If we look at the intensity of all movements (incoming + outgoing stones) we get the following intensity chart:

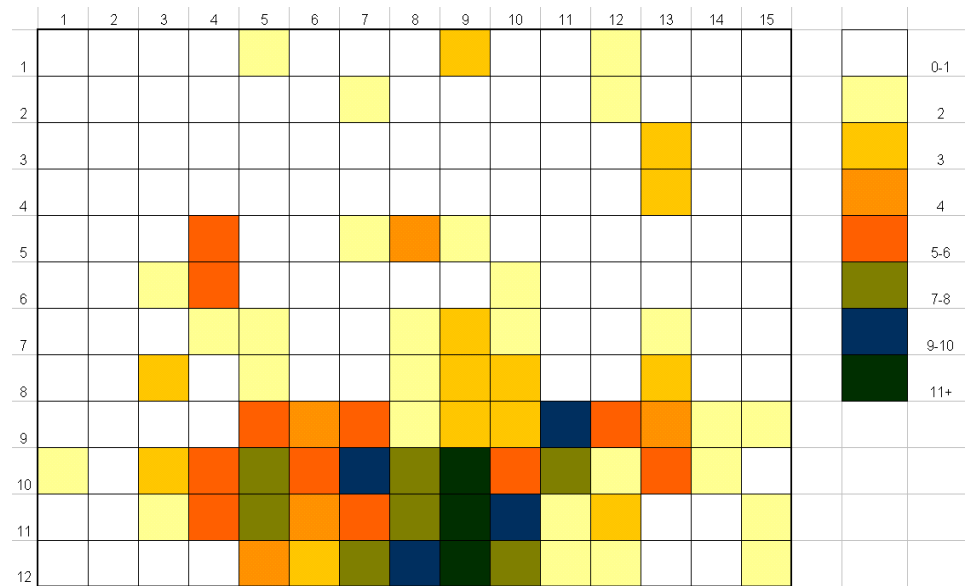


figure 4-27 Intensity of all movements, i.e. the total number of movements in the area considered.

Figure (4-27) shows that on the left side the intensity is slightly larger than on the right side. This could have something to do with the rotation direction of the propeller, but since the tangential velocity has decreased to almost zero at  $x = 0.7$  [m], this is considered to be highly unlikely. Since the difference is not significant and not important to this thesis it will not be looked into closer.

The place where the maximum damage occurs is much more important. This is found to be in the lower section of the slope. While the axis of the jet lays at  $z = 0$  [m], the maximum damage occurs at  $z = -0.15$  [m]. This is remarkable since the velocities of the undisturbed jet just in front on the slope are very low there. Some theories state that the centre of the jet slowly descends along the x-axis.

For instance Fuehrer, Pohl and Römisch (1987) state that the jet axis has an downward angle with the x-axis of 2.5 [degrees]. Even if this would be correct -something that is not justified by our measurements- this would still lead to a decrease in height of only 0.03 [m]. So this is not considered to be the explanation.

Van Veldhoven (2001) derived a hypothesis (which is explained in the next chapter) for this phenomenon and since there appears to be no former study on the matter, it is decided that more tests concerning the velocities near the slope should be carried out to gain more insight in the causes of this phenomenon and to find out if Van Veldhoven's hypothesis is correct.

---

#### 4.3.6 Conclusions on the stability of materials

- When a free propeller is used to model a bowthruuster the damage is significantly lower than in the case of a ducted propeller. The value of the rotation rate at which the material starts to move is 25 [%] higher for the free propeller than when using a ducted propeller. The main reason for it is the different rate at which the velocities decrease.
- The location of the most intense movements is at a considerably lower z-level then where it would be expected.

#### 4.4 Conclusions

The following can be concluded in relation to the question whether to use a ducted or a free propeller for modelling a bowthruuster:

- The velocity fields of the two models differ with respect to the rate of velocity reduction in x-direction. It is thought that higher relative turbulence intensities in the free-propeller jet cause the velocity to decrease faster than in the ducted-propeller jet.
- The diverging of the jets is almost equal.
- The damage done at the slope is very different between the two models if it is related to the rotation rate of the propeller: the free-propeller jet induces considerably less damage than the ducted-propeller jet.
- Remarkably, higher relative turbulence therefore eventually leads to less damage.

Taking the above into consideration it is concluded that:

When the goal is to model the damage induced by a bowthruuster, a free propeller should not be used in the model since a free propeller does not produce similar results as a ducted propeller (i.e. a bowthruuster) concerning velocity distribution and damage.



# 5 Damage location investigation

## 5.1 General

The results of the free-propeller jet in chapter 4 as well as the results of Van Veldhoven (2001) show that the maximum damage on the slope occurs at the lower part of the slope, approximately between 0 and 0.10 [m] from the toe (see figure (5-1) & (5-2)).

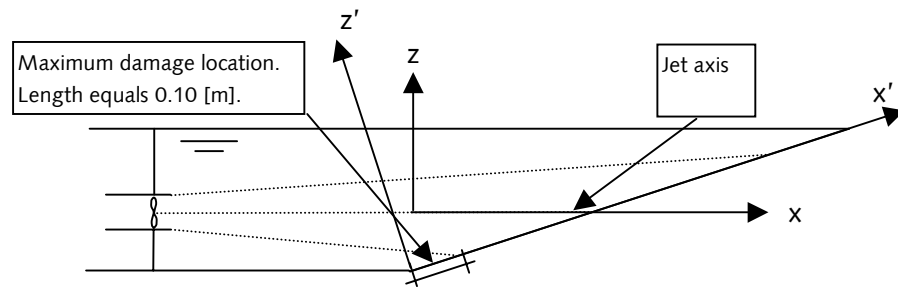


figure 5-1 Location of maximum damage, visualized in the x-z plane.

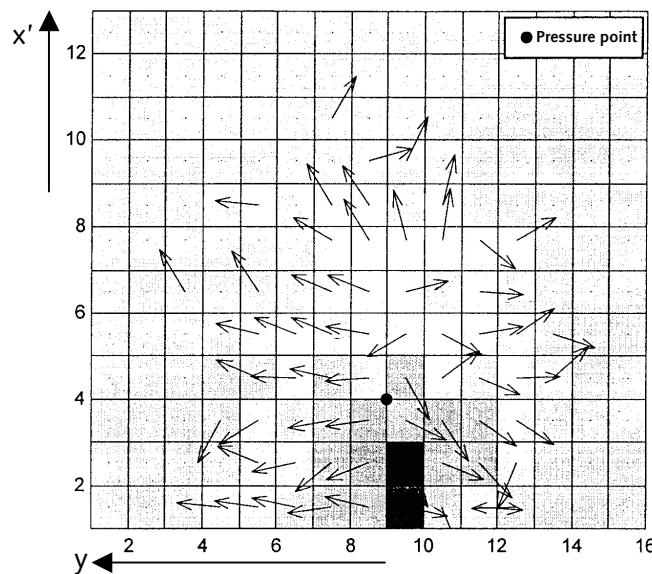


figure 5-2 Location and direction of the damages visualized in the x'-y plane. Dark areas are areas with intense movement of stones. Every square equals 0.05 [m] by 0.05 [m].

The black dot indicates the location that Van Veldhoven (2001) believes to be the point where the jet axis hits the slope, the so-called pressure point.

Since he did not perform any measurements near the slope, he derived a hypothesis based on a theory by Beltaos (1997). This hypothesis states that the jet axis, where the maximum velocities occur, changes direction towards the slope, hitting the slope at a much lower location (at the black dot in figure (5-2)) than when continuing straight ahead.

---

He also states that above this point the velocities will be positive (upward) and below this point they will be negative (downward). In order, for the jet axis, to hit the slope at such a low location, the jet would have to change its direction significantly. Van Veldhoven states that this direction change should start at 0.50 [m] ( $5 \cdot D_0$ ) from the propeller. Since his measurements do not show this, it is decided to perform measurements close to the slope to confirm or reject his hypothesis.

The goals of this chapter are therefore:

- To determine the cause of the location of the maximum damage.
- To determine if Van Veldhoven's hypothesis is correct.
- To give an idea of the velocity field in the vicinity of the slope.

To do this, the velocities have to be measured close to the slope. For practical considerations it was decided to do this with an EMS. Since the results of chapter 4 show that a bowthruster can best be modelled by a jet initiated by a ducted propeller, this is the way in which the jet was initiated during the measurements.

It was decided to use the same initial velocity at which Van Veldhoven (2001) found his maximum damage. This was at a rotation rate of approximately 900 [rpm]. For practical purposes it was increased to 1000 [rpm], which resulted in an initial velocity of 1.3 [m/s].

The velocities close to the slope are measured in three different ways:

- In the x-y plane,
- in the y-z plane,
- in the x-y plane related to the slope: the x'-y plane (see figure (5-1) for a definition of the different coordinate systems applied).

In this way more than 350 points were measured, each recorded in 2 directions.

In the remainder of this chapter the measuring methods are indicated as type I, II and III as explained in figure (5-3).



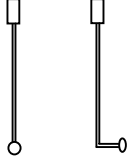
	<p><b>Type I</b> Horizontal measurements in the x-y plane</p>
	<p><b>Type II</b> Measurements parallel to the slope, in the x'-y plane</p>
	<p><b>Type III</b> Vertical/Horizontal measurements, in the x-z plane</p>

figure 5-3 Different types of measuring.

**Remark I:** Because of the large amount of points measured, it was decided to write a special numerical code that extracts and calculates the necessary data easily and quickly from the datasets. In appendix F the listing can be found.

## 5.2 The velocity field

### 5.2.1 General

Prior to looking at the damage location, the velocity field above the slope is first discussed in detail in the following order:

- The velocities parallel to the slope (x'-y plane).
- The vertical velocities (x-z plane).
- The horizontal velocities (x-y plane).

### 5.2.2 Velocities parallel to the slope

#### 5.2.2.1 General

The measurements parallel to the slope will be discussed here first. Ink was injected into the water to decide where to take the velocity measurements. It showed that there was only a small area in which little water activity took place. This area is located on the toe of the slope ( $0 < x' < 0.2$  [m],  $0.2$  [m]  $< y < 0.8$  [m]) and was not measured.

The following figure (5-4) shows the points that were eventually measured in the  $x'$ - $y$  plane:

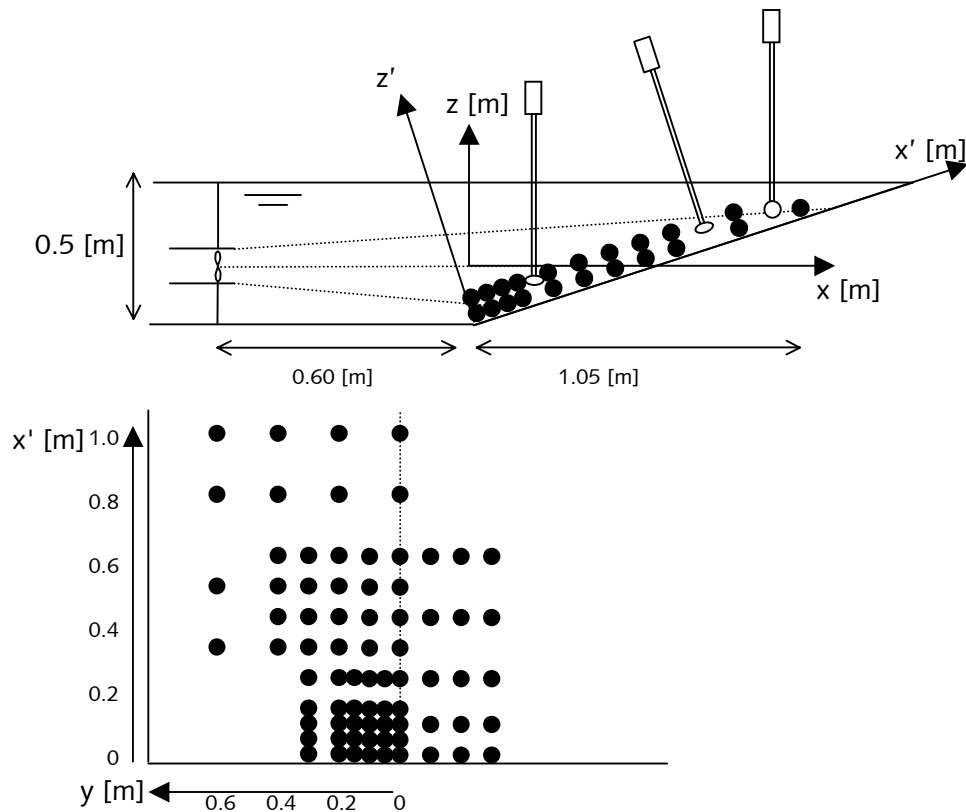


figure 5-4 Measured points in the  $x'$ - $y$  plane.

- The velocities were measured at  $z' = 0.025$  [m] and  $z' = 0.050$  [m] at the slope using the type II EMS (figure (5-5)).

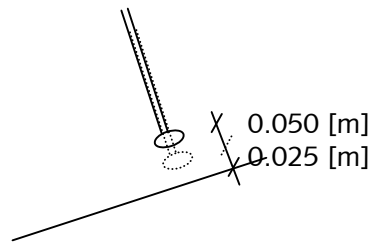


figure 5-5 The two heights at which the type II measurements were taken.

- Most of the points at  $z' = 0.025$  [m] were also measured with the type I EMS.
- The points at  $z' = 0.025$  [m],  $y = 0$  were also measured with the type III EMS.

### 5.2.2.2 Type II measurements

#### Difference between $z' = 0.025$ [m] and $z' = 0.050$ [m]

First the difference between the measurements at  $z' = 0.025$  [m] and  $z' = 0.050$  [m] is analysed. To do so figure (5-6) shows the velocity profile for  $z' = 0.025$  and  $z' = 0.050$  [m] at  $y = 0$ .

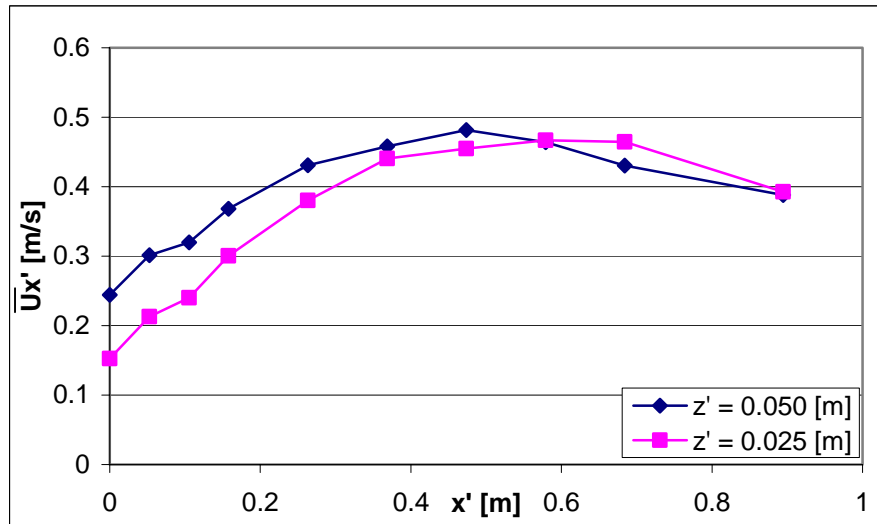


figure 5-6 The average velocities for  $z' = 0.025$  [m] and  $z' = 0.050$  [m].

An important fact that is concluded from figure (5-6) is that the velocities at  $y = 0$  along the entire slope are positive (upward).

Following from figure (5-6) it is furthermore concluded that the velocities measured at  $z' = 0.025$  [m] and  $z' = 0.050$  [m] differ slightly with a maximum of  $0.08$  [m/s] at  $x' = 0$  which decreases rapidly when the measurements are closer to the location where the original jet axis ( $z = 0$ ) hits the slope ( $x' = 0.6$  [m]).

Since the jet axis is defined as the axis where the velocities are highest it seems that this axis intersects the slope at  $x' = 0.6$  [m] since the average velocities are largest there. This is a first indication that the jet does not change direction, contradicting the hypothesis of Van Veldhoven.

It is clear that the maximum velocity for  $z' = 0.025$  [m] occurs at  $x' = 0.6$  [m] while for  $z' = 0.050$  [m] it occurs at  $x' = 0.5$  [m]. This is quite logical, considering the way the jet flows and the way the measurements are taken:

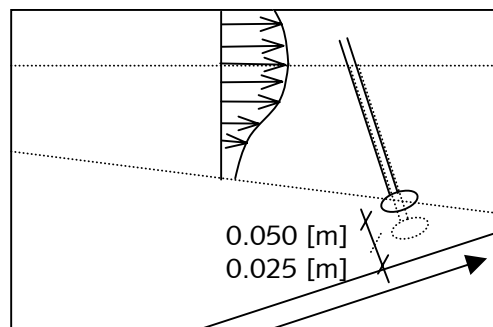


figure 5-7 Below the x-axis the velocity increases with increased height above the slope.

---

**z < 0:**

For  $z < 0$  (i.e. below the axis of the jet) the velocity increases as  $z'$  increases. This is caused by the fact that the closer one measures to the axis of the jet the higher the velocity will be (figure (5-7)).

**z > 0:**

The same applies for  $z > 0$  (i.e. above the axis of the jet) and the velocity decreases as  $z'$  increases. Therefore the graphs in figure (5-6) meet at approximately the location at which the x-axis of the jet hits the slope ( $x' = 0.6$  [m]).

The fact that the EMS disturbs the flow by its presence is neglected here. In section 5.2.2.4 this will be looked into further. The measurements at  $z' = 0.025$  [m] above the slope most likely contain an error caused by this phenomenon, only it is not known quite how large it is. Also it should be kept in mind that measuring at a distance of approximately 2.5 times the diameter of a stone, individual stones may very well be of great influence on the measurements (see also section 4.1.6).

Since the distance from slope to EMS is much larger for the measurements at  $z' = 0.050$  [m] than for  $z' = 0.025$  [m] it is assumed that the error due to the presence of the EMS is much smaller for  $z' = 0.050$  [m].

Another fact that may be important is that according to Booij (1992) and Hofland (2001) the size of the most effective vortices for moving a stone is approximately 1.5 to 2 times the diameter of this stone. When the EMS is at a similar distance from the slope as the size of these vortices it may be so that these vortices do not develop and that therefore the most effective vortices for the instability of the materials are not measured.

Keeping the above in mind, but trying to describe the situation at the slope as accurate as possible, it is chosen to apply the measurements at  $z' = 0.025$  [m] as indicative for velocities parallel to the slope.

**Velocities on the entire slope**

It is assumed that there is symmetry in the velocity field between  $y < 0$  and  $y > 0$ . To validate this, a number of points is measured at  $y > 0$ ,  $z' = 0.050$  [m] (figure (5-4)). These points are compared to the corresponding points at  $y < 0$ .

The difference turned out to have a maximum of 11% at location  $x' = 0.45$  [m],  $y = -0.20$  [m] with an absolute difference of less than 0.03 [m/s].

The difference in velocity is considered small enough to assume symmetry for the  $x'$ - $y$  velocities.

Figure (5-8) presents the combined average velocity

( $\bar{U} = \sqrt{(\bar{U}_x^2 + \bar{U}_y^2)}$ ) on the slope for all  $x'$  and  $y$  values, including

the flow direction.

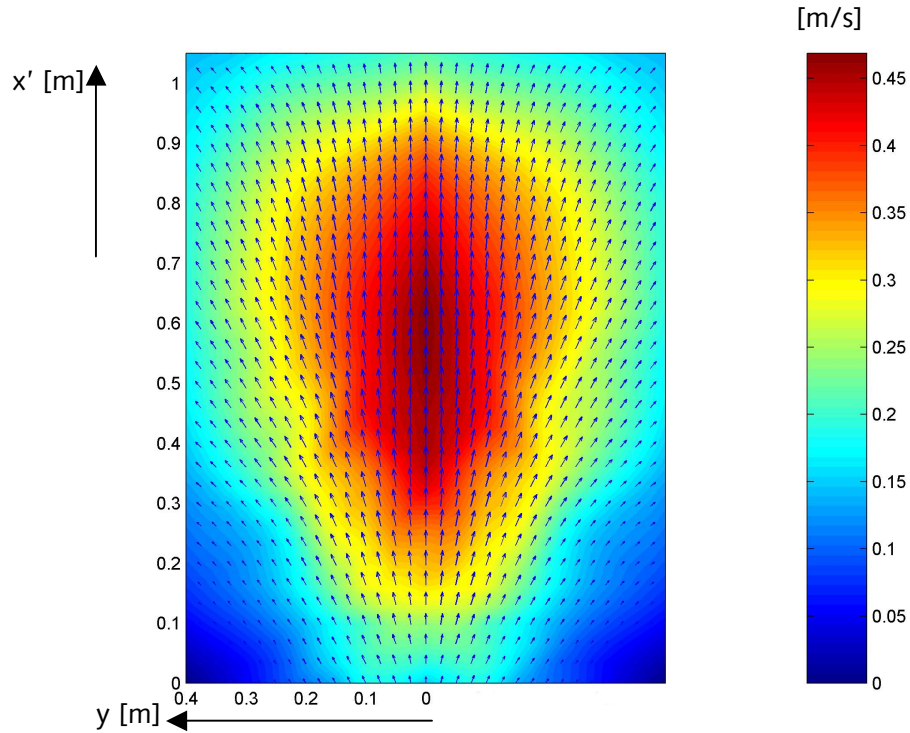


figure 5-8 Total average velocities and flow direction at  $z' = 0.025$  [m].

The maximum average velocity clearly takes place between  $x' = 0.45$  [m] and  $x' = 0.65$  [m],  $y = 0$ . This is in agreement with the idea that where the jet hits the slope ( $y = 0$ ,  $x' = 0.60$  [m]) the velocity is at its largest. For comparison, also a picture of the average velocities at  $z' = 0.050$  [m] is shown (figure (5-9)).

Since the location  $x' = 1.05$  [m],  $z' = 0.050$  [m] is practically at the water surface no measurements are taken at this point.

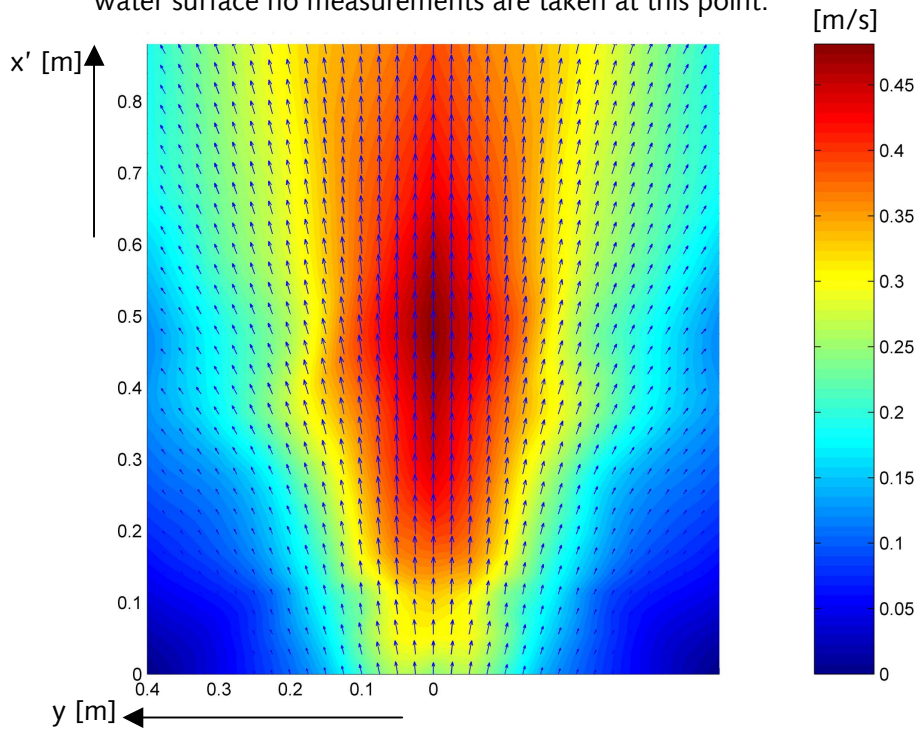


figure 5-9 Total average velocities and flow direction at  $z' = 0.050$  [m].

### 5.2.2.3 Type I measurements

Quite a few points were measured with the type I EMS (horizontal measurements in the x-y plane).

Figure (5-10) shows the velocities along the x'-axis for  $z' = 0.025$  [m].

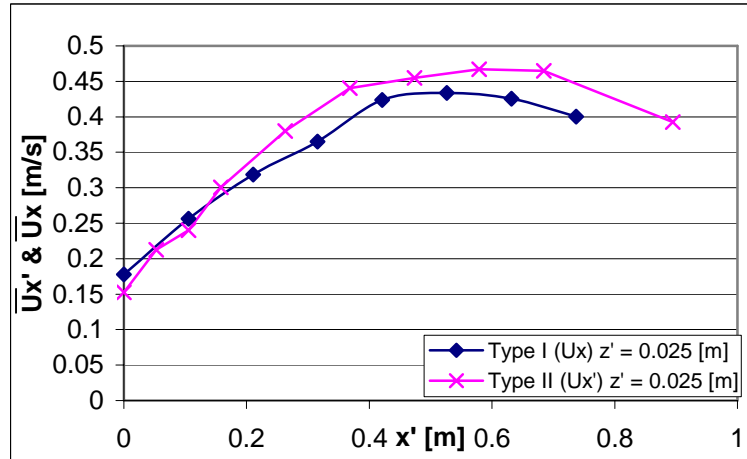


figure 5-10 Type I & II measurements at  $y = 0$ .

The results of the type I EMS do not differ much from the results acquired with the type II EMS for the points measured. The results of the type I EMS show a little bit lower average values than the ones measured with the type II EMS (the maximum difference is found to be 0.04 [m/s]). For the flow 0.025 [m] above the slope one can assume that  $U_x \approx U_{x'}$ . Since these results do not contribute much to the aims of this thesis and are considered to be less accurate for the type of flow we are interested in (flow parallel to the slope;  $U_{x'}$ ), the type I measurements will not be discussed here any further.

### 5.2.2.4 Type III (vertical) measurements

To find out the exact direction of the flow on the slope, measurements were taken at  $y = 0$ ,  $z' = 0.025$  [m] with the type III EMS (vertical measurements in the x-z plane). Since the velocity in y direction at  $y = 0$  is practically zero, in this case the EMS practically does not disturb the flow along the slope at  $y = 0$ , i.e. along the x'-axis (figure (5-11)), even if the flow is not parallel to the slope.

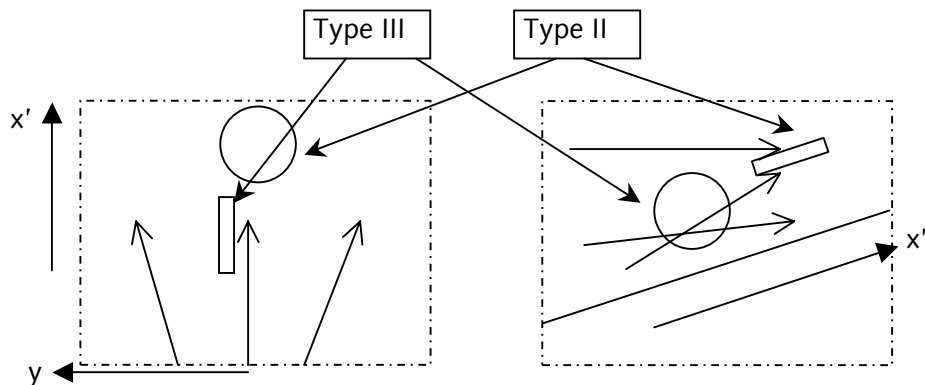


figure 5-11 EMS probes on the slope, top- and side view.



---

The results are compared to the results derived with the Type II measurements at  $y = 0$ . Figure (5-12) shows that the results are practically similar with a maximum difference of 0.04 [m/s].

So the results that are derived with an EMS that does disturb the flow are practically identical to the results derived by an EMS that does not disturb the flow. This leads to believe that the disturbance of the EMS when performing the type II measurements is not very big.

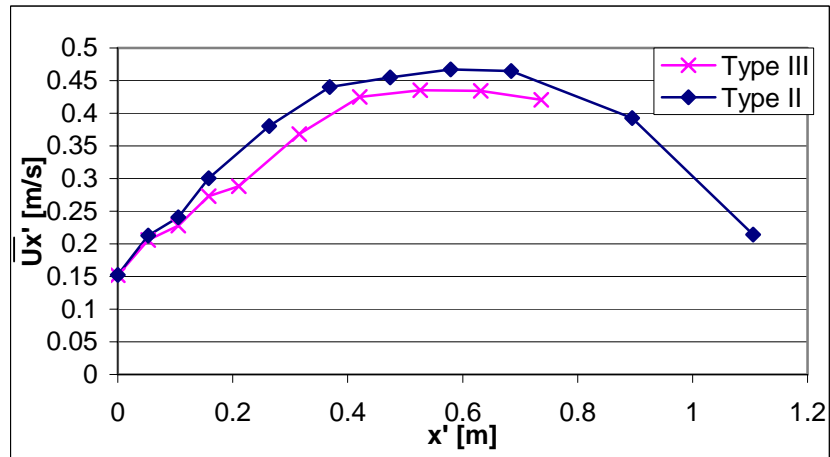


figure 5-12 Average velocities at  $z' = 0.025$  [m],  $y = 0$  for two different types of measuring.

However, it seems that the type III measurements have more irregularities than the type II measurements. This may be caused by the more free development of vortices around the stones, not hindered by the EMS.

Therefore, again, it should be kept in mind that measurements so close to bed may be significantly influenced by the presence or absence of one stone.

Figure (5-13) shows that the direction of the flow relative to the x-axis at  $y = 0$  varies between  $-2$  [degrees] and  $15$  [degrees]. The angle of the slope equals  $18$  [degrees]. So the water direction is not (yet) parallel to the slope anywhere. This causes the water to penetrate the protection material directly, which may be an important factor when looking at stability of the material (see section 5.3.4). It appears that higher on the slope the direction of the water starts to adapt more and more to the angle of the slope.

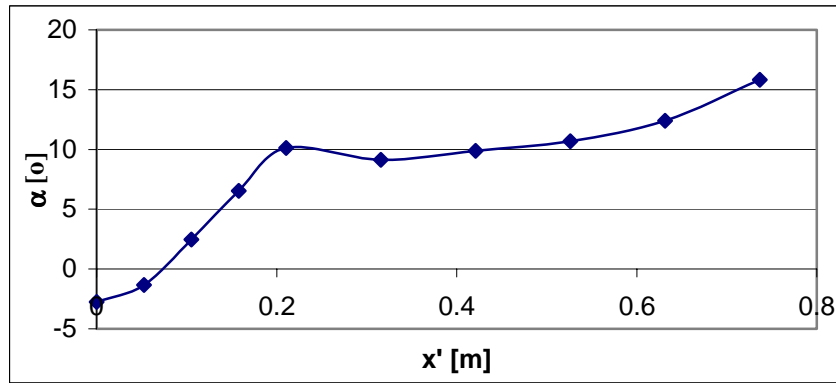


figure 5-13 The angle between the flow direction and the x-axis along the slope at  $z' = 0.025$  [m].

It is remarkable that the flow changes direction gradually between  $x' = 0$  and  $x' = 0.2$  [m] and then suddenly stabilises. In this thesis this phenomenon is not investigated further but it may be an interesting subject for further study.

### 5.2.3 Vertical velocities

The vertical velocities above the entire slope were measured at an interval of 0.10 [m] along the x-axis, starting at  $x = -0.05$  [m] in front of the slope. The maximum distance from the x-axis was chosen at  $y = 0.30$  [m].

The vertical values varied between  $z = -0.15$  [m] and  $z = 0.10$  [m] with an interval of 0.05 [m] (see figure (5-14)).

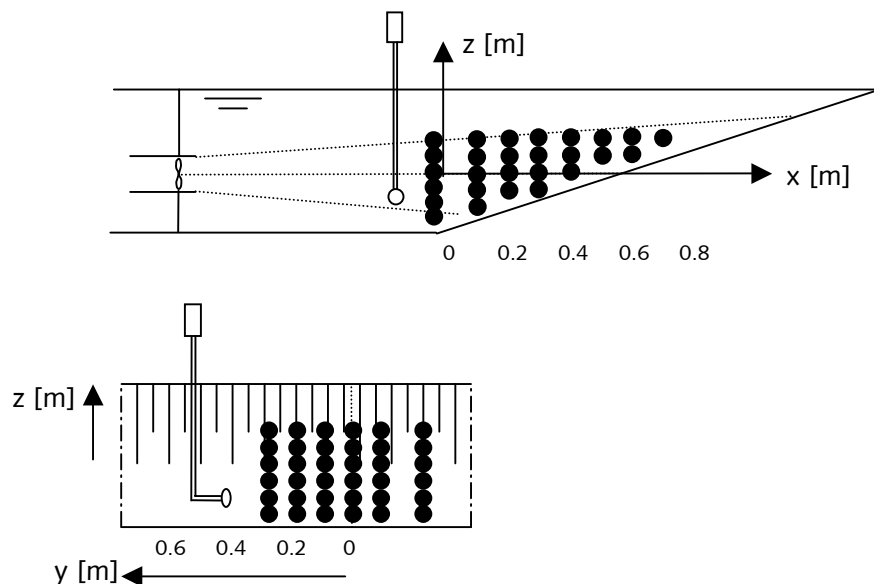


figure 5-14 The locations of the measurements in vertical direction (type III).

As an example the development of vertical velocities along the x-axis is shown in figure (5-15) for  $y = 0$  and  $z = 0.050$  [m].

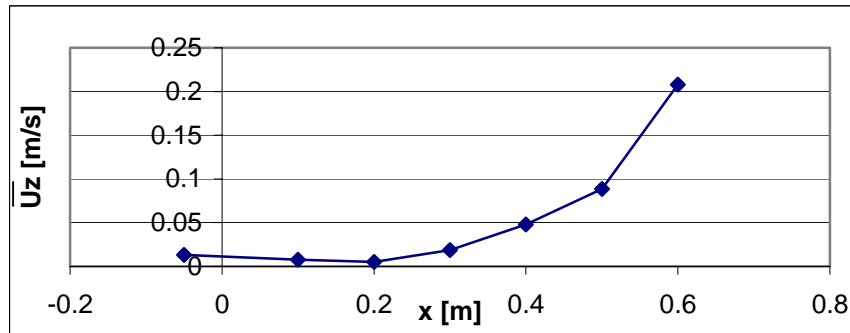


figure 5-15 Vertical velocities for  $z = 0.050$  [m].

It appears that (from all measurements taken) the average vertical velocities in the entire field are in general practically zero, with the exception of the locations close the slope. Approximately 0.3 [m] before the streamline would intersect with the slope the velocity direction changes from roughly horizontal to a direction of approximately 0 [degrees] related to the  $x'$ -axis, increasing the vertical velocities (see figure 5-15).

According to Schmidt and Römisch (1993) the pressure zone starts  $0.3 \cdot L$  [m]<sup>(25)</sup> in front of a vertical wall. If we apply the same principle here this would lead to  $0.3 \cdot 1.35$  [m] = 0.41 [m]. It seems that the value of 0.30 [m] found here is rather small. On the other hand, it seems logical that a vertical wall does not produce the same results as a slope. It also does not seem unlikely that a slope produces a less large pressure zone than a vertical wall does, since it deflects the jet more gradually.

For the entire field above the slope the velocities and their directions are shown for  $y = 0$  in figure (5-16).

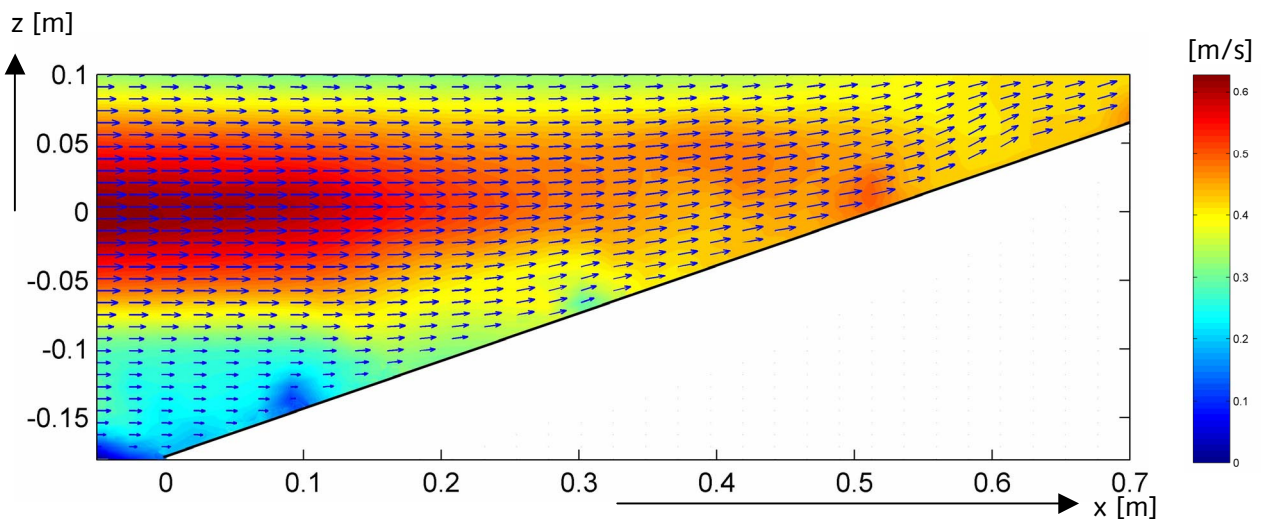


figure 5-16 Velocities in the  $x$ - $z$  plane for  $y = 0$ ,  $-0.050$  [m] <  $x$  <  $0.7$  [m],  $-0.18$  [m] <  $z$  <  $0.1$  [m].

It is clear to see here that the maximum velocity occurs at  $z = 0$  for  $-0.05$  [m] <  $x$  <  $0.3$  [m]. For  $x > 0.3$  [m] it seems that the maximum velocity occurs at a slightly higher  $z$ -level, in full contradiction with

<sup>(25)</sup>  $L$  is defined as the distance from the propeller.

the hypothesis of Van Veldhoven (2001), which states that the maximum velocity would occur on the lower part of the slope. Even lower the velocity would be negative, i.e. in a downward direction.

### 5.2.4 Horizontal velocities

To get an idea of the development of the horizontal velocities above the slope in the axis of the jet, measurements were carried out in the x-y plane at  $z = 0$ .

With an interval of 0.10 [m] the area was measured. Figure (5-17) shows the locations.

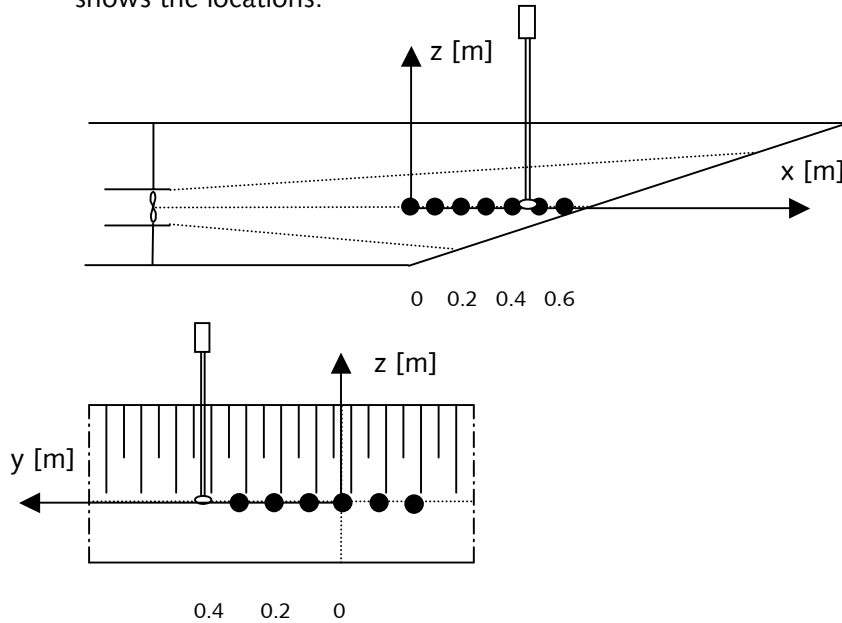


figure 5-17 Locations of the horizontal measurements. Between every point is a space of 0.10 [m]. Distances are in metres.

The interpolated velocities are shown in figure (5-18):

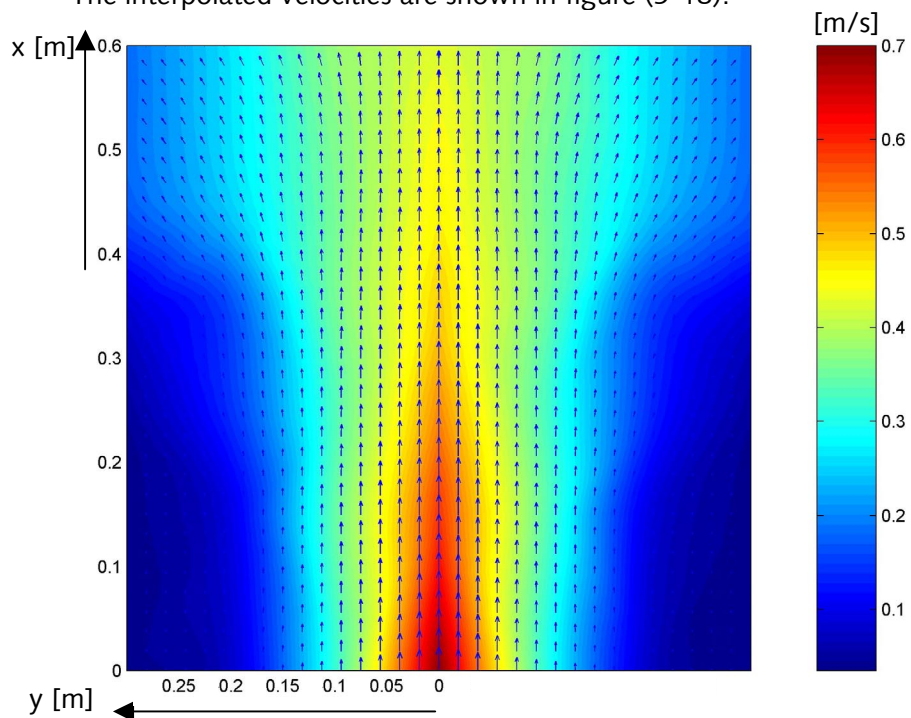


figure 5-18 Horizontal velocities for  $z = 0$ ,  $0 < x < 0.60$  [m],  $-0.3$  [m]  $< y < 0.3$  [m].

---

Figure (5-18) clearly shows that the width of the jet remains practically constant (approximately 0.3 [m]) until it reaches  $x = 0.4$  [m]. There it spreads out quickly and the velocities in the axis ( $y = 0$ ) die down quickly. It is therefore thought that the influence of the slope starts to be noticed at the axis at approximately that location ( $x = 0.4$  [m],  $z = 0$ , i.e. 0.20 [m] before the streamline hits the slope).

So the flow direction is parallel to the x-axis in the entire jet at  $z = 0$  if there is no influence of the slope. This influence is clearly noticeable when figure (5-18) is compared to figure (5-8) where the flow is only parallel to the x-axis on the x-axis itself.

### 5.2.5 Evaluation of the velocity field

The following describes the velocity field in the basin, based on the above description of the measurements.

The jet originates from the propeller with a similar diameter as the propeller and diverges slowly at an angle of approximately 6 [degrees]. The velocities in y and z direction are very small when the undisturbed jet reaches the vicinity of the slope (figure (5-19A&B)).

The slope forces the jet to spread out, creating a pressure zone in front of / above the slope. It is found from measurements that this happens approximately 0.2 [m] to 0.3 [m] before a streamline would intersect with the slope. In this pressure zone the flow velocity remains positive (upward on the slope) and its direction becomes more or less equal to the direction of the slope (figure (5-19A)). In the vicinity of the x'-axis the flow has no velocity component in y direction (figure (5-19C)). Outside the x'-axis the flow on the slope does have a horizontal velocity component perpendicular to the x'-axis, i.e. in y direction (figure (5-19C)), mirrored on the x'-axis.

Eventually the flow reaches the free water surface where it flows to the outlets or circulates in large cells. Otherwise the flow reaches the sidewalls first where it is forced either upwards to the outlets or downwards to circulate in the basin.

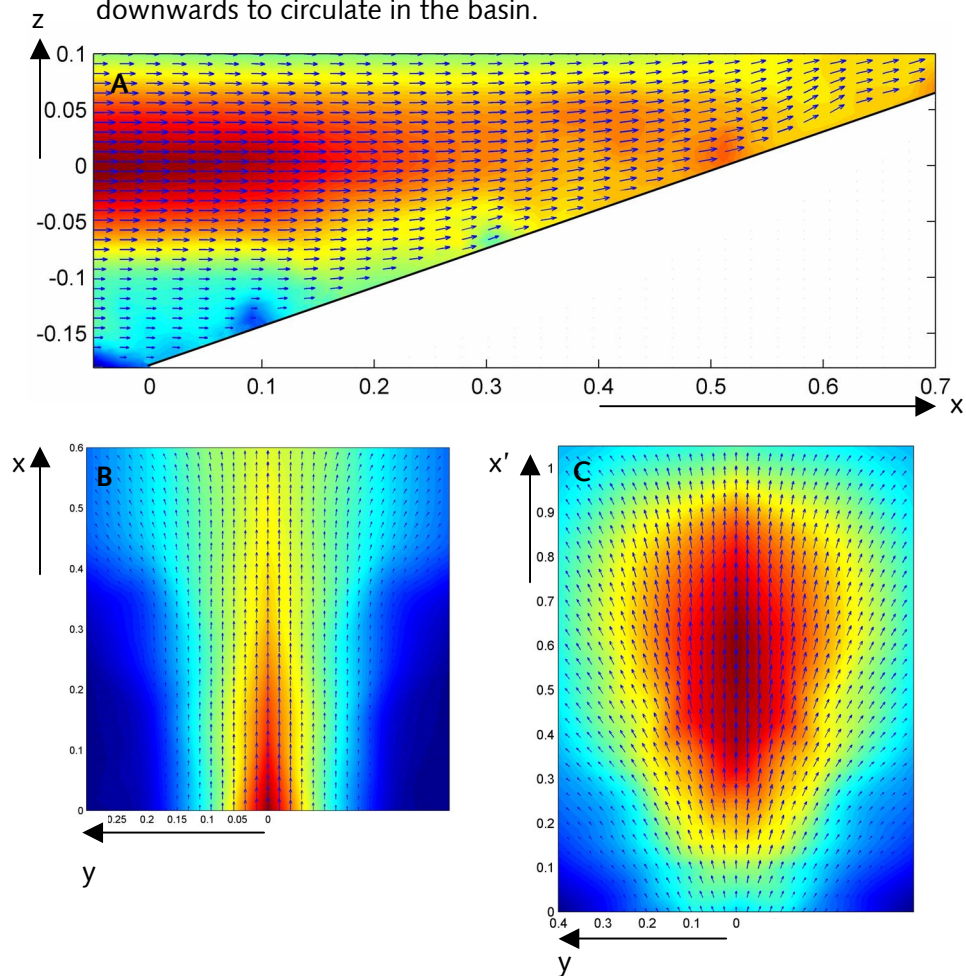


figure 5-19 Copy of the most important velocity field figures (all showing average velocities).

### 5.2.6 Conclusions on the velocity field

The following conclusions on the measured velocities are drawn based on the previous sections.

- All average velocities in x-direction and x'-direction are positive.
- Average vertical velocities are practically zero with the exception of locations close to the slope.
- At locations where vertical velocities do occur they are practically always positive.
- Approximately 0.2 [m] to 0.3 [m] before a streamline would intersect with the slope the influence of the slope becomes clearly noticeable.

## 5.3 Damage location

### 5.3.1 General

Van Veldhoven (2001) found that the maximum damage, induced by a ducted propeller, occurred at  $0 < x' < 0.10$  [m],  $y = 0$ . When looking at the average velocity, figure (5-6), and directly relating this to damage, it shows that the average velocity pattern does not explain the location of the maximum damage. Therefore it is believed that the average velocities are not the determining factor for a stone to move.

### 5.3.2 Peak velocities and turbulence

#### 5.3.2.1 Values along the slope

It is assumed that the peak velocities are the velocities that cause a stone to be lifted from its bed.

As already mentioned and explained in section (4.2.3) the peak velocities are calculated by use of the mean velocity and the turbulence intensity. The turbulence intensity is highest between  $0 < y < 0.10$  [m],  $0 < x' < 0.25$  [m].

In figure (5-20) the turbulence intensities along the x'-axis for  $z' = 0.025$  [m] and  $z' = 0.050$  [m] are shown.

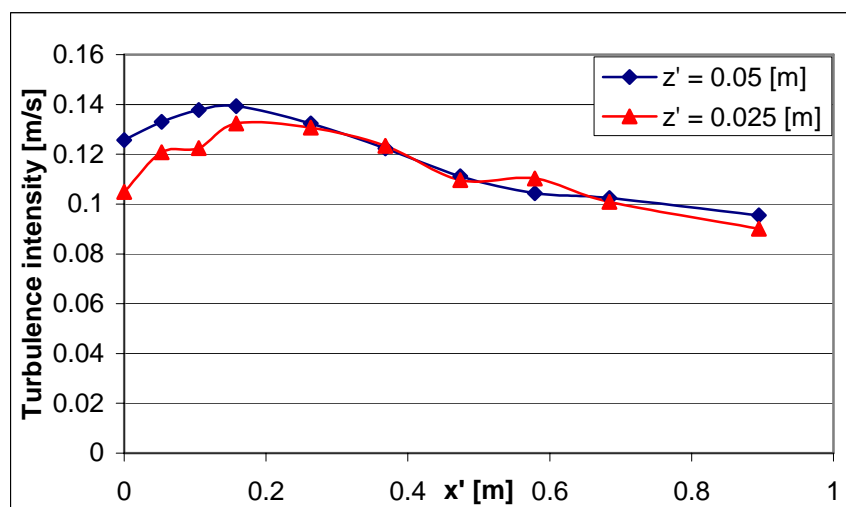


figure 5-20 Turbulence intensities along the slope for  $y = 0$ ,  $z' = 0.025$  [m] &  $0.050$  [m].

Figure (5-20) shows that the turbulence intensities along the x'-axis show quite some irregularities for  $z' = 0.025$  [m]. Since the turbulence intensity is a dominant factor when calculating the peak velocities it is questionable to use the values that are measured so close to the stones. It is believed that small irregularities on the bed combined with the short distance from the bed (2.5 [cm]) to the 3 [cm] large disc of the EMS may be responsible for the irregularities in the turbulence pattern.

In section 5.2.2.2 it was also mentioned that the vortices that are considered to be important to the movement of sediment may be suppressed by the EMS when measuring at 0.025 [m] from the slope.

It is therefore decided, taking all of the above into consideration, to use the values of  $z' = 0.050$  [m] when calculating the peak velocities (see also section (5.3.7) where this choice is justified).

The peak velocity is defined as:

$$\tilde{U}_{\max} = \bar{U} + a \cdot \sqrt{U'^2} \text{ [m/s]} \quad (4-10)$$

where

- $\tilde{U}_{\max}$  : peak velocity in the point considered [m/s]
- $\bar{U}$  : mean velocity in the point considered [m/s]
- $\sqrt{U'^2}$  : turbulence intensity in the point considered [m/s]
- a: constant; often the value 3 [-] is found during experiments.

Previously we found that 'a' equals 3.4 [-] in our model (section 4.2.3).

Furthermore, Izbash (1930) found a correction factor for the stability of stones on a slope, which is dependent on the slope angle and the flow direction (see section 2.2.1.2, Literature study).

Since the slope angle is a constant for every location on the slope, only the water flow direction is important. Since the highest (peak) velocities occur at  $y = 0$  where the flow direction is parallel to the x-axis for all locations it is not necessary to apply the factor of Izbash<sup>26</sup>.

Therefore it is decided to neglect the factor of Izbash. The peak velocities are shown in figure (5-21):

---

<sup>26</sup> This was verified with other locations on the entire slope where different flow directions occur. The locations at  $y = 0$  along the x'-axis however proved to be governing.



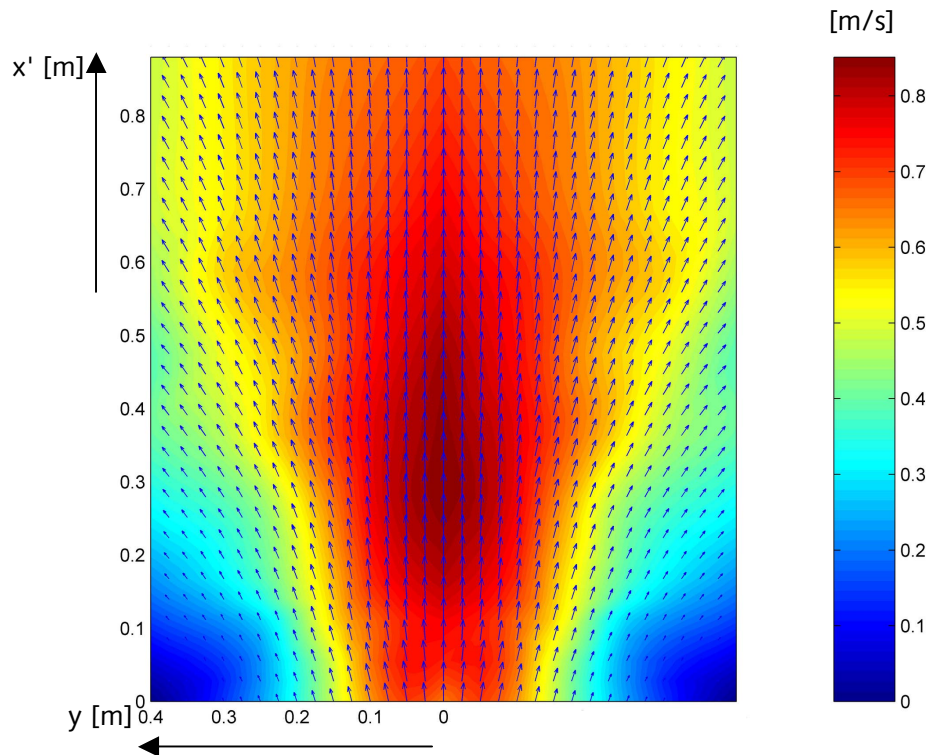


figure 5-21 Peak velocities on the slope,  $z' = 0.050$  [m].

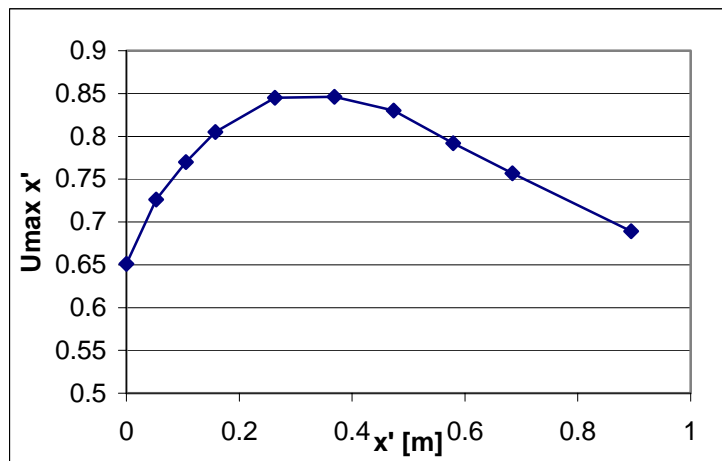


figure 5-22 Peak velocities along the slope at  $y = 0$ ,  $z' = 0.050$  [m].

The maximum peak velocities occur at  $x' = 0.35$  [m],  $y = 0$  [m] (see figure (5-21) & (5-22)).

Consequently, peak velocities also do not explain the location of the maximum damage.

### 5.3.2.2 Location of peak velocities

Van Veldhoven found the following relative turbulence intensities for several distances 'x' from the propeller (figure (5-23)):

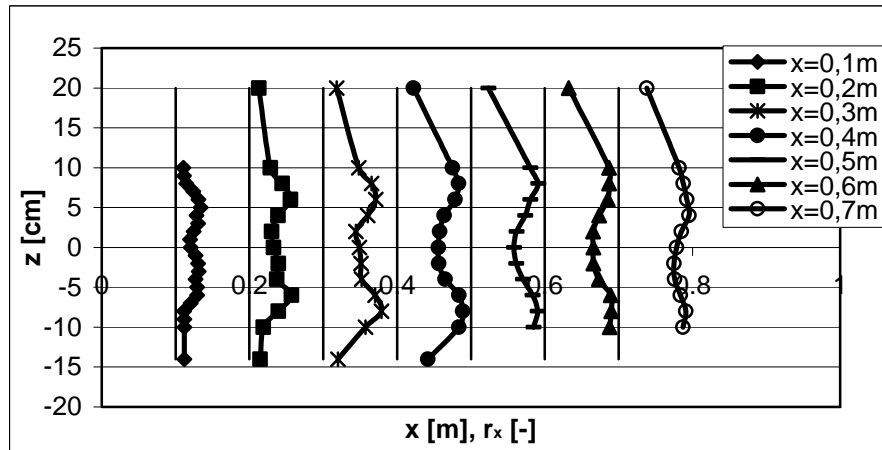


figure 5-23 Turbulence intensities ' $r_x$ ' in the ducted-propeller jet for different distances from the propeller.

The turbulence intensities are normalised with the average velocity on the x-axis resulting in the relative turbulence  $r_x$ . It is clear that the turbulence intensity<sup>27</sup> is highest just above and just below  $z = 0$ . For  $x = 0.7$  [m] the maximum values for the (relative) turbulence intensity occur at  $z = 0.05$  [m] and  $z = -0.09$  [m]. We now compare these values to the turbulence intensities found on the slope (figure (5-20)) since it is expected that high turbulence intensities in the jet will result in high turbulence intensities on the slope.

The high turbulence intensity in the jet found at  $z = -0.09$  [m] corresponds poorly to the maximum turbulence intensity found on the slope at location  $x' = 0.2$  [m] (the height  $z = -0.09$  [m] corresponds to  $x' = 0.3$  [m] on the slope. So the locations (expected versus measured) differ 0.1 [m] from each other).

The maximum turbulence intensity found in the jet at  $z = 0.05$  [m] can however not be related to a maximum on the slope at all since there is no peak found in the turbulence intensity on the upper part of the slope. The reason for this may be the following:

Schiereck (2000) found (from experimental results) that due to a convective<sup>28</sup> acceleration the fluctuations in the direction of the flow decrease.

This leads to the following explanation of the turbulence intensity pattern as found on the slope:

The increase in turbulence intensity in the first part of the slope (figure (5-20)) is explained by the fact that turbulence intensity is low in the lowest part of the jet ( $z < 0.10$  [m]) (figure (5-23)) and increases with increasing height until  $z = -0.09$  [m]. The growth of this turbulence is however negatively influenced by the acceleration

<sup>27</sup> Since the turbulence intensities at a certain distance from the propeller were all normalised with the same average velocity at the x-axis, the relative turbulence intensity at a certain distance from the propeller in figure (5-23) is also a measure for the turbulence intensity itself and can therefore be used to compare turbulence intensities within the same profile.

<sup>28</sup> A convective acceleration is an acceleration in space.

---

of the water. Therefore, when the increase of the turbulence intensity with increasing height in the jet stops at  $z = -0.09$  [m], the turbulence intensities on the slope start to decrease fast.

At  $x' = 0.75$  [m] one would expect to see the influence of the maximum turbulences in the jet at  $z = 0.05$  [m] (figure (5-23)), especially since we deal with decelerating water here which has a positive influence on the growth of turbulence intensities. However, this influence is not noticed. This might be caused by the longer distance to the slope: At  $x = 0.7$  [m] from the propeller the distance to the slope at a height of  $z = -0.09$  [m] equals  $0.2$  [m]. At a height of  $z = 0.05$  [m] this equals  $0.6$  [m]. The turbulent fluctuations therefore have more time to lose their energy and die down.

**Remark:** Even though the **relative** turbulence intensity (relative to the local velocity at the x-axis) seems to grow or remain constant as the distance from the propeller grows (figure (4-13)) the turbulence intensities themselves die down with increasing distance from the propeller. In the above we are dealing with the values of the turbulence intensities, not relative turbulence intensity.

### 5.3.3 Frequency and energy analysis of vortices

Some analysis on the data set will be carried out concerning autocorrelation and power density spectra (PDS). This is done to gain some more insight in the size and frequencies of vortices in the jet and of vortices in the vicinity of the slope. Since it does not directly contribute to the goal of this chapter (which is to find an explanation for the location of the damage on the slope) but since it is considered worth investigating, it is decided to put it in appendix D and it is only meant for the reader who is interested in the above mentioned subjects.

The conclusions are repeated here:

#### Conclusions

From the two sections, autocorrelation and power density spectrum, the following is clear:

- The average governing vortex at the slope has a diameter of approximately  $0.14$  [m]. The smaller governing vortices could not be detected with this method.
- It follows from the power density spectrum that the energy in the vortices at the slope is considerably less than the energy in the vortices just behind the propeller.
- From the power density spectrum it is also concluded that at the slope the energy is found in the relatively large vortices, with no distinct energy peaks at any frequencies. Just behind the propeller however there is a distinct increase of energy in vortices with a frequency of  $1$  [Hz] and  $5$  [Hz]. The size of these vortices is believed to be at most  $0.10$  [m] (which equals the diameter of the propeller) respectively  $0.02$  [m].

### 5.3.4 Flow direction and slope

As already noted in section 5.2.2.4 it is clear that the water direction makes an angle of less than zero degrees with the x'-axis at the lower half of the slope, whereas at the upper half of the slope this becomes practically zero. So the water is directly penetrating into the protection layer of the slope, which has a destabilising effect on the stones. However, since the (peak) velocities are small at the lower half of the slope it is believed that this may contribute to the greater damage, but is not solely responsible for it.

Therefore it is decided to look at the start of movement in some more detail.

### 5.3.5 Shear velocity

Let us consider a particle in a body of water (figure (5-24)):

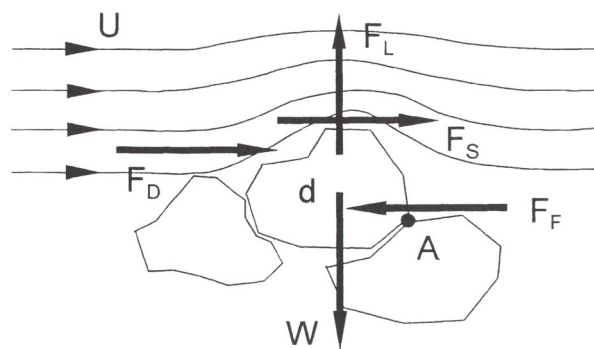


figure 5-24 The forces acting on a stone in a body of flowing water with a constant average velocity in time and space.

As long as the stone does not move there is equilibrium between the resisting force and the acting force.

Three acting forces can be distinguished:

$F_d$ :	Drag force [N]
$F_s$ :	Shear force [N]
$F_l$ :	Lift force [N]

These forces are balanced by the resisting forces of the stone:

$W$ :	Weight of the stone [N]
$F_f$ :	Friction force [N]

which are both directly related to the submerged weight of the particle.

The acting forces can be related to the particle diameter, water density and the water velocity.

In formula:

$$\rho_w \cdot u^2 \cdot d^2 \propto (\rho_s - \rho_w) \cdot g d^3 \quad (5-1)$$

Furthermore the following relationship holds, in which the shear stress, which represents all the acting forces, is defined as a function of the bed roughness and the velocity of the water:

$$\tau = \rho_w \cdot u^{*2} \quad [\text{N/m}^2] \quad (5-2)$$

where

$\tau$ : shear stress [ $\text{N/m}^2$ ]

$u^* = u \cdot \frac{\sqrt{g}}{C}$  shear velocity [ $\text{m/s}$ ]

$C = 18 \log(12 \cdot h/k)$  Chézy constant [ $\text{m}^{1/2}/\text{s}$ ]

$h$ : water depth [ $\text{m}$ ]

$k$ : roughness of the bed, equals 2 to 3 times the  $d_{50}$  [ $\text{m}$ ]

So the shear stress is related to the square of the velocity. If we calculate the resulting shear stress for each measured point at  $y = 0$  and multiply it with the area it acts on we derive the shear force 'Fs' ( $F_s = \tau \cdot A$ ).

For the area on which this shear stress acts the area of the sectional plane ( $\frac{1}{4} \cdot \pi \cdot d^2$ ) is taken. This leads to the following figure (5-25):

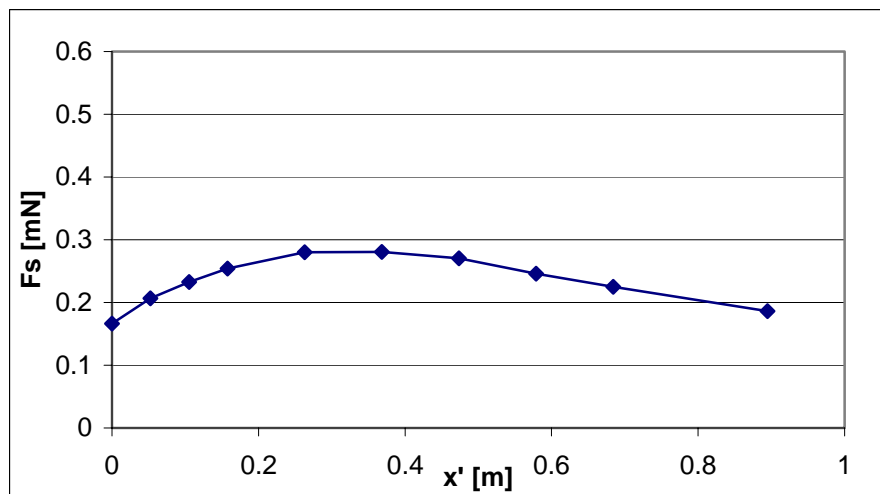


figure 5-25 Shear force for  $y = 0$  at the slope.

### 5.3.6 Pressure gradient

Figure (5-22) shows that there is a considerable convective acceleration in the first section of the slope. This acceleration causes a pressure difference 'dp' between two points along a streamline.

Let us consider a particle in an accelerating body of water (figure (5-26)):

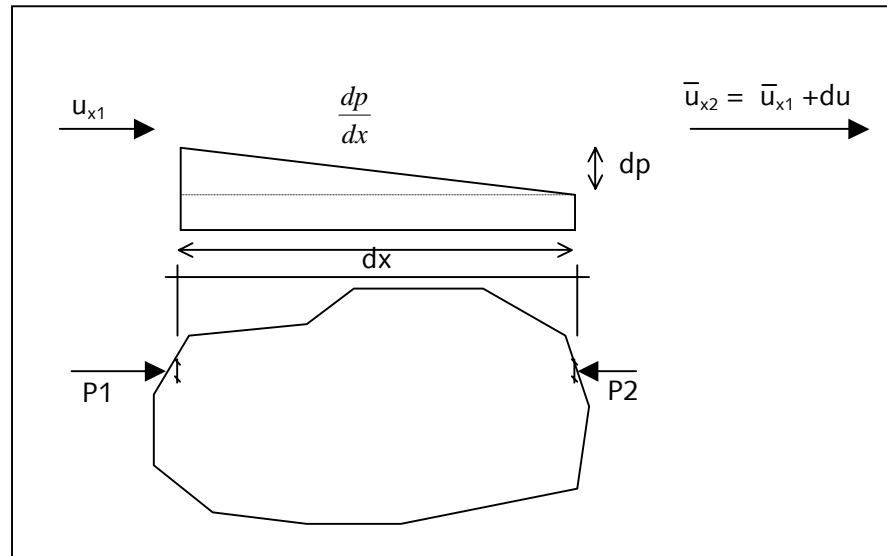


figure 5-26 Pressure difference over a stone in an accelerating body of water.

The pressure difference caused by the accelerating water in space results in a pressure difference over a distance  $dx$ , equal to

$$dp = \frac{1}{2} \rho \cdot (u_{x2}^2 - u_{x1}^2) \text{ [N/m}^2\text{]} \quad (5-3)$$

(This follows from Bernoulli's theorem:  $\frac{U^2}{2g} + \frac{p}{\rho g} + z = \text{constant}$

along a streamline)

We assume that over the (small) length of the stone that

$$\frac{dp}{dx} = \text{constant.}$$

The pressure difference  $dp$  between two locations  $x_1y_1z_1$  and  $x_2y_1z_1$  on the stone then equals:

$$dp = \frac{dp}{dx} \cdot dx \text{ [N/m}^2\text{]} \quad (5-4)$$

If we take a small area on the surface of the particle,  $dy \cdot dz$  [ $\text{m}^2$ ], the resulting force  $F$  on this area equals:

$$F = A \cdot dp = dy \cdot dz \cdot \frac{dp}{dx} \cdot dx \text{ [N]}. \quad (5-5)$$

---

The total force on the particle therefore equals

$$F_p = \iiint \frac{dp}{dx} dx dy dz \text{ [N]} \quad (5-6)$$

$\frac{dp}{dx}$  is a constant, and  $\iiint dx dy dz$  equals the volume of the particle 'V' [m<sup>3</sup>] when integrated to the boundaries of the particle.

The force on the particle then becomes

$$F_p = V \cdot \frac{dp}{dx} \text{ [N]} \quad (5-7)$$

We will use here

$$F_p = V \cdot \frac{dp}{dx} \cdot 1000 \text{ [mN]} \quad (5-8)$$

Since the maximum velocities and maximum acceleration takes place at  $y = 0$ , the rest of the slope is discarded. This leads to the following graph (5-27) for the pressure force 'F<sub>p</sub>' for  $y = 0$ .

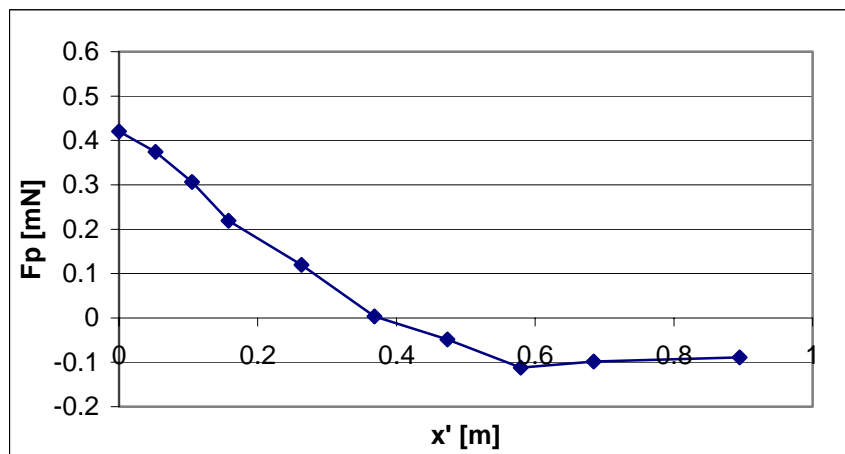


figure 5-27 Pressure force along the slope for  $y = 0$ .

### 5.3.7 Total force on a stone

If we add this force ' $F_p$ ' to the shear force found earlier on the stone ( $F_s$ ) this accumulates to the following graph (5-28):

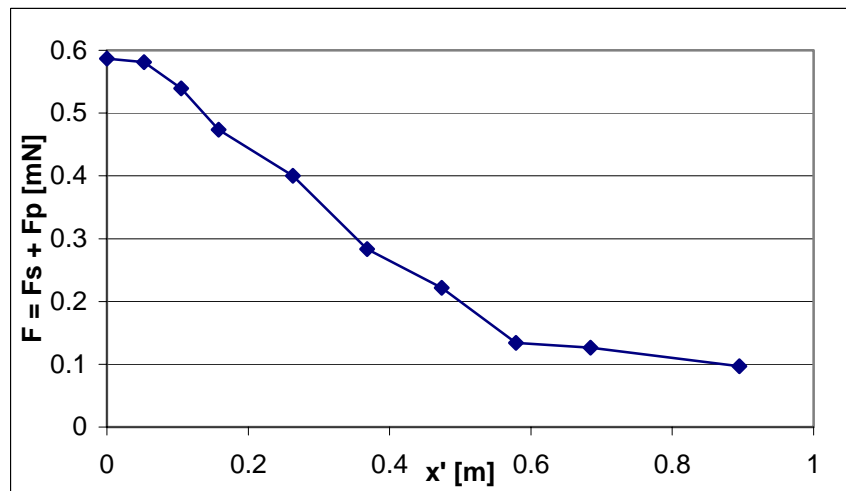


figure 5-28 Total upward force on the stone.

It appears that when the pressure difference caused by the accelerating water is taken into account the resulting upward force on the stones has a maximum between  $x' = 0$  and  $x' = 0.10$  [m], complying with the area of maximum movements<sup>29</sup>.

**Remark:** As mentioned in section 5.3.2.1, the choice was made to use the values for the average velocity and turbulence intensity of  $z' = 0.050$  [m] for calculating the peak velocities. Since these values are larger than the values at  $z' = 0.025$  [m] it was checked what the differences in the results between the two are.

Since the absolute values of velocity and turbulence intensity are smaller at  $z' = 0.025$  [m] than at  $z' = 0.050$  [m] but the acceleration at  $z' = 0.025$  [m] is larger than at  $z' = 0.050$  [m] the difference ended up to be small:

- The location of the maximum force is approximately the same, between 0 and 0.15 [m] from the toe of the slope.
- The difference in maximum total upward force was found to be 0.03 [mN] less for the measurements at  $z' = 0.025$  [m] than for the measurements at  $z' = 0.050$  [m], a difference of approximately 5 [%].

Therefore it is concluded that the choice of using the data derived at  $z' = 0.05$  [m] is justified.

<sup>29</sup> One can also add the penetration of the water at the lower half of the slope to this (section 5.2.2.4), which has a destabilising effect. Since this is assumed to be of minor influence due to its small velocity, no quantitative analysis is given here.



---

### 5.3.8 Direction of movement

In figure (5-29) it is noted that the stones have a propensity to move downward at the lower part the of damage area and to move upward at the upper part of the damage area.

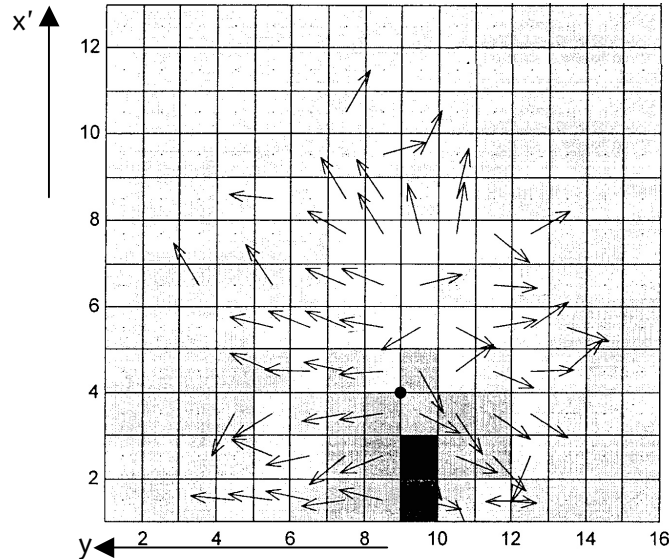


figure 5-29 Location of maximum movements and their direction. Every square equals 0.05 [m] by 0.05 [m].

As noted in section 5.2.2.2 the water velocity along the entire slope is positive (upward). When a stone is lifted and dragged out of its bed, it is believed that the direction of the stone's movement is determined by the following forces:

- The shear stress due to the average velocity.
- The pressure gradient.
- The gravity force.

Since the gravity force is constant (along the slope), we will focus here on the development of the shear stress and the pressure gradient along the slope at  $y = 0$ .

The average velocity at the bed at  $z' = 0.025$  [m]<sup>(30)</sup> is shown in figure (5-30):

---

<sup>(30)</sup> This height was chosen since as mentioned in section 5.2.2.4 there seems to be little error in the average velocity measurements at  $z' = 0.025$  [m] (in contradiction to the peak velocities at this height which are calculated with the use of the turbulence intensities).

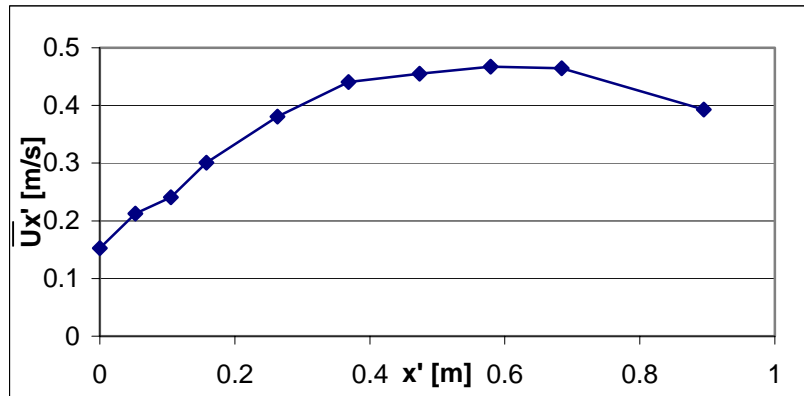


figure 5-30 Average velocity along the slope for  $z' = 0.025$  [m] and  $y = 0$ .

The following figure (5-31) shows the shear force, the pressure force and the resulting total force.

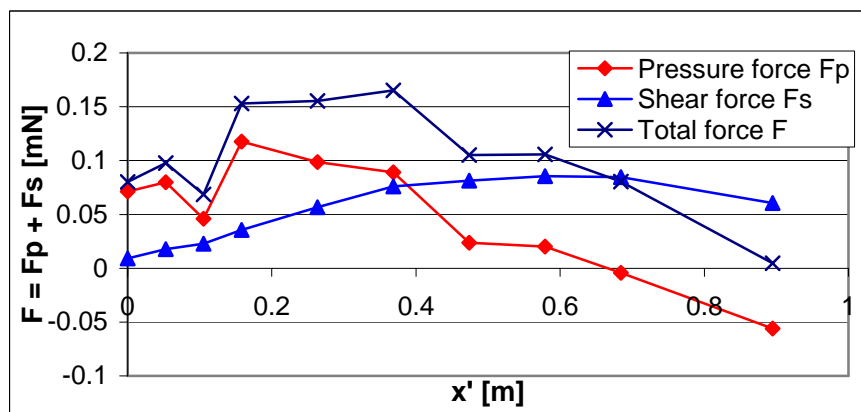


figure 5-31 Acting forces on stone lifted from its bed.

The graph shows that the total upward force is at its largest between  $x' = 0.15$  [m] and  $x' = 0.40$  [m]. This is approximately the area in which the stones move upward. It is therefore believed that in the other areas the downward force (gravity) is larger than the upward force when a stone is set in motion<sup>31</sup>.

<sup>31</sup> It is not useful to subtract this gravity force from the found acting force 'F' to derive a net force for two reasons: The accuracy of the found shear force 'Fs' is not known and furthermore all values were derived at a rotation rate of the propeller at which more than 100 stones would have moved already.

However, it seems that the influence of the small dip in the velocity at  $x' = 0.10$  [m] is quite large. If this point is neglected (to investigate the sensitivity of the theory) the following graph appears:

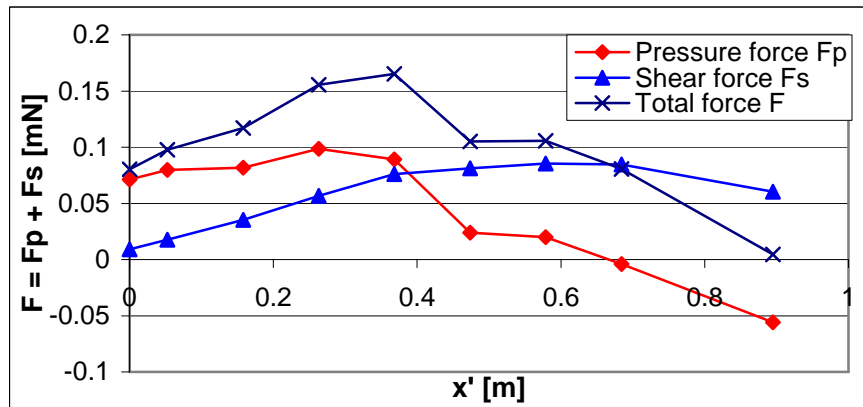


figure 5-32 Acting forces on stone lifted from its bed, point at  $x = 0.10$  [m] is neglected.

The maximum upward force is now largest between  $x' = 0.25$  [m] and  $x' = 0.45$  [m].

So a small discontinuity is of large influence on the resulting force, making the whole mechanism very sensitive for small errors in measuring or for discrepancies on the bed.

Since it is not known in which way the equation (5-2) is accurate in a situation like this<sup>32</sup> it is decided not to try and relate the direction of the stone to the total force, i.e. including the gravity.

When the particle is moving in a certain direction equation (5-2) cannot be used any longer. However, it seems justified to calculate the **initial direction** with equation (5-2) and (5-8) (the stone is lifted from its bed but does not have any velocity yet).

**Remark:** Another mechanism that may contribute to a gradient in the upward force along the slope is the fact that a fully exposed stone (lifted from its bed) experiences more drag force since it is no longer being (partly) protected by other stones. This also increases the shear force since the bottomside of the stone now experiences shear stress as well. The pressure difference remains constant. This mechanism would increase the effect of the average water velocity and it would therefore change the location of the area of maximum force slightly to the right in figure (5-32), and will also increase its maximum value.

<sup>32</sup> There are a few effects that are uncertain. Turbulences for instance are only used here to calculate the peak velocities. It is not clear what for instance the effect will be when a vortex occurs only at one side of a stone instead of occurring over the entire stone. Also the area on which the shear force acts is based on an assumption, making the outcome in exact numbers less certain.

---

### 5.3.9 Conclusions on the damage location

It appears, based on the previous section, that two mechanisms are responsible for the initiation of movement of a stone in a body of water, which is accelerating in space:

- The shear stress of the water on the stone.
- The pressure difference caused by the velocity difference over the stone.

The combined action of these two mechanisms is found to be largest at the toe of the slope in our model when the peak velocities are considered. When the average velocities are considered the combined action proves to give a maximum result higher on the slope.

This therefore indicates that the turbulences present in the water are largely responsible for the movement of a stone. Its direction is not determined by the turbulences.

## 5.4 Conclusions

It is concluded that neither the local average velocities nor the local peak velocities are solely responsible for the movement of a stone. The pressure difference caused by a difference in water velocity over a stone should be regarded as an important mechanism for the initiation of movement of the stone.

The turbulence intensities are largely responsible for the movement of the stones: directly by initiating an enlarged shear stress and indirectly by initiating an enlarged pressure difference over the stone.

The hypothesis of Van Veldhoven (2001) (see section 5.1) is rejected based on the following:

- There is no evidence found that the maximum velocity in the jet (i.e. in the jet axis) changes direction, neither in front of the slope nor above the slope. This is based on the measurements performed by the author and partly based on Van Veldhoven's own measurements. The highest velocities above the slope occur in the axis of the jet, and this axis continues in a horizontal line originating from the propeller axis and therefore reaches the slope much higher than where the maximum damage occurs.
- No 'pressure point' is found (i.e. the point of which Van Veldhoven believes that above this point the velocities would be positive, and below this point they would be negative).

---

## 6 Damage investigation

### 6.1 General

#### 6.1.1 Approach

In this chapter propeller induced-scour in the Dutch inland waterways will be treated.

Propeller-induced scour originates from either the mainthrusters or the bowthrusters of a ship.

The goal is to determine whether or not one should concern oneself with the effect of bowthrusters when looking at scour in the vicinity of quays.

One can assume that the maximum scour will be caused by the system that gives the maximum and longest hydraulic load. There is no general knowledge whether bowthrusters may be governing for the bottom protection in the inland waterways. This investigation will focus on the damage done by bowthrusters. In order to do that, it is necessary to make an inventory of all scour in the channel and then (try to) relate it to either bowthrusters or mainthrusters.

#### 6.1.2 Data collection

Since bowthrusters are mainly used during berthing and unberthing, possible scour related to bowthrusters can be found at berthing places. Most berthing places do not have any kind of bottom protection. An investigation was carried out to determine what the problems concerning scour in the vicinity of berthing places are and if there are indications that bowthrusters should be of concern to the maintenance and protection of these quays.

A very important role in an investigation like this is the kind of information that is available and where it is available. Sources inside the Rijkswaterstaat indicated that the Julianakanaal might be a good place to start since they might be encountering problems concerning scour induced by bowthrusters.

Decided was to start the investigation there. Contact was made with the operation and maintenance division of Limburg.

It proved difficult to get information like echo soundings of the channel or to find people who were under the impression that there were any problems in the Julianakanaal.

Eventually it was decided that the Julianakanaal was not a suitable location to acquire data from.

This was later justified by a letter from the local operation and maintenance division that there was no data available neither was anybody under the impression that there was a problem. Therefore a different location had to be found.

The ports of Rotterdam and IJmuiden also proved to be dead ends due to the unavailability of a helpful staff and/or data.

---

Eventually this led to the operation and maintenance division of the Amsterdam-Rijnkanaal. Here it was possible to acquire relatively up to date data and a helpful staff.

They were experiencing some scour problems in the Amsterdam-Rijnkanaal.

**Remark:** The data that is presented in this chapter and the conclusions that are drawn based on it are valid only for the Amsterdam-Rijnkanaal and does not apply on every canal in the Netherlands. It can therefore be considered as a case study.

A meeting took place with some of the maintenance engineers of the berthing places and also with the head of the vessel traffic department.

The situation appeared to be the following:

- The Amsterdam-Rijnkanaal is an artificial canal of about 70 kilometres long and 100 metres in width. It is defined as a class VIb waterway. It holds approximately 15 berthing places, either waiting places in front of a sluice, or places for spending the night.
- The water level varies between NAP  $-0.4$  [m] and NAP  $-0.6$  [m]. The guaranteed bottomlevel at the berthing places and in the channel is NAP  $-5.6$  [m]<sup>33</sup>.
- The Amsterdam-Rijnkanaal serves approximately 100.000 ships in one year.
- Echo-soundings of the entire depth profile of the channel are available.
- There are quite a few scourholes along the berthing places, but most of them are not close to the sheetpile construction. Of all the berthing places only two are of concern, namely the 'Plofsluis' near Nieuwegein. Also at a car-unloading-point<sup>34</sup> at the Roosenveltlaan they are experiencing scour.
- There is only one place that has a bottom protection, the northern berthing place at Wijk bij Duurstede.

### 6.1.3 Experience from practice

In a meeting the 'expert opinion' of the engineers and also of the head of vessel traffic department about scour caused by bowthrusters was investigated.

Based on their experience they all think that the bowthrusters induce considerably less damage than the main thrusters. Their explanation for this is that the duration of the use of bowthrusters is

---

<sup>33</sup> The maximum allowed draught of a ship in the Amsterdam-Rijnkanaal is 4.0 [m]. With 1.0 [m] keel clearance and a minimum water level of NAP  $-0.6$  [m] this leads to a minimum bottom level of NAP  $-5.6$  [m].

<sup>34</sup> At this location the skippers can unload their private vehicle from their vessel.

---

considerably less than the use of main thrusters and the power installed is much less for bowthrusters than it is for main thrusters.

A staff member of the department Limburg, among other things responsible for the data processing at the Julianakanaal, also asked some captains about their opinions<sup>35</sup>. The results were similar to the ideas of the personnel at the Amsterdam-Rijnkanaal. In addition, they thought that when departing the mainthruster passed the location of the bowthruster and would wash over whatever scour the bowthruster would have induced.

These findings are not based on any data or hard facts, but on their expert opinions, which are based on experience. This is a scientific report that mainly deals with facts rather than opinions. Obviously their opinions are not neglected here. These people are doing the maintenance of quays on the Amsterdam-Rijnkanaal for a long time and all experienced the growth of the ships and the growth of bowthrusters and their powers installed.

The captains of the ships have a good feeling of the powers they use to manoeuvre their ship and the impact it may have when they use them.

It is the opinion of the author that their common sense of the matter is obviously a justifiable fact for this report.

In the meeting at the Amsterdam-Rijnkanaal also echo soundings of all berthing places were retrieved. They were simple soundings made approximately 5 metres outside the berthing places. This gave a first indication of which might be interesting places to investigate.

---

<sup>35</sup> Unclear is in what way captains will respond in a conservative way to the question what they think about the damage their bowthrusters induce.

---

#### 6.1.4 Selected waterway

Figure (6-1) shows the Amsterdam-Rijnkanaal and the main places along the canal.

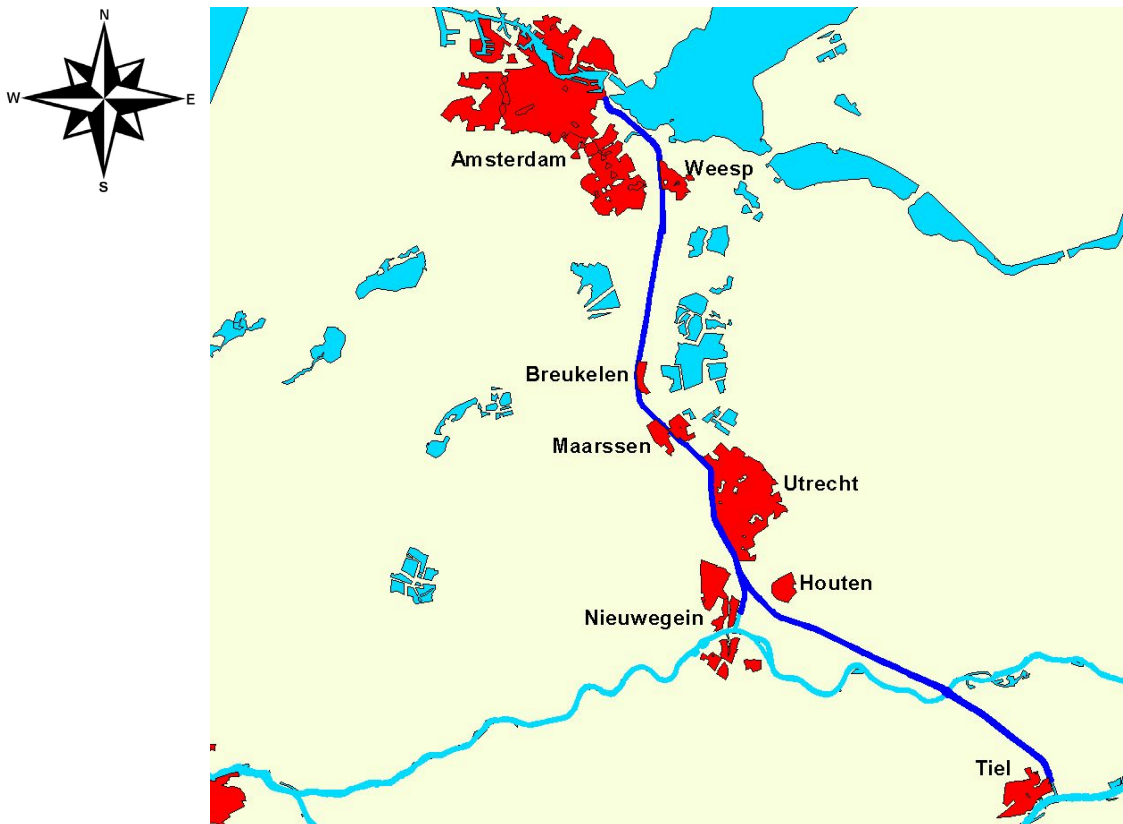


figure 6-1 The Amsterdam-Rijnkanaal with the main towns situated next to it.

Based on the first set of indicative echo soundings it was decided what locations to visit and to investigate.

#### 6.2 Background on berthing and scour

If one wants to relate scour to a certain mechanism, like a jet coming from a bow- or mainthruster, one must first establish whether this mechanism was solely responsible for the development.

To do this, we must consider the following:

Scour is a time dependent phenomenon. It needs a certain time of a certain load to derive a certain depth.

In order for this to happen a ship must use its bow- and mainthrusters long enough for the two (independent) scourholes to develop.

So if a scourhole has been developed by a berthing or unberthing ship, the next ship can enlarge it when it is at the same position as the first one. To have it enlarged by the same mechanism it also has to be berthed in the same direction (or the location and the



---

direction have to be different which could in the case of bowthrusters lead to a hydraulic load at the same location. In the case of mainthruster the direction of the flow will be opposite in that situation).

Since most berthing places are meant to serve both directions of the Amsterdam-Rijnkanaal ships will berth in two directions as well. The operations and maintenance division of the Amsterdam-Rijnkanaal indicated that there is no regularity at all in the berthing. Ships are allowed to berth at every spot and in every direction they like.

This also means that scour can be reduced by the next ship, filling up the scourhole with material coming from the hole he is developing at another location, resulting in a movement of the scourhole.

Further more, the transport along the quay induced by the mainthrusters may even out, only transporting the particles back and forth.

The following mechanism may also be (partly) responsible for levelling scourholes (Operation and maintenance division Limburg, 2002): When leaving, the ship passes the scourhole he just made with his bowthruster and fills and flattens it with his much more powerful mainthruster. This depends of course at how steep an angle the ship departs (at low angles the ship will surely pass the location of the bowthruster-induced scour, at a steep angle it will not). This again will be dependent on the length of the quay, whether or not the quay has an indentation and the presence or absence of other ships. At long quays, with no indentation and no other ships just in front of the departing ship there is not much reason to depart at a steep angle.

Taking all the above into account, it is unlikely that at these long quays the scour that develops comes from one mechanism, but it is more likely to be a combination of bow- and mainthruster-induced scour.

In the next sections it is concluded whether or not the above statement is true.

## **6.3 Uniform quays**

### **6.3.1 General**

First some uniform quays were selected. A uniform quay is defined in this study as a long quay ( $L > 500$  [m]) with no distinct geometrical anomalies.

The quays at Maarsse, Nieuwegein, Houten and Breukelen were selected to investigate in more detail (figure 6-1).

At each of these quays the scour patterns appeared to be similar. As an example Maarsse will be treated.

---

## 6.3.2 Examples of uniform quays

### 6.3.2.1 Maarssen

The quay at Maarssen is located just north of Utrecht (figure (6-1)). It has a berthing place on the east side of the Amsterdam-Rijnkanaal only. The occupancy rate is approximately 25 [%].

It serves ships both coming from north and south. It is a long quay (approximately 1 [km]) with an average depth of 5.5 [m] to 6.0 [m]. Figure (6-2) shows the berthing place with the city of Utrecht on the background<sup>36</sup>.



figure 6-2 Berthing place at Maarssen.

---

<sup>36</sup> In the case shown in the photograph the vessel sailed all the way to the end of the quay before berthing, a manoeuvre noticed regularly.

Some parts of the bathymetry along the quay are shown in figures (6-3) and (6-4). The upper panel of these figures shows the bathymetry map and the lower panel the depth profile parallel to the quay at a distance of approximately 5 [m] from the quay, from north to south.

(The colours in the depth profiles in the entire section represent relative depths. Dark red means relatively shallow water, light red means relatively deep water).

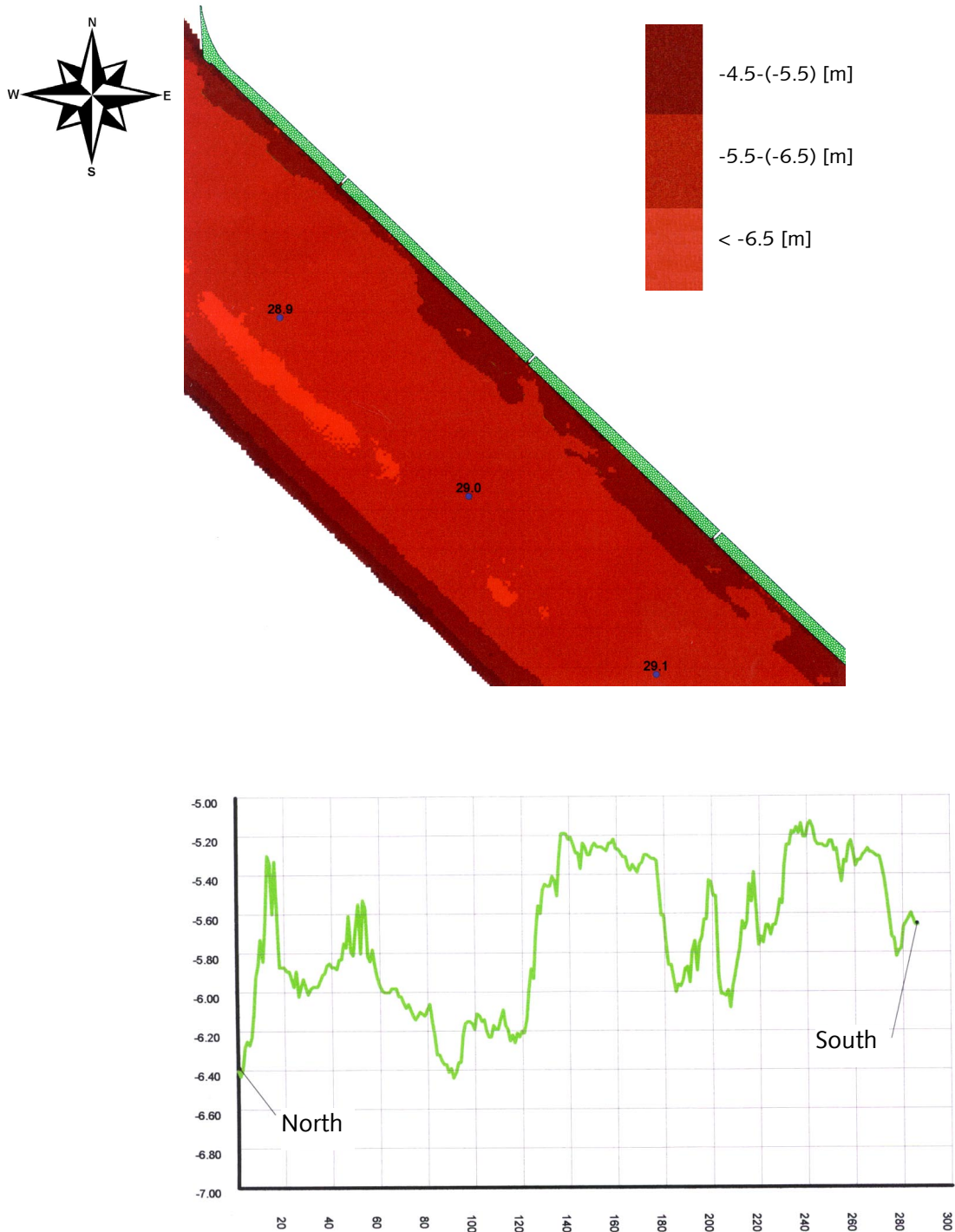


figure 6-3 Bathymetry at Maarsse. All values are in metres. Reference level for depth profile (5 [m] outside the quay) is NAP.

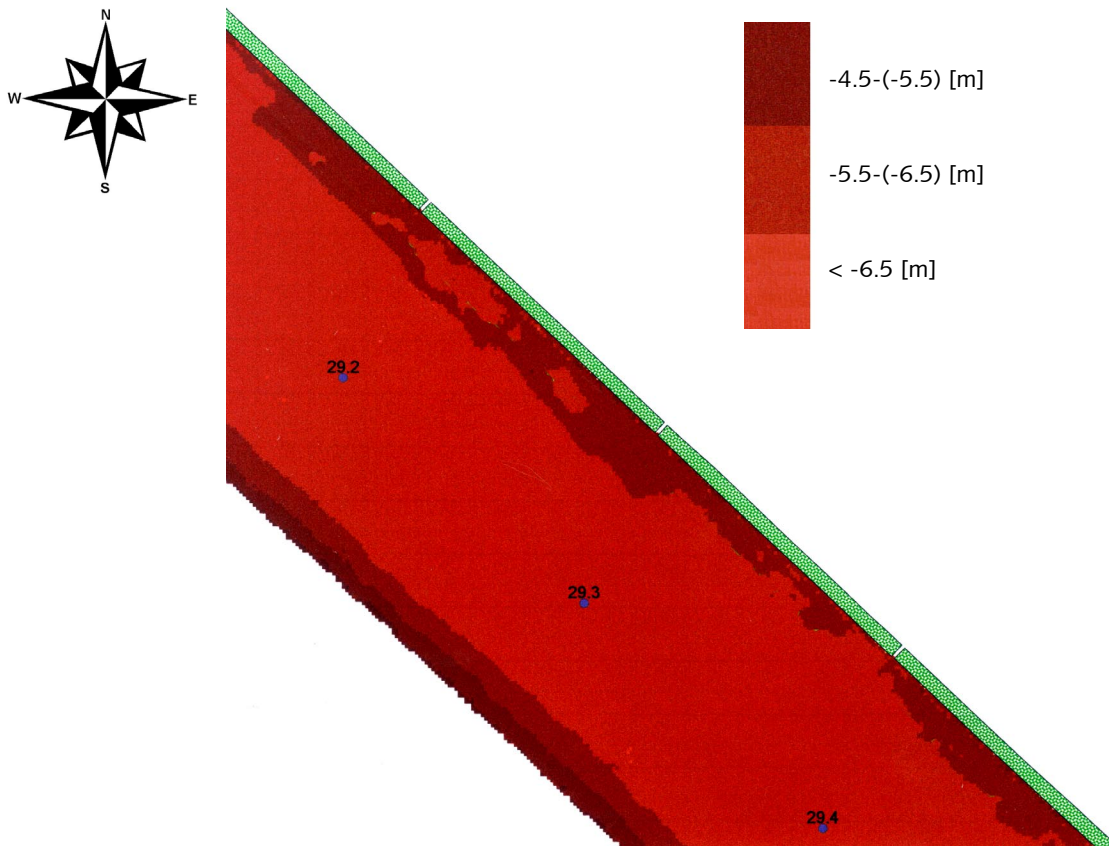


figure 6-4 Bathymetry at Maarsse. All values are in metres. Reference level for depth profile (5 [m] outside the quay) is NAP.

As can be seen in figure (6-3) and (6-4) the depth is smallest close to the quay, with some local scourholes. The scour is not connected to the sheet pile structure, except for location 29.38 [km]. The deepest hole found here has a bottom level at NAP  $-6.50$  [m],

---

which means a depth of 0.90 [m] compared to the surrounding bottom level.

### 6.3.2.2 Other quays in the Amsterdam-Rijnkanaal

In the Amsterdam-Rijnkanaal also the berthing places at Nieuwegein, Houten and Breukelen were investigated. They all show similar scour patterns as mentioned above. They are all fairly long quays (approximately 1 [km]) and they all serve ships in two directions (at Houten and Nieuwegein there is also a possibility to berth at the other side of the canal, but they are considerably shorter, so at busy times ships from both directions will berth at the long quays)

### 6.3.2.3 Douanekade Sas van Gent

As an example of a quay outside the scope of the Amsterdam-Rijnkanaal the quay at Sas van Gent was visited and investigated. It complies with the definition of a uniform quay and is located on the border of the Netherlands and Belgium. Only the Dutch part was investigated.

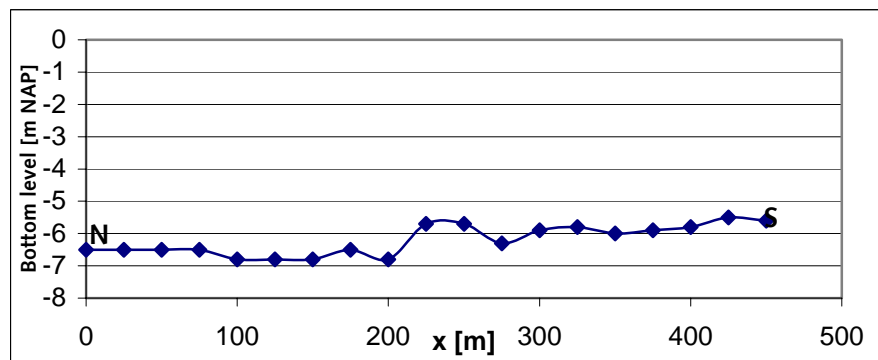


figure 6-5 Bathymetry at Sas van Gent. All depths are in metres. Reference level is NAP.

The depth profile (figure (6-5)) shows that on the northern part the depth is largest, approximately 1 [m] deeper than on the south side of the Dutch part. Also here, as in Maarsssen, there is no regularity in the berthing of ships (direction and location wise). Since the profile does not show large fluctuations it is believed that the deeper section on the north side is caused by more intense use than the south side, possibly because of the orientation of the border. Because of the irregularity in berthing, the scour caused by bow and main thrusters is evenly distributed over the entire length, causing no distinct large holes.

---

### 6.3.3 Conclusions on uniform quays

From the investigation on uniform quays the following is concluded:

- The scour is shallow.
- It is not possible to separate bow- and mainthruster-induced scour.
- There are two dominant mechanisms that are believed to lead to shallow scouring:
  - The irregularity of the location of bow- and mainthruster when scour is induced.
  - The interaction between bow- and mainthruster on a certain scour location.

This leads to the following two consequences:

- Scourholes along uniform are not suitable to derive data from when the aim is to make a separation between scourholes that originated from mainthrusters and those who originated from bowthrusters.
- Scourholes along uniform quays will in general not endanger the sheetpile structure.

Therefore it is concluded that to investigate the problems related to bowthruster one needs to do this were the ships are forced to berth in a logical and consistent way, which leads to non-uniform quays.

**Remark:** It is known that during hazardous situations ships are sometimes forced to use their thrusters more intense and for long intervals. This may lead to very high local scour depths. Even though this scour will be replenished in a natural manner, a situation like this may momentarily endanger the sheetpile construction.

## 6.4 Non-uniform quays

### 6.4.1 General

The hypothesis is that along non-uniform quays (for instance short quays, or quays with distinct geometrical anomalies) it is likely to see larger erosion depths and possibly a difference in scour pattern between bow- and mainthrusters.

It is for instance known that in ports where large ferries berth, which berth at exactly the same spot every time, a different protection is used at different locations. Loose stones for instance are used at the location of the bowthruster, and bituminised larger stones (heavy protection) are used at the location of the mainthruster.

Some locations in the Amsterdam-Rijnkanaal are selected that probably do have some regularity in their berthing. They were visited for a visual inspection to determine whether the layout leads to the so-called logical berthing, i.e. berthing at approximately the same location and in the same direction each time.



## 6.4.2 Examples of non-uniform quays

### 6.4.2.1 Roosenveltlaan

The Roosenveltlaan is the location with the largest scour depth in the Amsterdam-Rijnkanaal. This scour depth occurs at the car-unloading-point. At this spot a scourhole of 3.5 [m] developed. When the ships drop of the car, they attach their bow to the quay with a line and keep their main thrusters running to keep tension on it. Since this scour is so dominant at this location and closely and logically related to mainthrusters this proved to be an uninteresting point to look at the phenomenon of bowthruuster-induced scour.

### 6.4.2.2 Location Plofsluis

At kilometre number 42.7 the Lekkanaal joins the Amsterdam-Rijnkanaal. See figure (6-6) and (6-7). The operation and maintenance division is concerned about the scourholes that have developed<sup>37</sup> at this location.

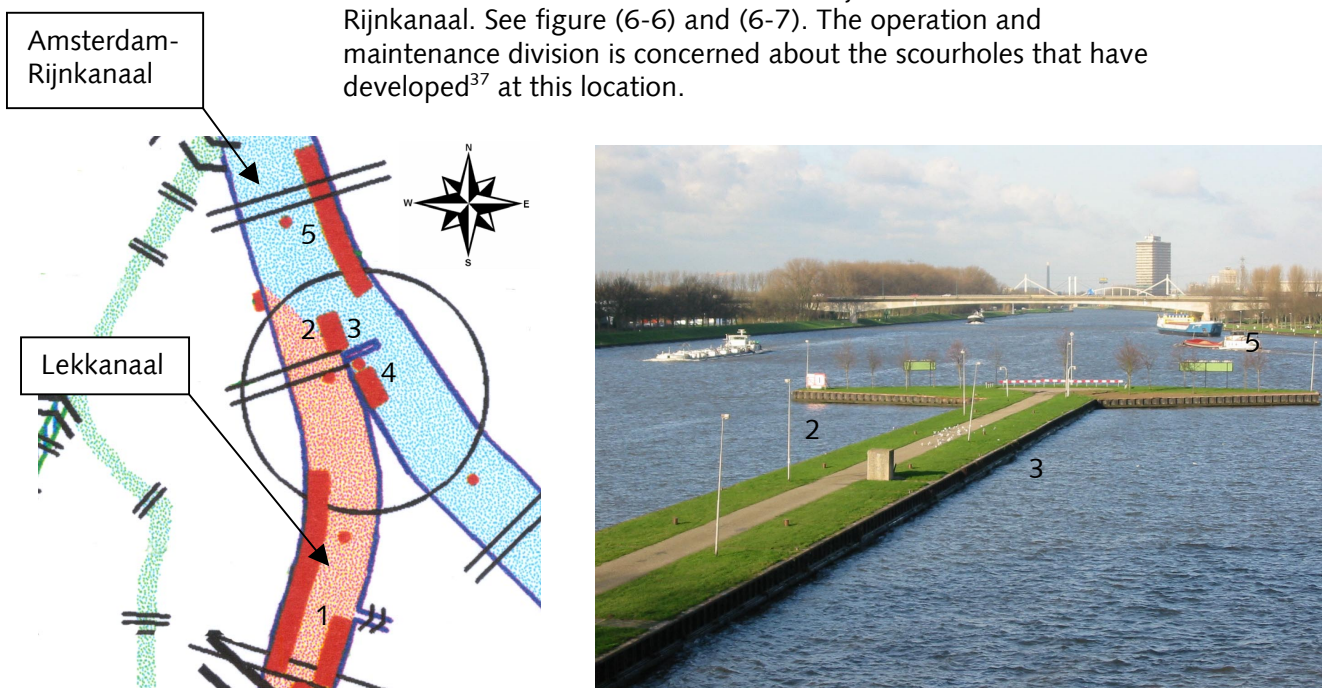


figure 6-6 Berthing places in the vicinity of Nieuwegein and Houten.

At this point there are several berthing places that give access to ships on the Amsterdam-Rijnkanaal and on the Lekkanaal as can be seen in figure (6-6). In the Lekkanaal the berthing places at Nieuwegein are situated (1). At the intersection itself there are three berthing locations (2, 3 & 4) and just to the north on the east side is the quay of Houten (5) (figure (6-6)).

Since we are focussing here on the Amsterdam-Rijnkanaal we will neglect the western part (2).

<sup>37</sup> In February 2002 two divers went down to visually inspect the sheetpiles since the operation and maintenance division was afraid the toe might be exposed. It proved that this was not (yet) the case.

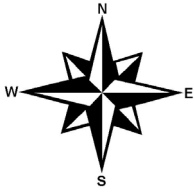


figure 6-7 Aerial photograph of the area shown in figure (6-6).

There is an obstacle between the berthing places (3) and (4) (figure (6-7)), the so-called Plofsluis<sup>38</sup>. Because of this, it is likely that most ships coming from the south will berth on the south side (4) or at Houten (5), and ships coming from the north will berth on the north side (3), not having to make a sharp turn around this obstacle. When departing this is not much of a problem, since a ship's velocity is still low when unberthing.

Therefore, the idea arises that on the east side of the structure (3) ships will mainly berth with their bow to the south. Their location will be to the north as much as possible to keep as much distance as possible from the obstacle.

This makes this a suitable location to look closer at the scouring phenomena.

Figure (6-8) shows the bathymetry around the west and east side of the northern part of the berthing facility.

---

<sup>38</sup> Some historical background: The Plofsluis was built between 1937 and 1940 as part of the Dutch 'Waterlinie' (a strip of land flooded as a defense line). In case parts of the Netherlands would be flooded by the military, the thin bottom of the Plofsluis could be blown away by explosives, releasing 40.000 tons of loose stones in the water, blocking the canal, making sure the water in the inundated areas could not flow away and they would stay flooded. The Plofsluis was never used.



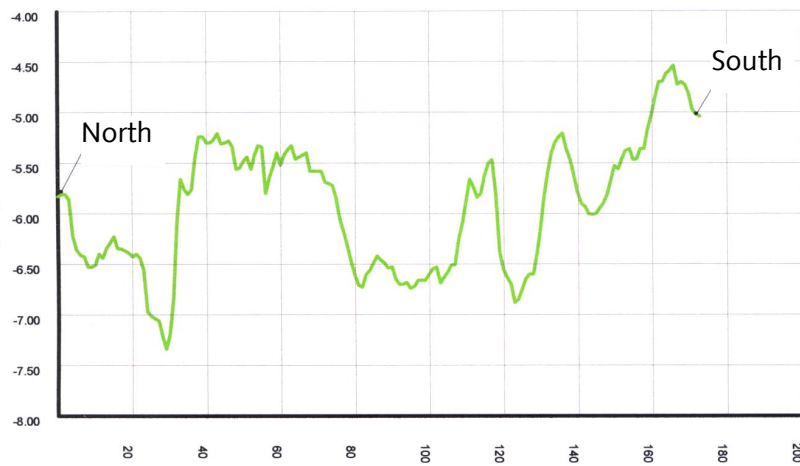
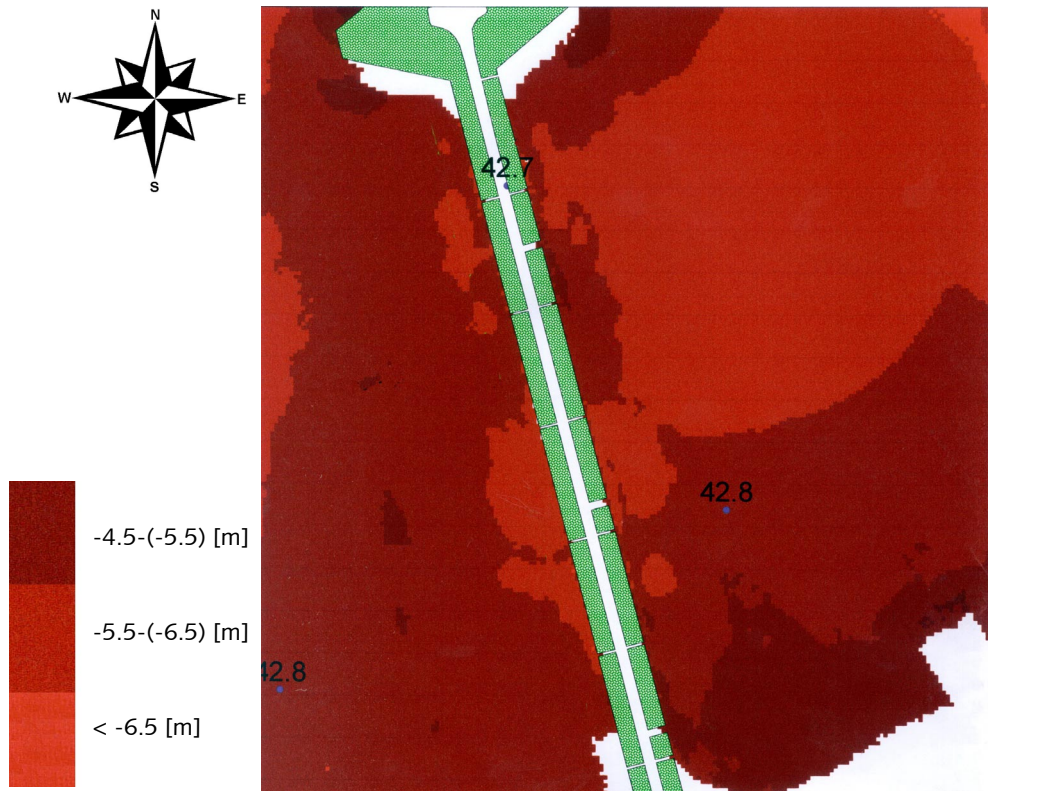


figure 6-8 Bathymetry at the Plofsluis, east side. All values are in metres. Reference level for the depth profile (5 [m] outside the quay) is NAP.

The focus will be on the east side. Two scourholes can be distinguished. One approximately at 42.7 [km] and one close to 42.8 [km]. A similar situation is visible on the west side.

The depth profile (figure (6-8), lower panel) shows that the bottom level of these holes is at approximately NAP  $-7.0$  [m].

---

Looking at figure (6-8) the reader can distinguish some interesting features:

- The maximum scour depth is located at 42.7 [km].
- The scourhole at 42.8 [km] is connected to the sheetpile construction.
- The area of the scour at 42.8 [km] is much larger than the area at 42.7 [km].

Following the hypothesis on the location and direction of the ship, we derive the following picture:

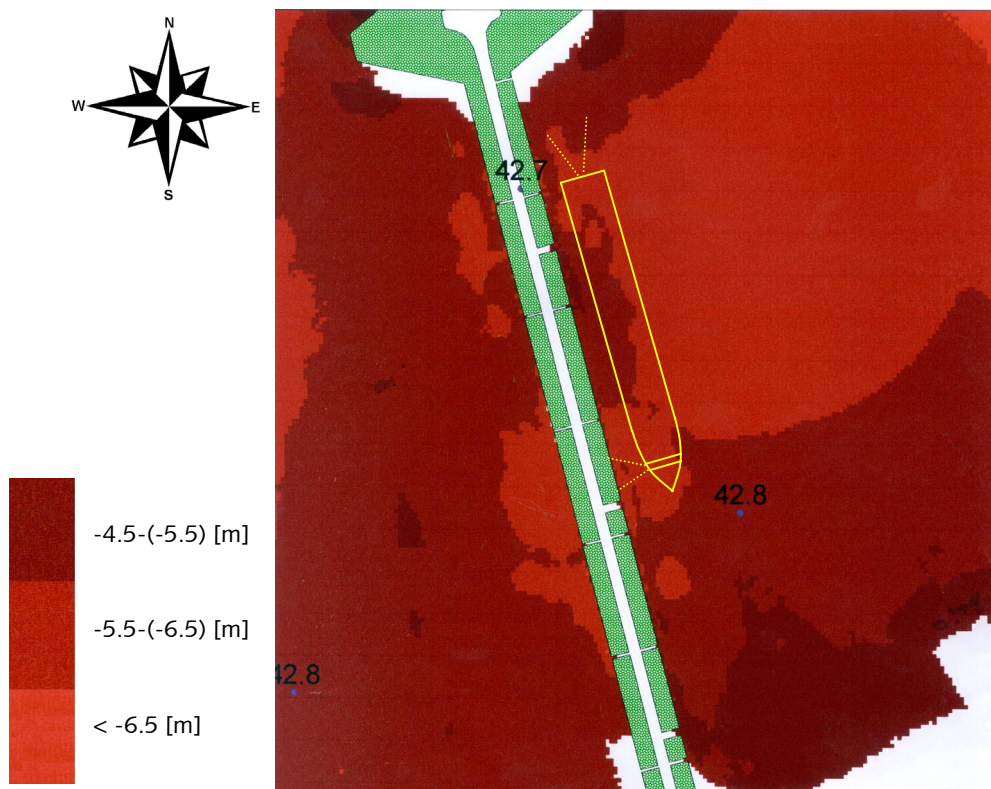


*figure 6-9 Bathymetry at the Plofsluis with the believed location and direction of most ships berthing here.*

The fact that the scour at 42.8 [km] is connected to the sheetpiles may be explained by the fact that a jet originating from a bowthruster hits perpendicular to the wall. The maximum velocity at the bottom occurs next to the sheetpiles causing scour. A main thruster is located further away from the quay and hits at an angle much less than 90 degrees. This could explain the scouring pattern as found at the Plofsluis.

The fact that the scour area, which is believed to be caused by the bowthrusters, is larger than the scour area caused by the mainthrusters may be caused by the following:

Ships of different lengths berth at the quay, but as already said, they berth as much to the north as possible, attaching their stern to the first possible bollard. This means that the mainthruster is located at

the same position for different ships, but the location of the bowthruster varies with the length of the ship, causing relatively widespread scour.

However, this also means that the intensity of the bowthrusters is less, causing a scour depth that is less than when it would be located on the same spot each time.

Some more examples of places with one directional berthing:

#### 6.4.2.3 Wijk bij Duurstede south side

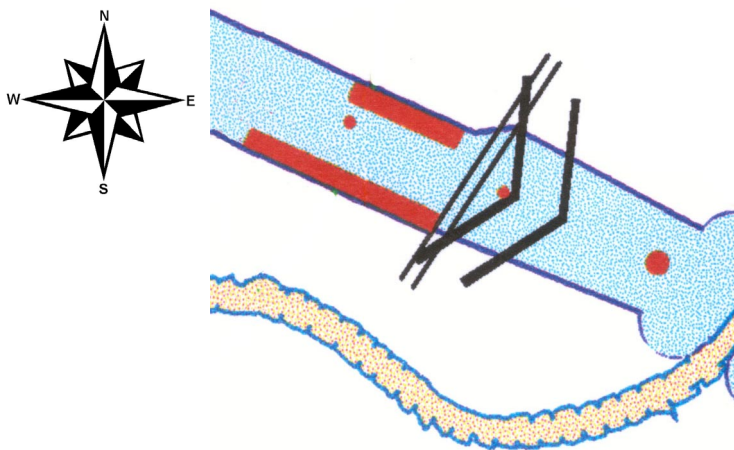


figure 6-10 Situation at Wijk bij Duurstede.

In figure (6-11) a part of the bathymetry of the quay at Wijk bij Duurstede is shown. Since there is a berthing place on the north side as well (figure (6-10)), the assumption is made that only ships coming from the west will berth here. That means that there will always be a bowthruster located on the east side of the indentation (figure (6-11)).

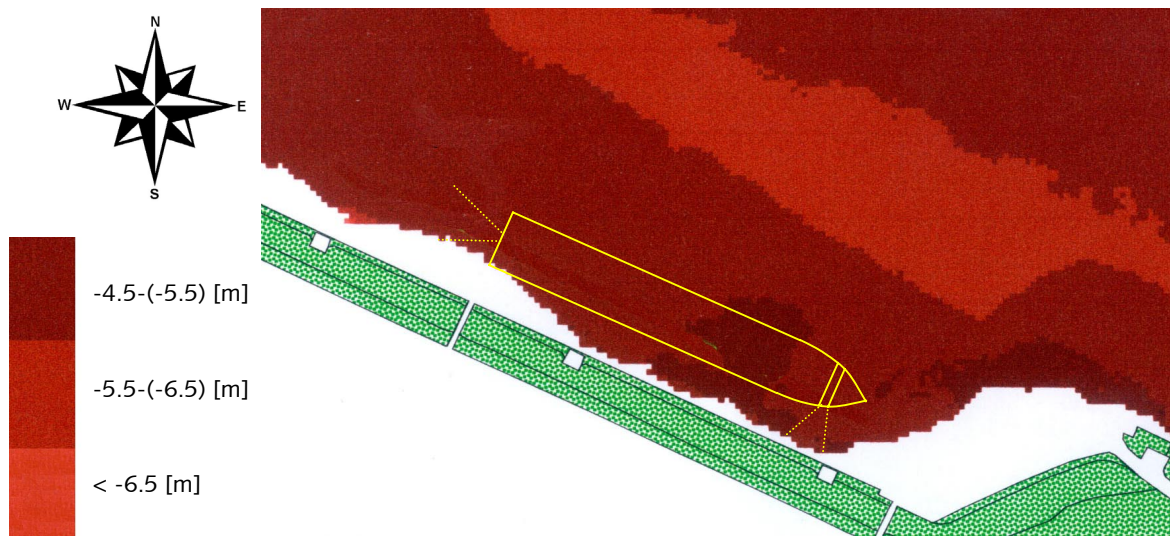


figure 6-11 Bathymetry at Wijk bij Duurstede. All values are in metres. Reference level for the depth profile (8 [m] outside the quay) is NAP.



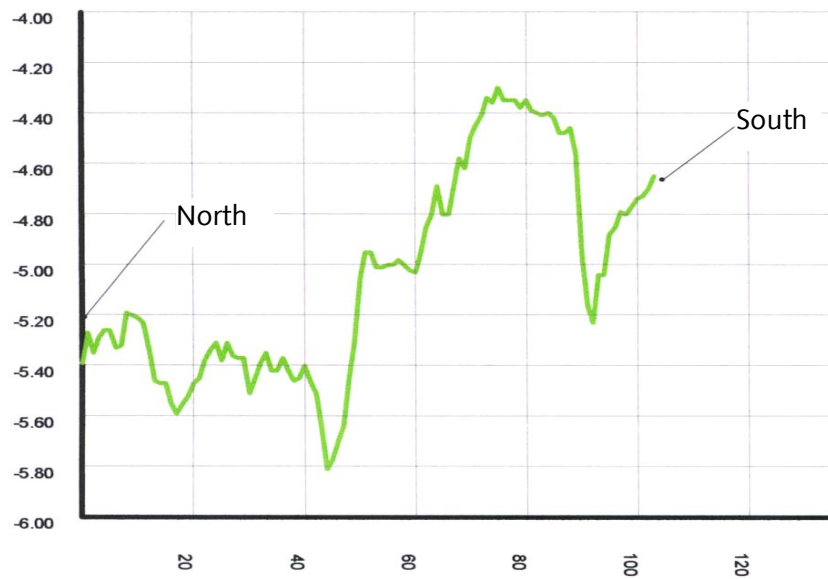


figure 6-11 Bathymetry at Wijk bij Duurstede. All values are in metres. Reference level for the depth profile (8 [m] outside the quay) is NAP.

The profile shows that the bottom level at the east side is considerably lower than on the western part, where, consequently, the mainthrusters are located.

#### 6.4.2.4 Nigtevecht

As an example of a short quay 'Nigtevecht' is used.

Figure (6-12) shows the short (185 [m]) berthing place near Nigtevecht.

There is no berthing place at the other side of the canal but just to the north there is one on the other side of the Vecht.



figure 6-12 Aerial photograph of the situation at Nigtevecht.

It is therefore not clear in what direction the ships will berth. Skippers have the tendency to berth as much forward as possible, giving them easy access for unberthing, with no ships in front of them.

This leads to the following two possible directions (figure (6-13)):

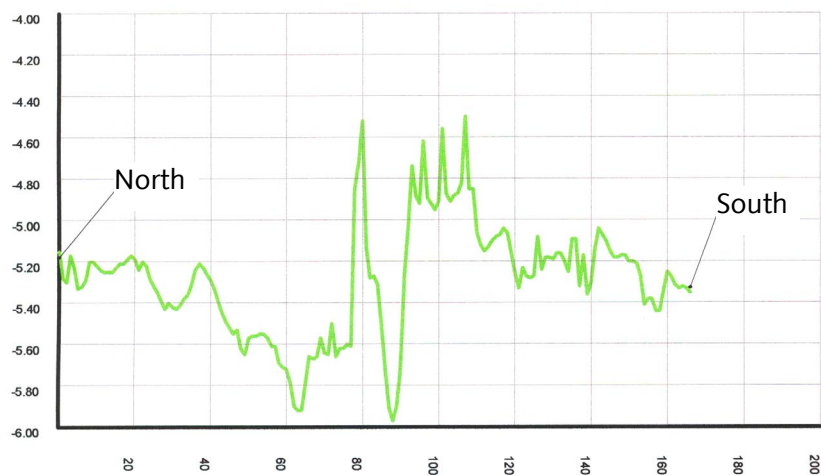
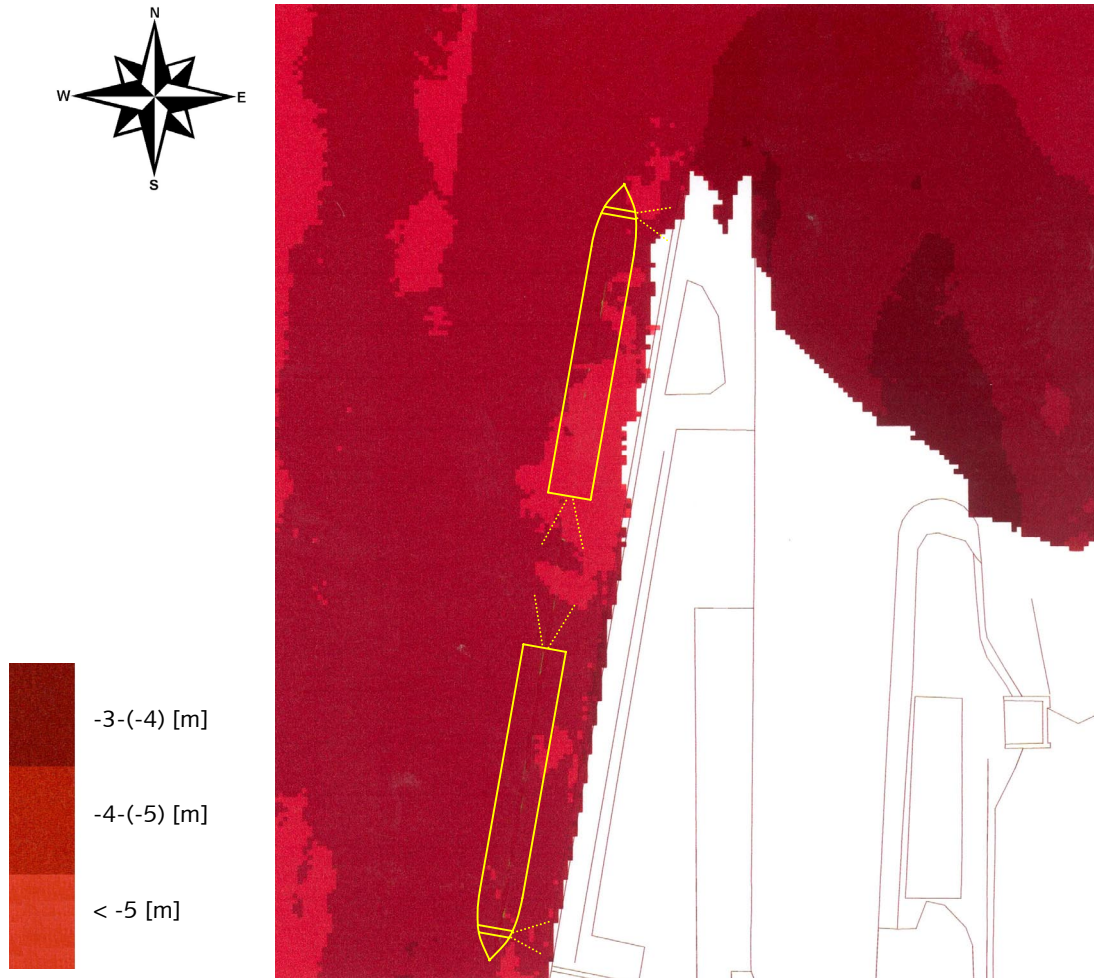


figure 6-13 Bathymetry at Nigtevecht. All values are in metres. Reference level for the depth profile (8 [m] outside the quay) is NAP.

---

When more than one ship berths at the same time in the same direction, it becomes a different story. However, one of the two situations above is likely to be the most common one.

Scour is clearly most intense on the north side. The average depth here appears to be approximately 5.3 [m]. The minimum bottom level is NAP -6.0 [m], i.e. a scour depth of 0.7 [m].

On the south side hardly any scour is found. This leads to the idea that not many ships berth at this spot. The accretion of sand at approximately 100 [m] from the north (figure (6-13)) may very well be caused by the parallel transport of the mainthruster of the ship berthed on the north side of the quay.

At the location where the bowthruster should be located, hardly any scour is visible. This might be caused by the fact that the ships do not use their bowthruster much, since they do not intent to make a turn to the left but can continue straight ahead (figure (6-12)).

---

#### 6.4.2.5 Tiel

At the north and south side of the sluice at Tiel there are short ( $L < 300$  [m]) waiting places designed for ships larger than 60 [m]. They both serve only one direction of the canal since they are only meant as waiting places in front of the sluice. The type of quay is slightly different than the ones discussed until now. It has a separate row of dolphins in front of the quay, approximately 15 [m] outside the quay. This is an excellent place to see what the effect of the propeller is when there is no quay wall present (or at least at a considerable larger distance than at uniform quays). Figure (6-14) and (6-15) show the southern quay.

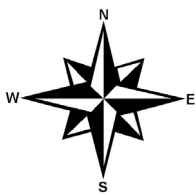


figure 6-14 Aerial photograph of the situation at Tiel.



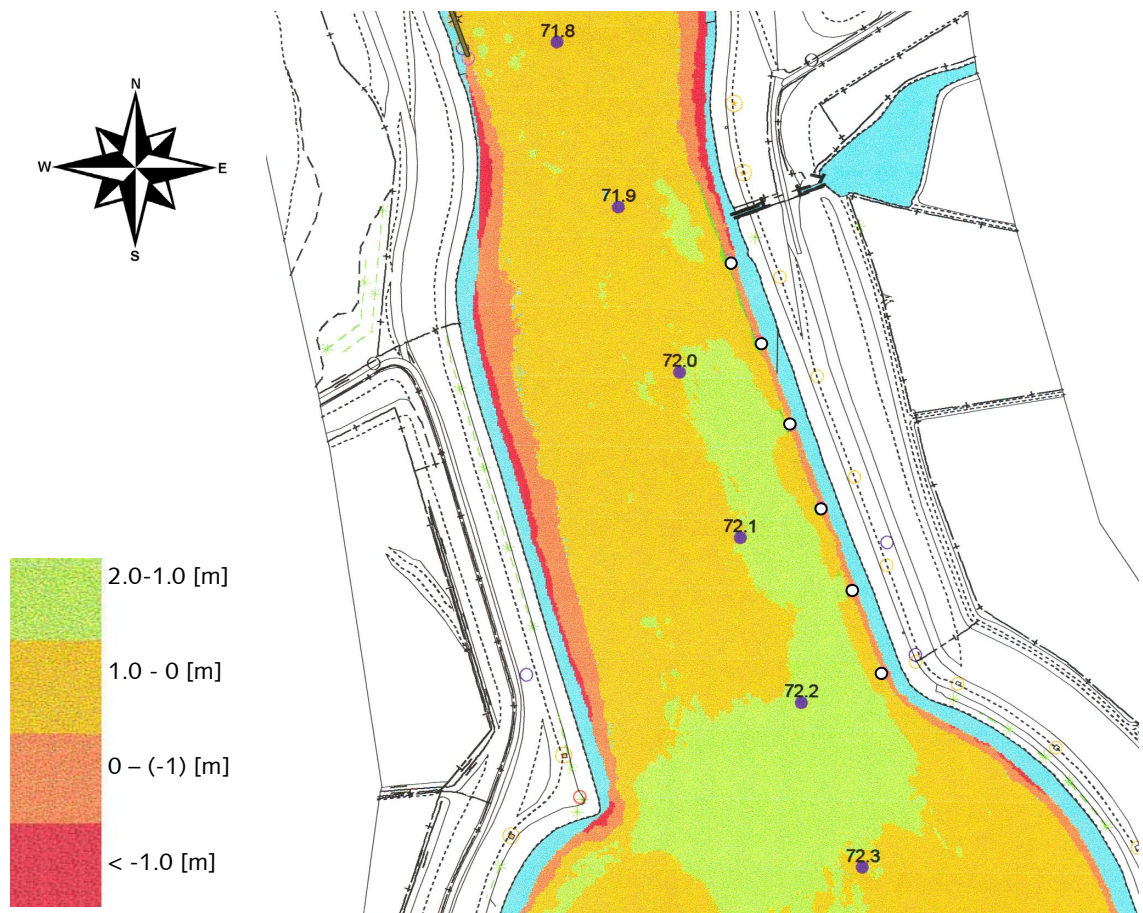


figure 6-15 Bathymetry at Tiel. All values are in metres. Reference level is NAP.

The berthing place is located on the east side, from kilometre number 71.95, to 72.20. It appears that the depth is smallest at the location where the ships berth. This is quite strange, since at all the other berthing places this was the other way around. It is also clear that the closer one gets to the quay the deeper it gets. (The orange/dark scour pattern in between the dolphins is the closest measurement to the quay as possible).

The explanation for the accretion at the ship's location may be the following:

The sediment originating from the scour close to the sheetpiles appears to settle at approximately the location of the ship. Especially when using a bowthruster, the flow is directed inward the canal after being deflected by the sheetpiles. This can cause accretion at the location where the ships berth. This pattern is not noticed at any of the other quays. Perhaps the difference in distance between propeller and quay wall is the reason for the difference in scouring and accretion pattern<sup>39</sup>.

<sup>39</sup> This may be an interesting variable when conducting physical model tests on a vertical wall.



#### 6.4.2.6 Wijk bij Duurstede north side

As an example of a berthing place with a bottom protection the profile of Wijk bij Duurstede north side is shown in figure (6-16)). A bottom protection is applied at this location, hence the bathymetry looks quite different than from those dealt with in previous sections.

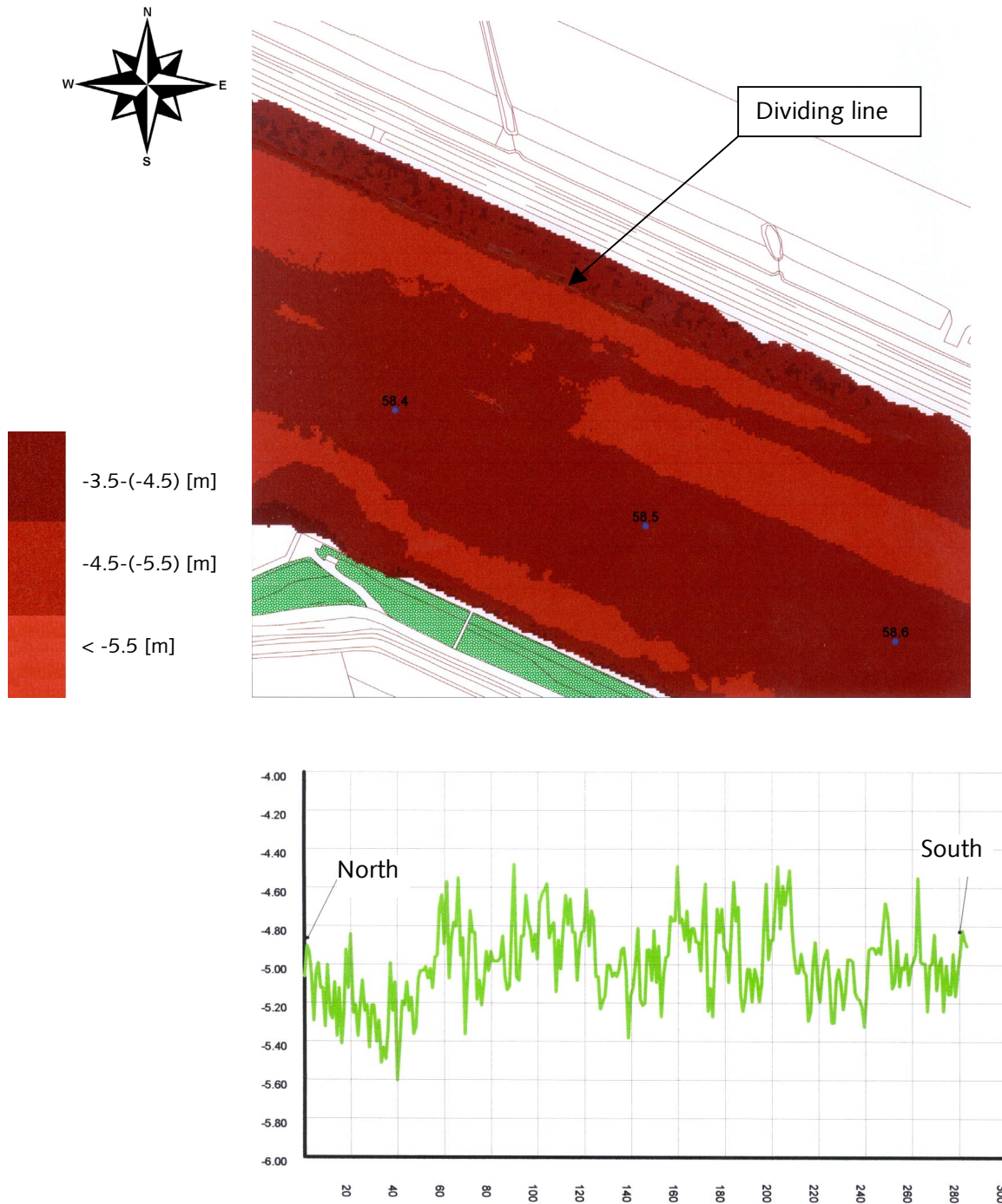


figure 6-16 Bathymetry at Wijk bij Duurstede north side. All values are in metres. Reference level for the depth profile (10 [m] outside the quay) is NAP.

It is clear to see where the protection is applied and where it stops. A straight dividing line is visible in figure (6-16). Since no really deep holes can be distinguished, it appears that the protection is adequate.

If one however considers the guaranteed depth of 5.60 – NAP it seems that the top level of the protection is wrong. It is most likely that the protection was applied before the maximum draught in the Amsterdam-Rijnkanaal was increased from 3.5 [m] to 4.0 [m].

### 6.4.3 Conclusions on non-uniform quays

Some non-uniform quays show scour that may very well be caused by bowthrusters. There is however no evidence found that these scourholes are endangering the sheetpiles or that they are larger than the scour believed to be caused by mainthrusters.

## 6.5 Comparison with theory

In this section the findings at the Plofsluis are compared to theoretical values. The quay at the Plofsluis was chosen since the distinction between the holes induced by either bow- or mainthruster is quite clear. At the end also some theoretical results on scour depths at other quays will be listed in a table.

### 6.5.1 Governing vessel

The DWW (1997) did some research on scour in the Amsterdam-Rijnkanaal as well and compared several vessel that are common in the Amsterdam-Rijnkanaal. They found that a large Rhine-vessel is governing for the maximum scour, based on calculations of draught, engine power installed and propeller diameter.

Although their findings for scour appear to be doubtful<sup>40</sup>, the vessel seems appropriate to get an indication of the possible scour.

Some characteristics of the vessel:

length [m]	110
beam [m]	11.4
draught [m]	4
manoeuvring power [kW]	1000
number of main propellers [-]	2
effective diameter ( $D_0$ ) [m]	1.45
draught main propellers [m]	3.10
power of bowthruster [kW]	200
effective diameter of bowthruster [m]	0.80
draught bowthruster [m]	3.50

table 6-1 Characteristics of a large Rhine vessel.

<sup>40</sup> The results they found for the maximum scour are questionable.

---

## 6.5.2 Example: Plofsluis

### 6.5.2.1 Bottom velocity

#### Bowthruster

The average bottom depth at the Plofsluis is NAP –6.0 [m]. Based on the characteristics of table (6-1) this leads to the following situation for the bowthruster (figure (6-17)):

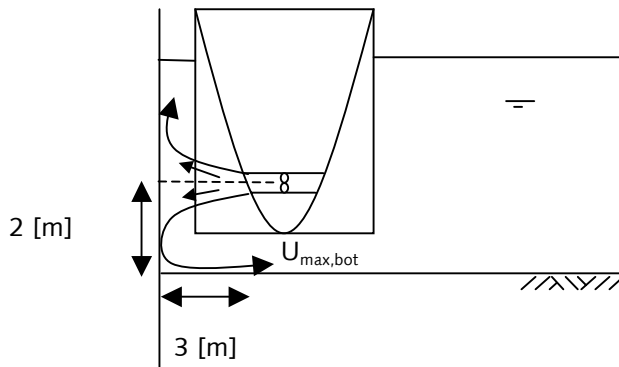


figure 6-17 Situation at the Plofsluis when a large Rhine vessel is unberthing.

To determine the maximum scour depth the method of Blokland<sup>41</sup> is used to calculate the water velocity at the bottom which is used as input in the formula of Hoffmans to calculate the maximum scour depth.

In addition, the results following from these calculations will be compared to calculations based on the formulas of Römisch and also compared to the actual –measured- scour depth.

The initial velocity  $U_0$  is calculated using the formula of Blaauw and Van de Kaa (1978):

$$U_0 = 1.15 \cdot \left( \frac{P}{\rho \cdot D_0^2} \right)^{\frac{1}{3}} \text{ [m/s]} \quad (6-1)$$

With the characteristics of table (6-1) this leads to  $U_0 = 7.8 \text{ [m/s]}$ <sup>42</sup>.

This initial velocity is then used in the formula of Blokland to calculate the maximum velocity at the bottom  $U_{\max, \text{bot}}$ :

---

<sup>41</sup> The reader is referred to chapter 2, Literature study, for a detailed description of the formulas used in this section.

<sup>42</sup> For the power 'P' 100 [%] of the installed maneuvering power is used. It is believed that this is correct for the use of the bowthruster, but it may be on the high side for the mainthruster.

$$U_{\max,bot} = 1.0 \cdot \frac{U_o \cdot D_0}{z} \quad [\text{m/s}] \quad \text{for} \quad \frac{L}{z} < 1.8 \quad [-] \quad (6-2)$$

in which  $L = 3$  [m] and  $z = 2$  [m] (figure (6-17)).  
This leads to  $U_{\max,bot} = 3.1$  [m/s]

### Mainthrusters

The found maximum bottom velocity for the bowthruster is compared to the maximum bottom velocity initiated by the mainthrusters when the ship is at an angle of  $\alpha = 45^\circ$  with the quay<sup>43</sup>:

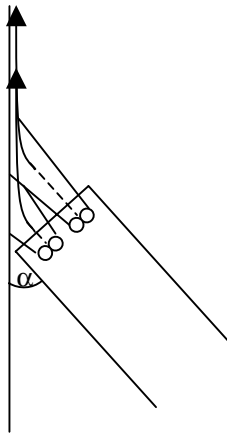


figure 6-18 Situation at the Plofluis when a large Rhine vessel is unberthing.

With the characteristics of table (6-1) and the formula of Blaauw & Van de Kaa (1978) this leads to:

$U_o$  of a single propeller equals 7.1 [m/s].

This is used in the formula of Blokland:

$$U_{\max,bot} = 2.8 \cdot \frac{U_o \cdot D_0}{L + z} \quad [\text{m/s}] \quad \text{for} \quad \frac{L}{z} \geq 1.8 \quad [-] \quad (6-3)$$

With  $L = 6$  [m] and  $z = 2.5 \cdot \sqrt{2}$  [m]<sup>(44)</sup>

$U_{\max,bot} = 2.7$  [m/s] for a single propeller.

Since we are dealing with two mainthrusters here we have to calculate the combined action.

According to WL (1996):

<sup>43</sup> An angle of 45 [degrees] was chosen here since it is considered the maximum angle at which a ship will depart, initiating the maximum load on the sheetpile structure.

<sup>44</sup> This value for  $z$  is taken here since it is believed that the jet will also reach the bottom at an angle less than 90 degrees with the sheetpiles since the vessel itself is at an angle less than 90 degrees with the sheetpiles. Therefore 45 [degrees] is used.

$$U_{\max, \text{bot}} = \sqrt{2} \cdot U_{\max, \text{bot single}} \quad (6-4)$$

This leads to  $U_{\max, \text{bot}} = 3.8$  [m/s] for the combined action of the propellers.

So there is a small difference in maximum bottom velocity between the two systems (bow- and mainthruster).

### 6.5.2.2 Scourdepth at the Plofsluis

#### Hoffmans

First the results of section 6.5.2.1 for the maximum bottom velocity are used in the formula of Hoffmans (1995):

$$h_{\text{hole}} = c_{3H} \left( Q \cdot \frac{U_{\max, \text{bot}}}{g} \right)^{\frac{1}{3}} \text{ [m]} \quad (6-5)$$

where

$c_{3H}$ : constant, equals 2.0 [-]

Q: discharge (=  $U_0 \cdot A$ ) [m<sup>3</sup>/s]

this leads for the bowthruster to:

$$\text{with } Q = U_0 \cdot \frac{1}{4} \cdot \pi \cdot D_0^2 = 3.9 \text{ [m}^3\text{/s]}$$

$$h_{\text{hole}} = 2.1 \text{ [m]}$$

And for the main thruster:

$$\text{with } Q = \sqrt{2} \cdot Q_{\text{single}} = 16.5 \text{ [m}^3\text{/s]}$$

$$h_{\text{hole}} = 3.7 \text{ [m]}$$

There is a **75 [%]** larger scour depth found for the mainthruster compared to the depth found for the bowthruster.

#### Römisch

Römisch also defined a formula for the maximum scour depth (see literature study, section 2.2.3.1):

$$\frac{h_{\text{hole}}}{d_{85}} = C_m \cdot 0.1 \cdot \left( \frac{B}{B_{\text{crit}}} \right)^{13} \quad \text{for } 1.0 < \left( \frac{B}{B_{\text{crit}}} \right) < 1.4 \text{ [-]} \quad (6-6)$$

$$\frac{h_{\text{hole}}}{d_{85}} = C_m \cdot 4.6 \cdot \left( \frac{B}{B_{\text{crit}}} \right)^{2.25} \quad \text{for } \left( \frac{B}{B_{\text{crit}}} \right) > 1.4 \text{ [-]} \quad (6-7)$$

---

where

$$B = \frac{U_{\max,bot}}{\sqrt{\frac{\rho_s - \rho_w}{\rho_w} \cdot g \cdot d_{85}}} \quad [-] \quad (6-8)$$

$C_m$  : constant [-] (0.3 [-] for manoeuvring ships, 1.0 [-] for ships at rest)

For both the bow- and mainthruster it will be calculated what the scour depth will be for the ship at rest and for a manoeuvring ship.

For the bowthruster with  $C_m = 1.0$  [-] (ship at rest) this leads to the following:

$$U_{\max,bot} = 3.1 \text{ [m/s]}$$

$$d_{85} = 150 \mu\text{m}^{45}$$

$$B = 63 \text{ [-]}$$

$$B_{\text{crit}} = 1.25 \text{ (Römisch (1977))}$$

$$h_{\text{hole}} = 4.6 \text{ [m]}$$

and for  $C_m = 0.3$  [-] (manoeuvring ship)<sup>46</sup>

$$h_{\text{hole}} = 1.4 \text{ [m]}$$

For the mainthruster it follows with  $C_m = 1.0$  [-]:

$$U_{\max,bot} = 3.8 \text{ [m/s]}$$

$$B = 77 \text{ [-]}$$

$$h_{\text{hole}} = 7.3 \text{ [m]}$$

and for  $C_m = 0.3$  [-]

$$h_{\text{hole}} = 2.2 \text{ [m]}$$

A **60 [%]** larger scour depth is found for the mainthrusters than found for the bowthrusters.

It appears that there is quite a difference in results from different formulas.

---

<sup>45</sup> Value for the  $d_{85}$  of sandy clay.

<sup>46</sup> It is not clear if this parameter is based on the time dependent character of scour, the use of smaller engine power during maneuvering or both.

### 6.5.2.3 Evaluation and conclusions

The following scour depths are found for bow- and mainthruster when using different formulas and coefficients :

Plofsluis	Hoffmans	Römisch C = 1.0 [-]	Römisch C = 0.3 [-]	Measured (in front of quay)
<b>Bowthruster</b>	2.1 [m]	4.6 [m]	1.4 [m]	1.3 [m]
<b>Mainthruster</b>	3.7 [m]	7.3 [m]	2.2 [m]	1.7 [m]

table 6-2 Results of maximum scour from different formulas compared to the measured values at the Plofsluis.

It appears from table (6-2) that for the situation investigated, the mainthrusters will cause considerably larger scour depth than the bowthrusters.

The maximum scour depth in reality was found to be 1.7 [m]. It appears that the values derived from the formula of Römisch for manoeuvring ships do not differ much from the measured values.

Some remarks may be made on the calculations made in this section:

- There are quite a few assumptions made on dimensions, initial velocity, etc. For instance it is not certain how and where the jet of the mainthruster induces maximum damage (this is depending on the angle at which the ship departs). Based on the bathymetry and assumptions on the ships location and direction it is expected that the maximum damage occurs approximately 5 [m] from the quay.
- For calculating the initial velocity, 100 [%] of the engine power is used. As already noted, it is believed that this is in practice a correct assumption for the use of bowthrusters, however, for the use of mainthrusters is may be on the high side.
- Also the ship used for the calculations here is quite large. The average ship is less damaging. Since scour is time dependent the scour pattern will be an average resulting from all loads, not just from the largest.
- Furthermore the formula of Hoffmans (1995) was derived for sand. This is however not exactly the case here. According to the geotechnical laboratory in Delft the soil is sandy clay. Since clay has a greater cohesion the maximum scour will be less.
- Also all the formulas used in section (6.5.2.2) give a maximum scour depth, since the formulas are independent of time. But it is not certain that the final stage is reached yet.

It is concluded that theoretical values do not differ very much from the measured values when using the formula of Römisch for manoeuvring ships. The fact that all formulas result in high values

for scour depth can be explained by the errors in the assumptions that are made.

It is also concluded that based on the present theories, it is considered unlikely that bowthrusters will cause greater damage than mainthrusters.

### 6.5.3 Other examples: Maarsse and the Roosenveltlaan

From two other quays the theoretical scourdepth is also calculated, namely from Maarsse and the Roosenveltlaan. The results are presented in tables (6-3) and (6-4):

Maarsse	Hoffmans	Römisch C = 1.0 [-]	Römisch C = 0.3 [-]	Measured (in front of quay)
<b>Bowthruster</b>	2.3 [m]	7.8 [m]	2.3 [m]	0.9 [m]
<b>Mainthruster</b>	4.0 [m]	11.3 [m]	3.4 [m]	

table 6-3 Results of maximum scour from different formulas compared to the measured values at Maarsse.

Roosenveltlaan	Hoffmans	Römisch C = 1.0 [-]	Römisch C = 0.3 [-]	Measured (in front of quay)
<b>Bowthruster</b>	2.2 [m]	5.4 [m]	1.6 [m]	3.5 [m]
<b>Mainthruster</b>	3.9 [m]	10.2 [m]	3.1 [m]	

table 6-4 Results of maximum scour from different formulas compared to the measured values at the Roosenveltlaan.

It follows that for Maarsse all predicted values, including the ones derived from Römisch's theory for manoeuvring ships, are much to large. This justifies the idea that along these uniform quays the scour does not fully develop anywhere.

For the Roosenveltlaan it appears that again the equation of Römisch for manoeuvring ships predicts a good value. However, this is a location where it is believed that the ships are in the same position while operating their mainthrusters for relatively long times (unloading their car). One would therefore expect that the coefficient C should equal 1 [-]. Apparently this is not the case.

It is however interesting to see that Hoffmans' value for the mainthruster-induced scour at the Roosenveltlaan is also not much different than the measured value. This may indicate that Hoffmans' formula is applicable when ships are using their thrusters for long times at a certain location without moving/manoeuvring.

### Conclusions

This section substantiates the idea that the equations that are used produce valid results for locations where regular berthing occurs and scour therefore has time to develop. However, it seems that Römisch's equation for ships at rest does not produce valid results under any circumstances investigated here.



---

At locations where irregular berthing occurs time independent scour formulas should not be used.

This section therefore consequently also substantiates the idea that at uniform berthing places scour is much less than at non-uniform berthing places due to the lack of time for a scourhole to develop.

## 6.6 Conclusions and recommendations

### Conclusions

#### *Uniform quays*

- At uniform berthing places in the Amsterdam-Rijnkanaal the maximum scour depth was found to be 1.2 [m], located at the berthing place at Nieuwegein. The width of the scourhole is approximately 5 [m].
- In no case scour along uniform quays led to serious problems.
- It is not possible based on the available data to separate scour initiated by mainthrusters from scour initiated by bowthrusters.

#### *Non-uniform quays*

- In the entire Amsterdam-Rijnkanaal the maximum scour depth was found to be 1.8 [m] at the Plofsluis near Nieuwegein (not taking the car-unloading-point into account). This maximum scour is probably related to the mainthruster. The width of the hole is approximately 10 [m].
- The bowthrusters may very well cause scour of the same order as mainthrusters do. Measurements, however, indicate that they should probably not be regarded as the criterion for the maximum scour, which is supported by theory.
- The development of scour seems very sensitive to the geometry of the berthing place and the distance from the sheetpile structure. Non-uniform berthing places should therefore be monitored more closely than uniform ones.

### Recommendations

Based on the findings in this chapter it is recommended to Rijkswaterstaat to regard the mainthrusters governing for scour along quays walls. In most cases one does not need to bother oneself with the effects of this scour, even when no bottom protection is applied (not taking hazardous situations into account. If such a situation occurs, it is recommended to closely monitor the scour and its natural replenishment in order to gain more insight into this phenomenon.).

Further more, more attention should be paid to the so-called non-uniform quays than to uniform quays when dealing with maintenance of these quays. It can be assumed that this is not only the case in the Amsterdam-Rijnkanaal but also in similar inland waterways.

---

Since scour is time dependent it would be useful to replenish a location with new bottom material where it is known that bowthruuster-induced scour takes place (for instance at the Plofsluis). After that it can be regularly monitored where and how fast the scourholes develop again.

Since it is believed that bowthrusters may produce scour in the same order as mainthrusters do, it may very well be that if the size and power of bowthrusters continues to increase, bowthrusters may become governing. Therefore it is wise to increase the knowledge of bowthruster-induced scour.

To do so, it is recommended to perform physical model tests concerning scour in front of a vertical wall. The results from these tests can be used to eventually perform prototype tests. When conducting these model tests a ducted-propeller jet should be used. Further more, not only should one concern oneself with stability of material, but also with the actual development of (time dependent) scour.

---

# 7 Conclusions and recommendations

## 7.1 General

Based on the previous three chapters conclusions are drawn and recommendations are made. They are divided into two categories:

Conclusions and recommendations concerning:

- The results of the experimental model investigation (aims 1a and 1b).
- The damage investigation in the Dutch inland waterways (aim 2).

## 7.2 Model (aim 1a&b)

### 7.2.1 Free-propeller jet

Conclusions:

- The free-propeller jet has a similar diverging pattern as the ducted-propeller jet.
- The ratio at which the velocity decreases with distance from the propeller is higher for the free-propeller jet than it is for the ducted-propeller jet. This is caused by larger turbulence in the free-propeller jet.
- The ducted-propeller jet causes more damage at the slope than the free-propeller jet at the same rotation rate. The different ratio of velocity decrease is the cause of this.
- Measurements of the velocities in the jet differ slightly from calculated values.
- The maximum damage resulting from a free-propeller jet as well as resulting from a ducted-propeller jet occurs at the toe of the slope.
- A ducted-propeller jet should be used when modelling a bowthruster.
- The distribution of turbulent fluctuations in the jet seems to comply with a normal probability density function distribution. In the boundary layer the distribution becomes asymmetric.

Recommendations for further study on the free propeller:

- There are no recommendations concerning a further study to the free-propeller jet when concerned with bowthrusters.

### 7.2.2 Damage location on the slope

Conclusions:

- The flow direction is upward on the entire slope.
- Most severe damage occurs on the toe of the slope.
- Stones move downward at the toe of the slope and move upward at a higher location on the slope.
- The damage is initiated by a combination of the following two mechanisms:

- 
- Shear stress.
  - A pressure force, resulting from a pressure gradient along the slope, which is induced by a convective acceleration of the water.
  - The peak velocities should be applied for calculating the values for the two mechanisms mentioned above when looking at damage. These peak velocities are largely dependent on the turbulence intensities.
  - The average velocities should be applied for calculating the values for the two mechanisms mentioned above when looking at the initial direction of movement.
  - Turbulent energetic vortices in the jet are found with approximately the same size as the diameter of the propeller.

Recommendations for further study on the slope:

- See recommendations in general, section 7.2.3.

### 7.2.3 Recommendations in general

A further study will give more insight in the relations between velocities, turbulences and stability. Possible studies include:

- A more correct representation of the prototype<sup>47</sup>. The return current around the bow of the ship, or underneath the ship may be an important feature of the water flow. If possible, this should be done in a larger basin. If this is not available, it should be kept in mind that circulation occurs that may not occur in the prototype situation, of which the effect on the stability of stones is not known.
- The use of more precise instruments that do not disturb the flow, for instance a Laser-Doppler Anemometer.
- The use of a different slope. Van Veldhoven states that in prototype situations the slope varies between 1:1.33 [-] and 1:2.6 [-]. It is not clear why he chose a less steep slope for the model. It may be possible that for a steeper slope, the flow will be partly downward on the slope as well, thereby creating a pressure point, which would change the stability of the stones on the slope drastically. Eventually also a vertical wall could be investigated, shifting the point of erosion to the bottom, in front of the vertical wall. Possible variables should also include the roughness of the wall, for example the influence of a horizontal plate to deflect the wall jet originating from the bowthruster, preventing it to reach the bottom.
- The use of different distances from the propeller to the slope.
- The use of different sediment sizes. This will give more insight in the relations between velocities and stability.
- Performing extensive analysis on derived data concerning frequencies and energies of vortices. This might provide

---

<sup>47</sup> In the case of this investigation it was not necessary to build a sophisticated model, since the goal was to derive fundamental insight in the differences between several types of jets.

---

more insight in the movement of stones and the mechanisms responsible for it.

### 7.3 Damage investigation in the Dutch inland waterways (aim 2)

Conclusions (based on the case study Amsterdam-Rijnkanaal):

- Quays are separated in this study in uniform quays and non-uniform quays. A uniform quay is a long quay with no distinct anomalies at which ships berth from both directions of the waterway and at random locations. A non-uniform quay is a short quay or a quay with distinct geometrical anomalies, i.e. a quay that does not comply with the definition of a uniform quay.
- At uniform quays there is little concern for scour induced by bowthrusters. The present scour is believed to be caused by both main- and bowthruster; due to the randomness in berthing these scourholes are usually shallow.
- At non-uniform quays there seem to be indications that bowthrusters can produce scour of the same order of magnitude as mainthrusters. The scourholes here are large (as much as 3.5 [m], mainthruster-induced) and are therefore reason for concern. However, no evidence has been found that the use of bowthrusters results in larger scour than the use of mainthrusters.

Recommendations with respect to the maintenance of inland waterways:

- There is little reason to be concerned about scourholes at uniform quays as long as no hazardous situations<sup>48</sup> occur.
- It is meaningful to pay more attention to the so-called non-uniform quays, since large scourholes have the tendency to develop here.
- If hazardous situations occur, development of the scourholes should be closely monitored to increase insight in the development of scour and accretion.

Recommendations for further investigations

- When extending this investigation concerning scour along quay walls, it is recommended to focus on non-uniform quays. More investigations at locations in different waterways and also harbours will (probably) substantiate the findings of this report.
- Full-scale testing is an efficacious method for gaining insight in the actual scour development in time. Due to large costs it is recommended to perform model tests on a vertical quay wall first to get insight in the points of interest for full-scale tests.

---

<sup>48</sup> Hazardous situations are defined here as dangerous situations caused by the ships, resulting in extensive thruster use.



---

# Nomenclature

Variable	Description	Symbol
a	constant	-
B	stability parameter of Römisch	-
C	coefficient of Chezy	$m^{1/2}/s$
$C_m$	Shipfactor of Ducker and Miller	-
$c, c_1, c_2$	constant in the equations for velocity distributions in the jet	-
$C_{3H}$	constant in the equation of Hoffmans	-
$C_f$	friction coefficient	-
D	diameter of propeller	m
d	particle diameter	m
$D_0$	diameter of jet at maximum contraction	m
E	stability parameter of Rajaratnam	-
F	force	N
$F_d$	drag force	N
$F_f$	friction force	N
$F_l$	lift force	N
$F_p$	pressure force	N
Fr	Froude number	-
$F_s$	shear force	N
g	gravitation constant	$m/s^2$
$h_d$	draught of ship	m
$h_{hole}$	depth of hole	m
$h_k$	keel clearance	m
$h_w$	waterdepth	m
I	momentum	$kg \cdot m/s^2$
$K(\alpha)$	correction factor	-
$K_T$	thrust coefficient	-
$K_{T(dps)}$	thrust coefficient of a ducted-propeller system	-
$K_{T(prop)}$	thrust coefficient of the propeller	-
L	distance from wall	m
$L_d$	length of duct	m
m	slope	-
n	revolutions per second	$s^{-1}$
$n_b$	number of blades	-
P	(engine) power	Watts
Q	discharge	$m^3/s$
r	radial distance from x-axis	m
$r, r_x, r_y, r_z$	relative turbulence	-

---

Re	Reynolds number	-
T	thrust	kg·m/s <sup>2</sup>
t	time	s
T <sub>(dps)</sub>	thrust of a ducted-propeller system	kg·m/s <sup>2</sup>
T <sub>(prop)</sub>	thrust of the propeller	kg·m/s <sup>2</sup>
u*	shear velocity	m/s
U, U <sub>x</sub> , U <sub>y</sub> , U <sub>z</sub>	velocity	m/s
U'	fluctuation velocity	m/s
U <sub>0</sub>	initial velocity after exit at propeller	m/s
U <sub>1</sub>	velocity gained in actuator disc	m/s
U <sub>2</sub>	initial velocity after exiting the disc	m/s
U <sub>A</sub>	velocity of surrounding water	m/s
U <sub>cr</sub>	water velocity at which the sediment starts to move	m/s
U <sub>max</sub>	maximum velocity at distance x from the propeller, occurring at the x-axis	m/s
$\tilde{U}_{max}$	peak velocity	m/s
U <sub>max,bot</sub>	maximum velocity at the bottom	m/s
V	volume	m <sup>3</sup>
V <sub>(dps)</sub>	volume moved by a ducted-propeller system	m <sup>3</sup>
W	maximum beam of ship	m
W	weight	N
w	fall velocity of sediment	m/s
x	distance along x-axis from propeller	m
x <sub>0</sub>	length of flow establishment zone	m
z	height above bottom	m
Δ	relative density	-
α	angle	degrees
β <sub>iz</sub>	stability parameter of Izbash	-
φ	angle of internal stability	degrees
φ'	contraction coefficient	-
λ	constant	-
ν	kinematical viscosity	m <sup>2</sup> /s
ρ <sub>s</sub>	sediment density	kg/m <sup>3</sup>
ρ <sub>w</sub>	water density	kg/m <sup>3</sup>
τ	shear stress	N/m <sup>2</sup>
ψ	stability parameter of Shields	-

---



---

## References

- Blaauw, H.G., and Kaa, E.J. van de, *Erosion of bottom and sloping banks caused by the screw race of manoeuvring ships*, WL publication 202, 1978.
- Blokland, T., Smedes, *In situ tests of current velocities and stone movements caused by a propeller jet against a vertical quay wall*, Rotterdam public works, 1994.
- Bok, A., *De stabiliteit van de bodembescherming voor een kademuur bij het gebruik van boegschroeven*, DUT M.Sc. thesis, 1996.
- Booij, R., *Erosie onder een geometrisch open filter*, DUT report, 1998.
- Chatfield, *The analysis of time series*, Chapman & Hall, 1996.
- Ducker, H.P. and Miller, C., *Harbour bottom erosion at berths due to propeller jets*, Proceedings 11<sup>th</sup> Int. Harbour Congress, Antwerpen, 1996.
- DWW, *Advies bodembescherming aanlegplaatsen Amsterdam-Rijnkanaal*, project Oevers, 1997.
- Gemeentewerken Rotterdam, *Schroefstraal tegen kademuur*, report: 61.00\_R94.038, 1996.
- Giger, M., Jirka, G.H., Dracos, T., *Entrainment and mixing in plane turbulent jets in shallow water*, Journal of hydraulic research vol. 29, 1991, p. 615-642.
- Hamill, G.A., Johnston, H.T., Stewart, D.P.J., *Propeller wash scour near quay walls*, Journal of waterway, port, coastal and ocean engineering, 1999, p. 170-175.
- Hinze, J.O., *Turbulence*, 2nd edition, McGraw-Hill, 1975.
- Johnston, H.T., Elsayy, E.M., Hamill, G., McKillen, H.G., *A study of scour and deposition near a berth structure caused by propulsion action of manoeuvring ships.*, 21st IAHR Congress, Melbourne, 1985, p. 117-122.
- Kraatz, W., *Flüssigkeitsstrahlen*, Technische Hydromechanik, V 2, 1989.
- Meijer, D.G., Verheij, H.J., *Stroomsnelheden bij de oever veroorzaakt door boegschroeven*, WL report, 1993.

---

Rajaratnam, N., *Turbulent jets*, Elsevier, 1976.

Rajaratnam, N., Aderibigbe, O., *Erosion of loose beds by submerged circular impinging vertical turbulent jets*, *Journal of Hydraulic Research*, 34, 1, p. 19-33, 1996.

Rajaratnam and Beltaos, *Erosion by impinging circular turbulent jets*, *Journal of Hydraulics Division*, 103, 10, p. 1191-1204, 1977.

Rijkswaterstaat, *Schroefstraalerosie bij aanlegplaatsen langs het Amsterdam-Rijnkanaal*, nota S 85.105, 1985.

Römisch, K., and Fuehrer, M. *Effects of modern ship traffic on inland- and ocean waterways and their structures*, 24<sup>th</sup> Int. Navigation Congress, Leningrad, S.I-3, p79-94, 1977.

Römisch, K., and Fuehrer, M., *Criteria for dimensioning the bottom and slope protections and for applying the new methods of protecting navigation channels*. PIANC's 25<sup>th</sup> Int. Navigation Congress, Edinburgh, S.I-1, p.29-37, 1981.

Römisch, K., *Der Propellerstrahl als erodierendes Element bei An- und Ablegmanövern im Hafenbecken*, *Seewirtschaft*, 7, 7, p. 431-434, 1975.

Römisch, K., *Propellerstrahlinduzierte Erosionserscheinungen in Häfen*, *Hansa*, 1993, p. 62-68.

Schiereck, G.J., *Introduction to bed, bank and shore protection*, DUT lecture notes, 2000.

Schmidt, E., *Ausbreitungsverhalten und Erosionswirkung eines Bugpropellerstrahles vor einer Kaiwand*, Leightweiss-Institut für Wasserbau der Technischen Universität Braunschweig, *Mitteilungen Heft 143/1998*, 1998.

Shields, A., *Anwendung der Ähnlichkeitsmechanik un der Turbulenzforschung auf die Geschiebebewegung*, *Mitteilungen der Preussischen Versuchanstalt für Wasserbau und Schiffbau*, Berlin, 26, 1936.

Velden, E.T.J.M., van der, *Coastal Engineering*, DUT lecture notes, 2000.

Veldhoven, V., van, *Vooronderzoek schroefstraal op een talud met breuksteen*, DUT M.Sc. thesis, 2001.

Verheij, H.J., *The stability of bottom and banks subjected to the velocities in the propeller jet behind ships*, 8<sup>th</sup> Int. Harbour Congress, Antwerp, 303, p. 1-11, 1983.

---

Verheij, H.J., *Voorspellen stroomsnelheden en ontgroningen bij schroefstralen*, WL publication, 2000.

Weijde, R.W., van der, Heijndijk, P.J.M., Noordijk, A.C., Kleijheeg, J.T., *Scouring by ships' propellers*, 10<sup>th</sup> int. harbour congress Antwerp, 1992, s. 6.1-6.17.

Westrich, B., and Kobus, H. *Einfluss stationärer und pulsierender Strahlen auf die Erosion eines Sandbettes*, Universität Karlsruhe, Bericht des Sonderforschungsbereiches 80, 1974.

WL, *Aantasting van dwarsprofielen in vaarwegen*, Physical Model Research, WL, M115.V7, 1985.

## APPENDICES

A.	Experimental model dimensions	A-1
B:	Pictures of the model	A-5
C:	Velocity profiles for ducted and free propeller	A-9
D:	Autocorrelation and Power Density Spectra of the jet	A-15
E:	PASCAL program 'diameter of opening in board'	A-23
F:	PASCAL program 'dataset analysis'	A-25
G:	Velocities and turbulences in the free-propeller jet	A-29
H:	Depth profile of the Amsterdam-Rijnkanaal at Houten	A-33
I:	Principle of operation of the EMS	A-35



## **A. Experimental model dimensions**

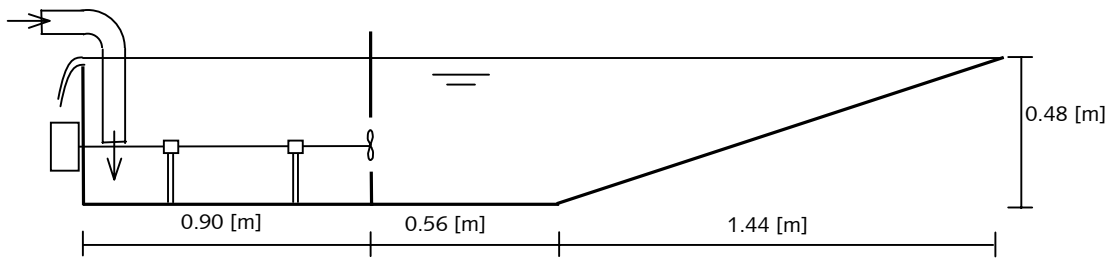


figure A-1 Side view and dimensions of the free-propeller model.

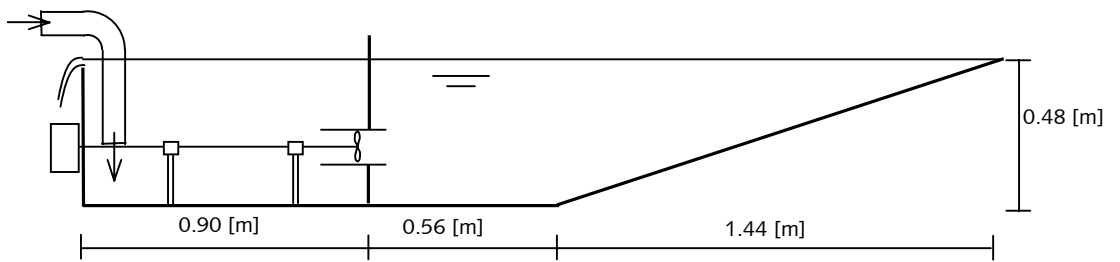


figure A-2 Side view and dimensions of the ducted-propeller model.

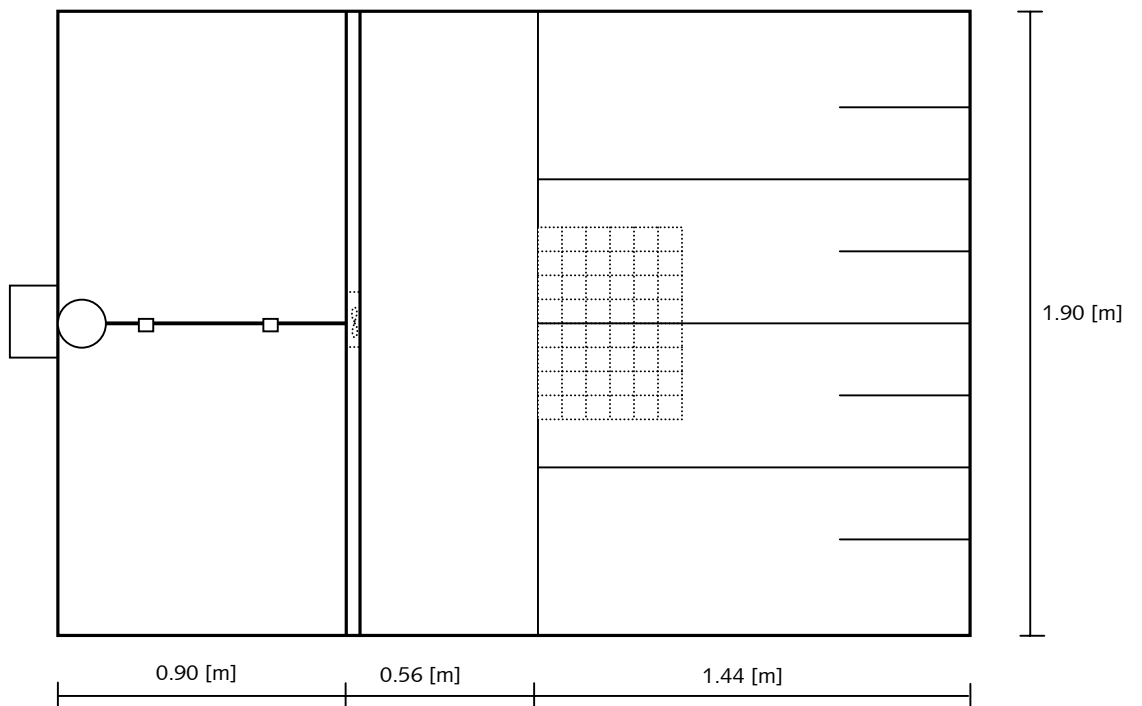


figure A-3 Top view and dimensions of the free-propeller model.

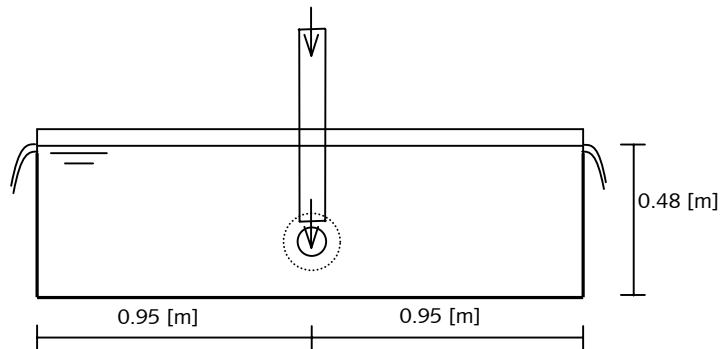


figure A-4 Front view of the ducted- and free-propeller model (dotted line is the size of the opening for the free propeller).

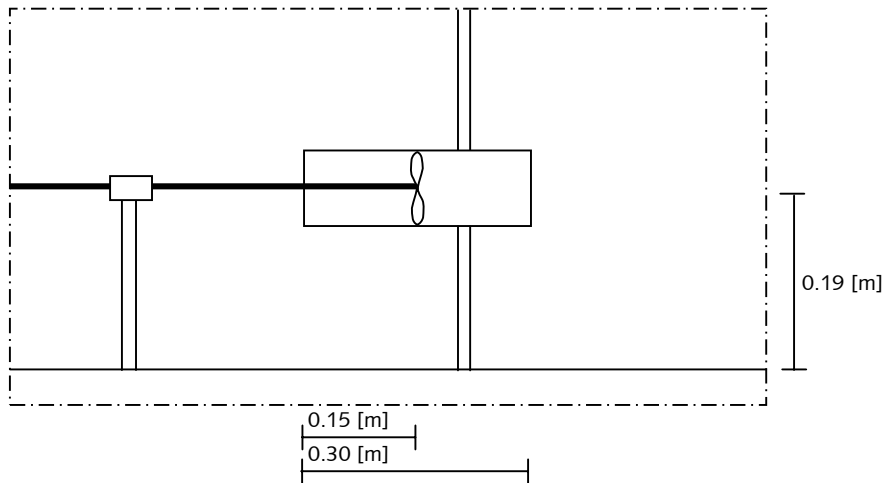


figure A-5 Detailed side view of the propeller in ducted situation.





## **B. Pictures of the model**



figure B-1 The ducted propeller and the coloured stones on the slope.

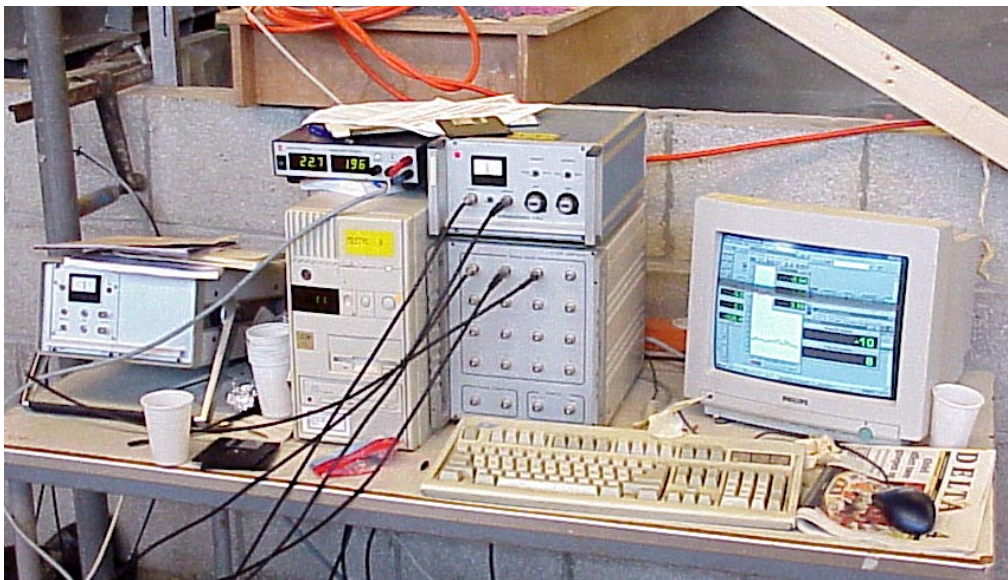
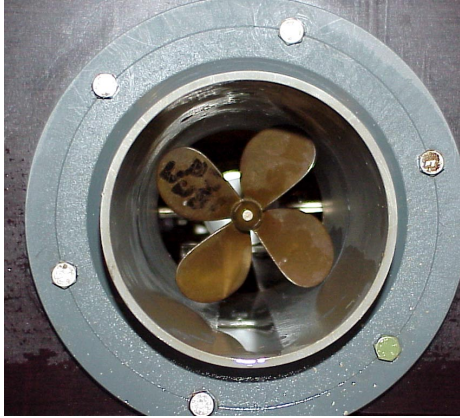


figure B-2 The data-processing equipment.





brand: Raboesch  
type: 167-31 R M5  
diameter: 0.100 [m]  
number of blades: 4 [-]  
material: brass

*figure B-3 The propeller in the duct.*

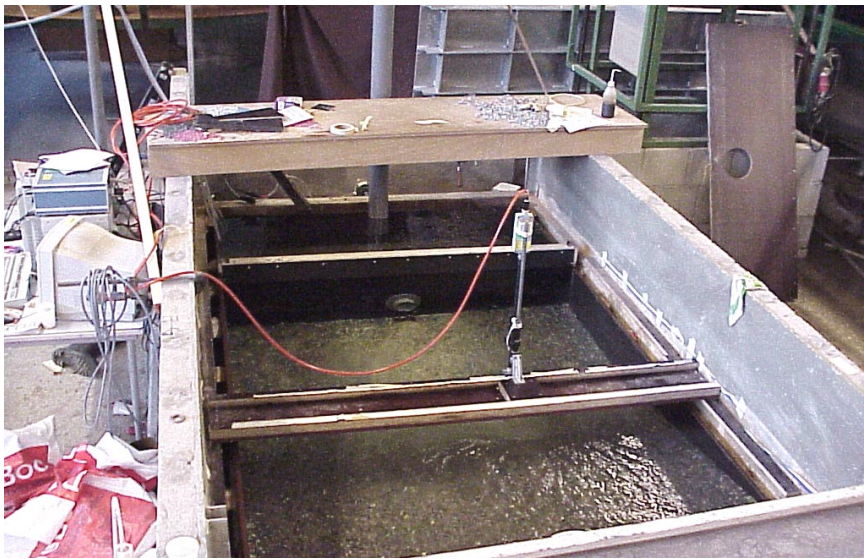


*figure B-4 The EMS during velocity measurements. On the right the board for the free propeller.*



*figure B-5 The coloured squares of stones on the slope.*



## **C. Velocity profiles for ducted and free propeller**

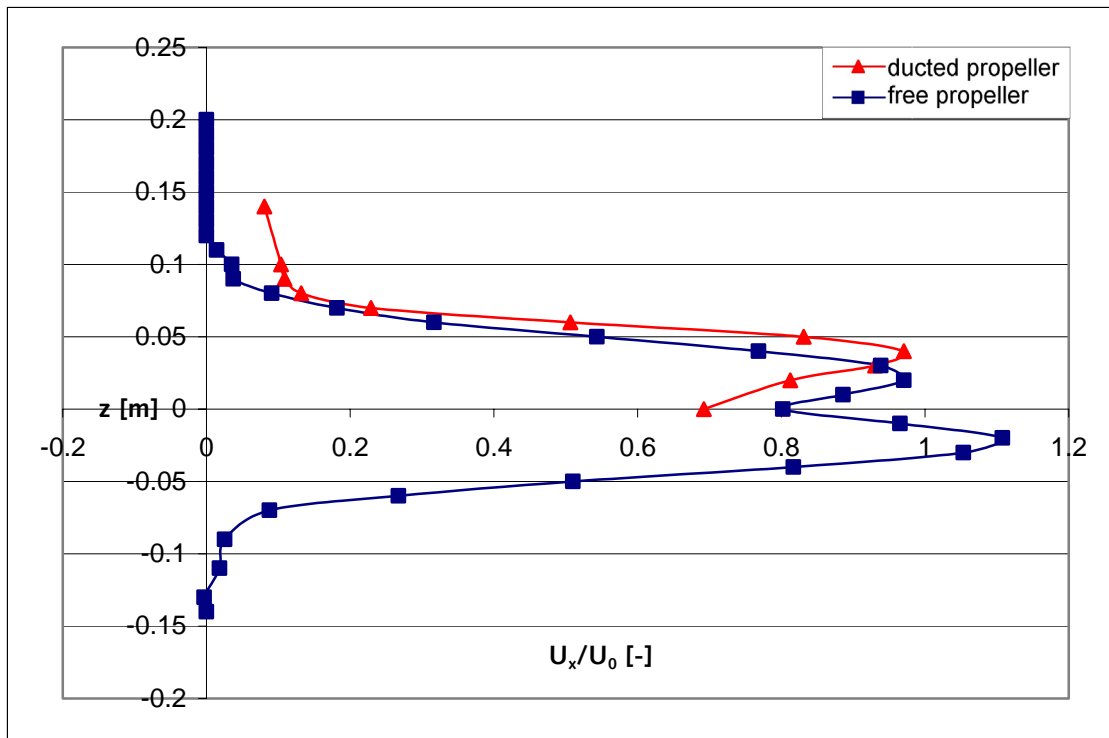


figure C-1 Velocity distribution over the height of the jet for the ducted and free propeller at  $X/D = 1$  [-].

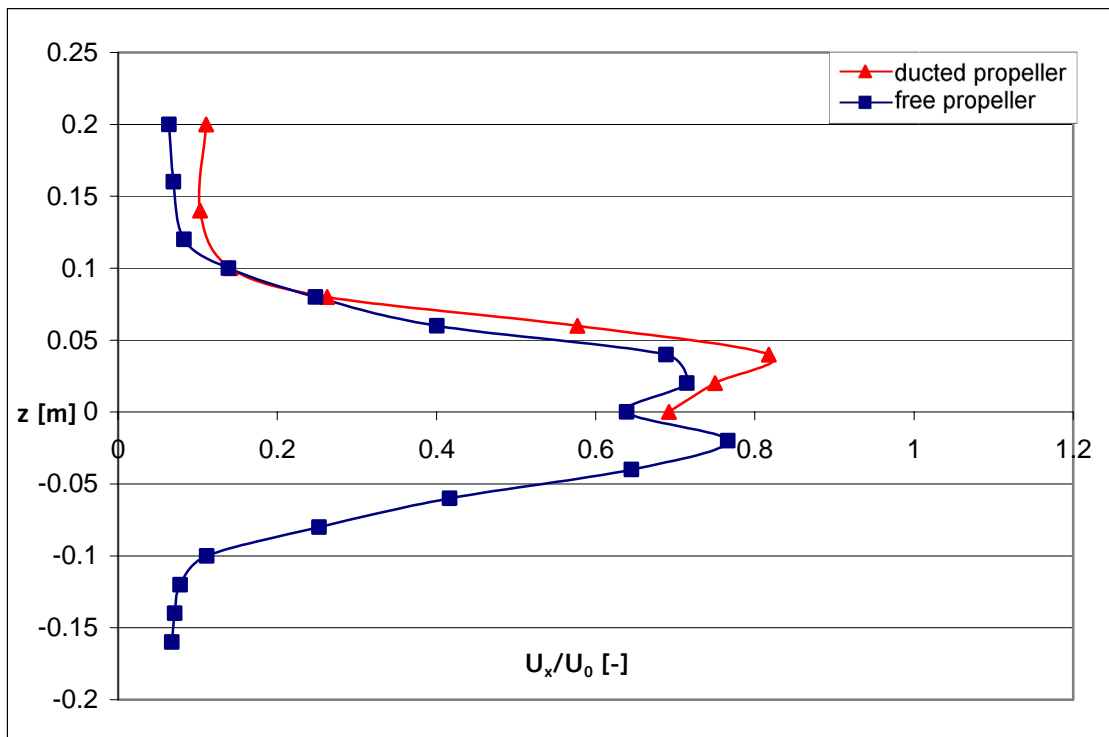


figure C-2 Velocity distribution over the height of the jet for the ducted and free propeller at  $X/D = 2$  [-].

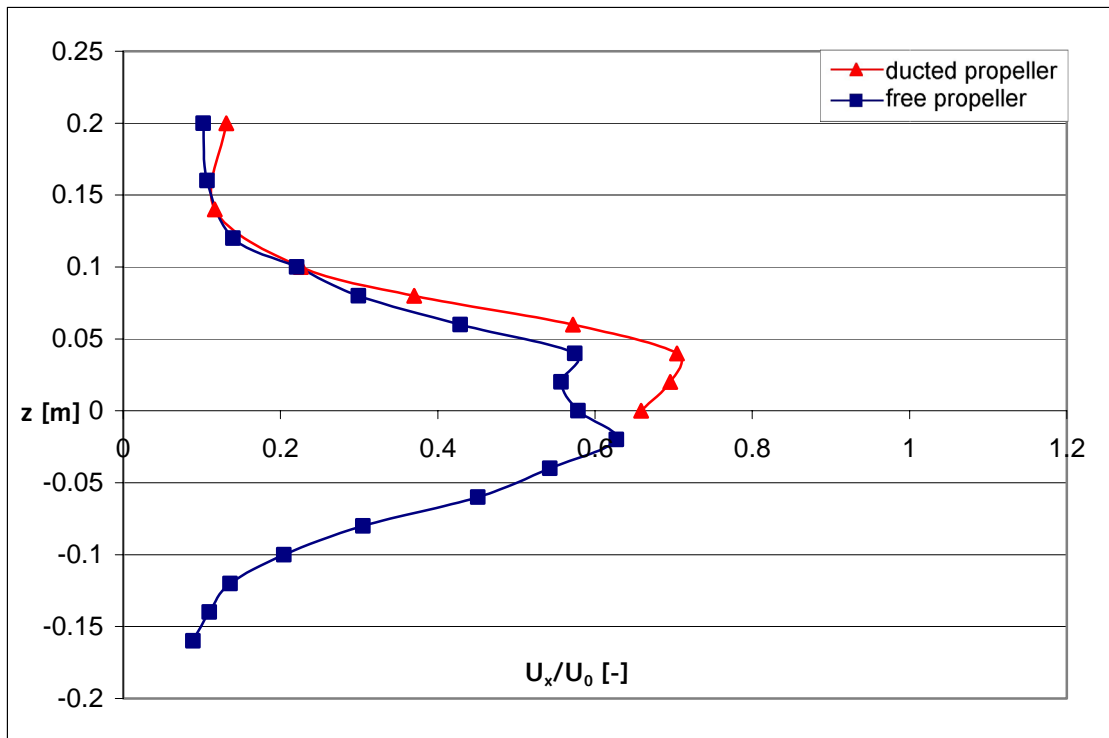


figure C-3 Velocity distribution over the height of the jet for the ducted and free propeller at  $X/D = 3$  [-].

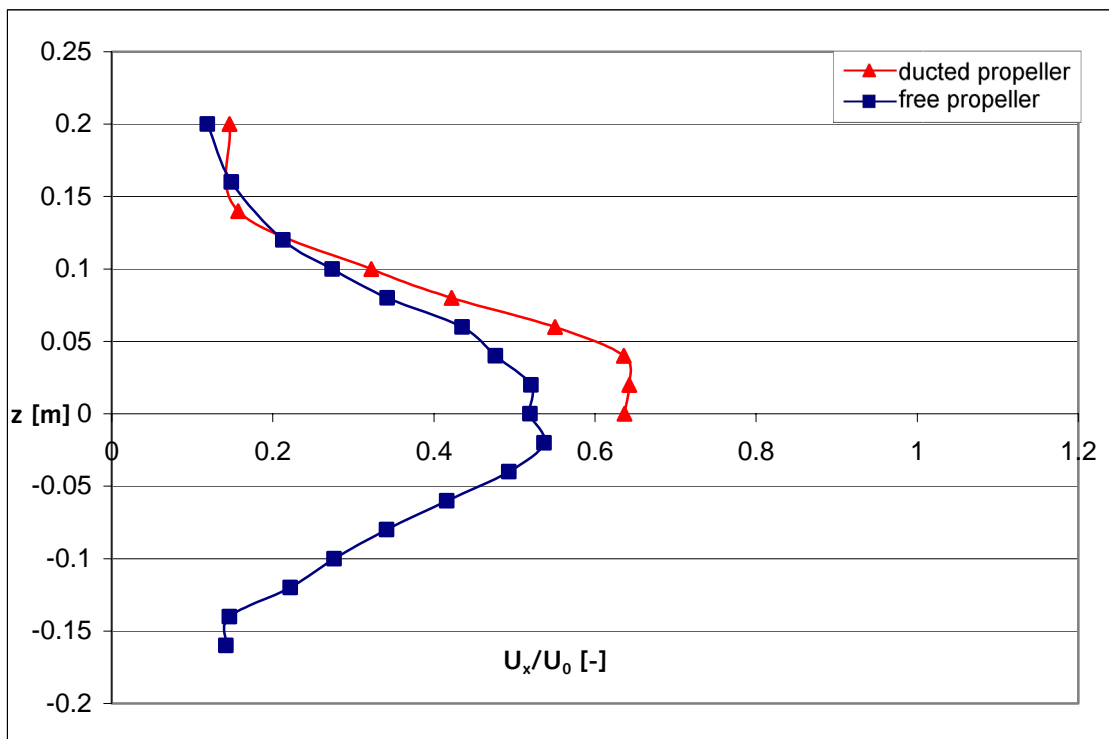


figure C-4 Velocity distribution over the height of the jet for the ducted and free propeller at  $X/D = 4$  [-].



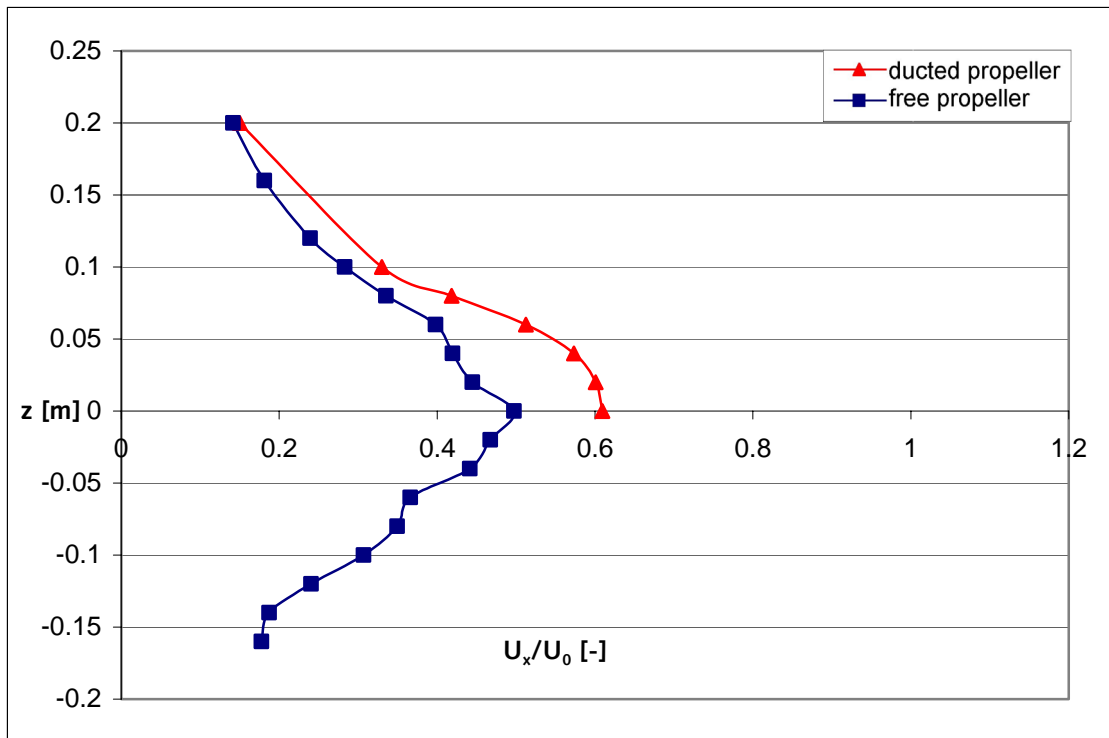


figure C-5 Velocity distribution over the height of the jet for the ducted and free propeller at  $X/D = 5$  [-].

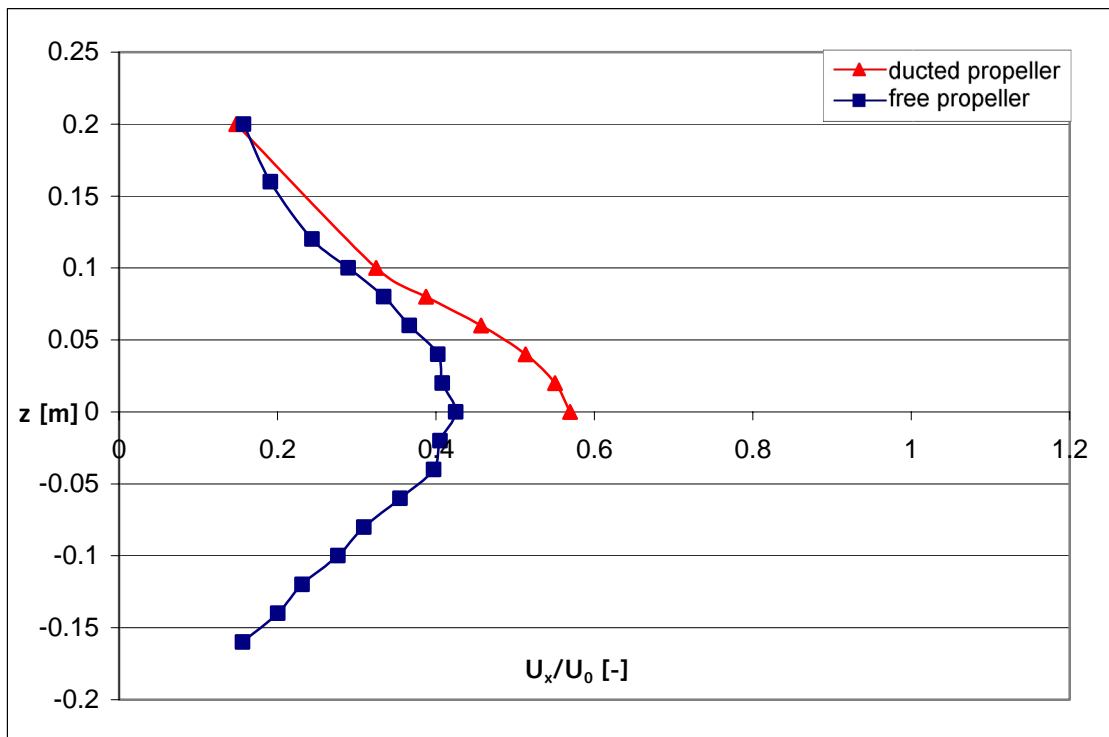


figure C-6 Velocity distribution over the height of the jet for the ducted and free propeller at  $X/D = 6$  [-].

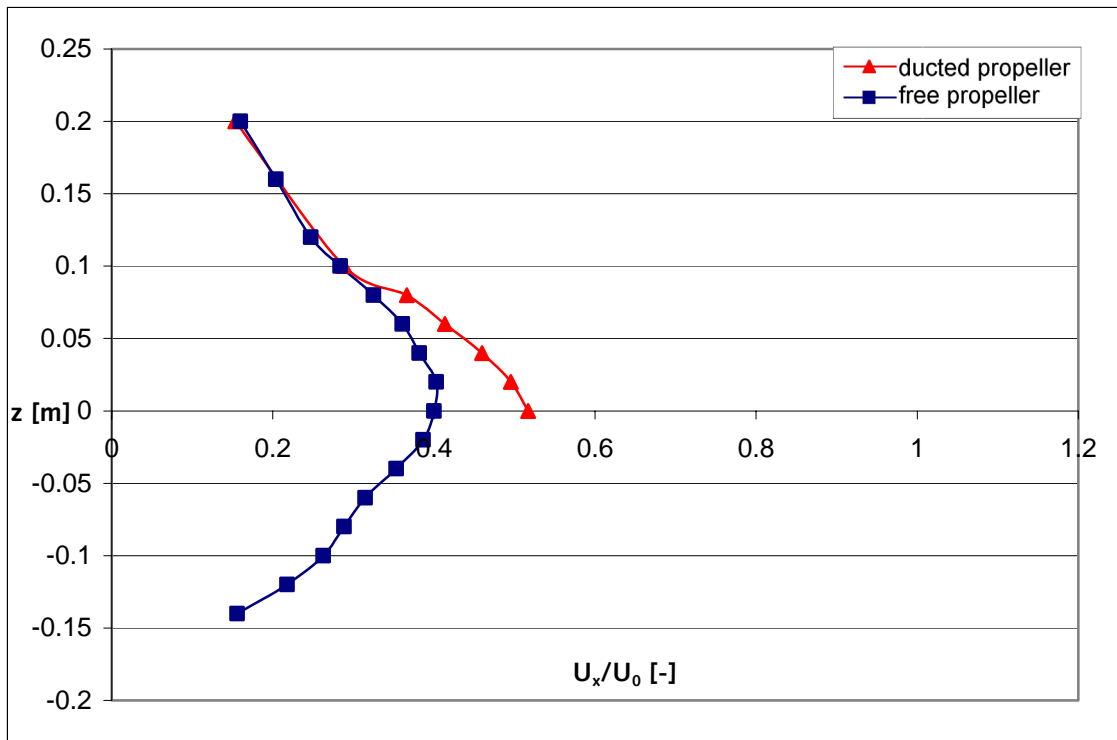


figure C-7 Velocity distribution over the height of the jet for the ducted and free propeller at  $X/D = 7$  [-].



## **D. Autocorrelation and Power Density Spectra of the jet**

### Autocorrelation

Autocorrelation coefficients measure the correlation between observations at different distances or time steps apart. The coefficient can be used to get an idea of the size of the average vortex in the water. A vortex is transported by the average water velocity. As long as the correlation between several lags 'k' is positive, the fluctuations in those steps have a similar direction. During this time ( $T = k_q - k_0$  [s]) the vortex passes the (measuring) point with a velocity equal to the average water velocity.

The size of the vortex ( $\lambda$  [m]) then equals:

$$\lambda = \bar{U} \cdot T \quad [\text{m}] \quad (\text{D-1})$$

In a given dataset with time step 't' the following equation gives the autocorrelation coefficient<sup>A1</sup> for two given points  $x_t$  and  $x_{t+1}$ :

$$r_1 = \frac{\sum_{t=1}^{N-1} (x_t - \bar{x}_{(1)})(x_{t+1} - \bar{x}_{(2)})}{\sqrt{\left[ \sum_{t=1}^{N-1} (x_t - \bar{x}_{(1)})^2 \sum_{t=1}^{N-1} (x_{t+1} - \bar{x}_{(2)})^2 \right]}} \quad [-] \quad (\text{D-2})$$

In practice the series of autocorrelation coefficients are usually calculated by computing the series of autocovariance coefficients  $\{c_k\}$ . We then compute  $r_k$  in the following manner:

$$r_k = c_k / c_0 = \frac{\frac{1}{N} \sum_{t=1}^{N-k} (x_t - \bar{x})(x_{t+k} - \bar{x})}{\frac{1}{N} \sum_{t=1}^N (x_t - \bar{x})^2} \quad [-] \quad (\text{D-3})$$

Here we will use it to calculate the correlation of the fluctuations in time at a certain point.

If we now compute these values of  $r_k$  for every lag 'k' we derive the following figure (D-1) (chosen is to use the point at  $x' = 0.45$  [m],  $y = 0$ ,  $z' = 0.025$  [m], measured with the type II EMS at the slope. This type is chosen since it gives the opportunity to compare the measurements at the slope with the measurements which Van Veldhoven (2001) took in the jet):

---

<sup>A1</sup> For further explanation of autocorrelation the reader is for instance referred to 'The analysis of time series' by Chatfield, published by Chapman & Hall 1996.

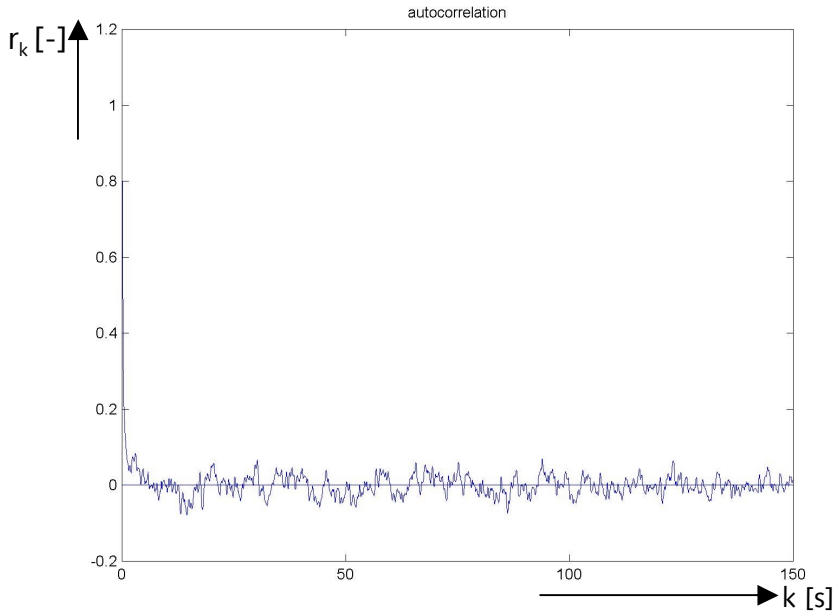


figure D-1 Autocorrelation for  $0 < k < 150$  [s] at  $x' = 0.45$  [m],  $y = 0$ ,  $z' = 0.025$  [m].

At  $k = 0$  the autocorrelation coefficient  $r_k$  equals 1 [-] (by definition) and decreases fast. If regular sinusoids can be detected this would tell us something about the sizes of vortices that are present in the water. From figure (D-1) it seems that no regular sinusoids can be visually detected.

However, it is possible to detect the average vortex size in the following manner: At the point where it becomes zero for the first time there is no correlation anymore between lag  $k_0$  and lag  $k_q$ . The time period 'T' that is needed to reach this point is used to calculate the size of the average vortex using equation (D-1).

In figure (D-2) the first part of figure (D-1) is shown in some more detail:

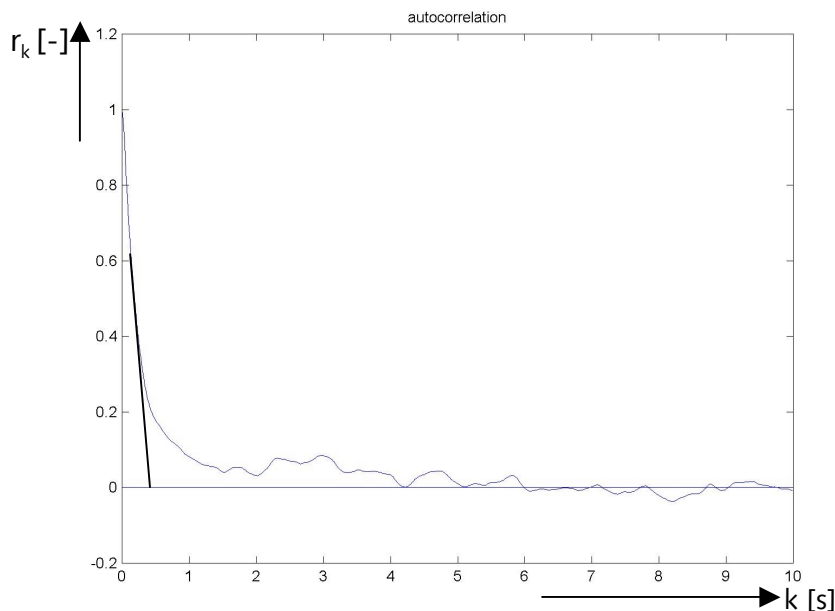


figure D-2 Correlogram for  $0 < k < 10$  [s] at  $x' = 0.45$  [m],  $y = 0$ ,  $z' = 0.025$  [m].

It appears that at  $k_q = 4.2$  [s] the graph crosses the x-axis for the first time.

It is however clear that this is not a smooth line, but that it shows ups and downs before it crosses the x-axis. It is believed that smaller vortices are superimposed to larger vortices, giving fluctuations on fluctuations. To calculate the smallest governing vortex made visible by this method we use the initial direction of the graph at  $k = 0$  and discard all superimposed vortices.

When following this initial direction of the line it would cross at approximately  $k = 0.3$  [s] (see figure (D-2)). With an average velocity at the measured point of  $0.46$  [m/s] this leads to a vortex of  $0.14$  [m] using equation (D-2).

It is decided to compare this correlogram to the correlogram of a point in the developing jet. Chosen was to do this at  $x = 0.10$  [m] from the propeller,  $y = 0$ ,  $z = -0.05$  [m]. The two compared points are practically on the same height, making an interesting comparison. Figure (D-3) shows the correlogram of the point in the jet at  $x = 0.10$  [m] from the propeller,  $y = 0$ ,  $z = -0.05$  [m].

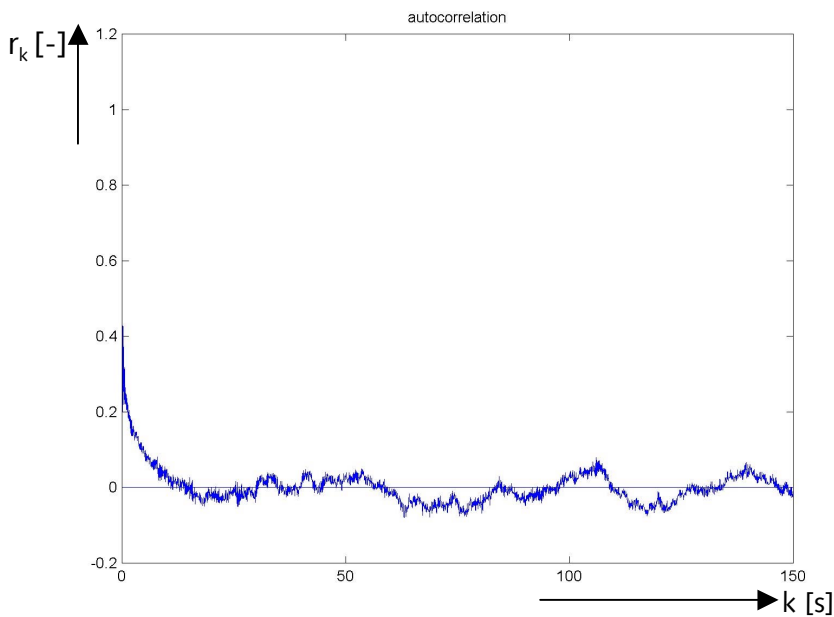


figure D-3 Autocorrelation at  $x = 0.10$  [m] from the propeller,  $y = 0$ ,  $z = -0.05$  [m].

There is clearly a large difference between the two points (see figure (D-1) and (D-3)). There seems to be a distinct sinusoid in the correlation pattern with a large period of approximately 30 [s]. When looking at figure (D-1) it shows that there may also be a sinusoid with a large period in the correlation pattern at the slope, but if so, it is much less clear than for the point in the developing jet. The cause of this sinusoid can be various; a standing wave in the basin or an irregularity in the rotation rate of the engine are possible causes.

We will look at the correlogram of this point (figure (D-3)) in some more detail in figure (D-4).

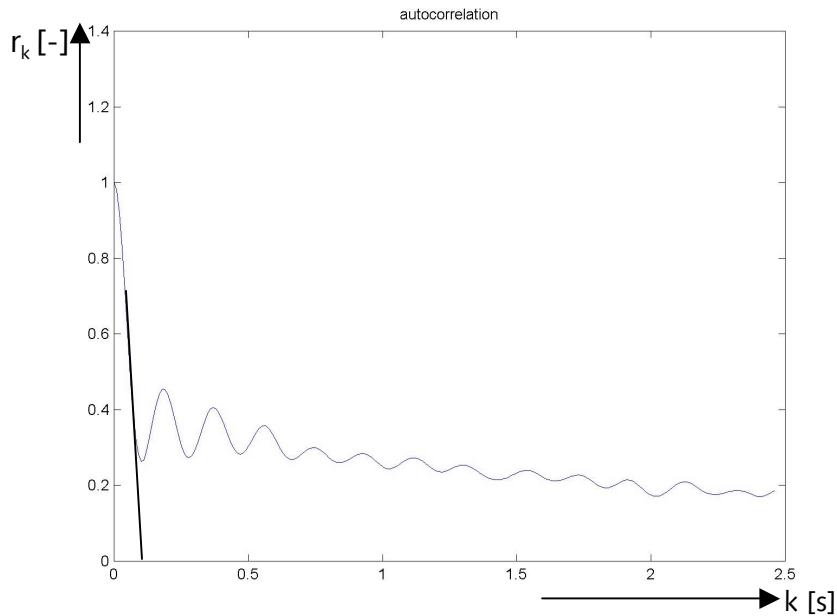


figure D-4 Autocorrelation at  $x = 0.10 [m]$  from the propeller,  $y = 0, z = -0.05 [m]$ .

The initial direction of the graph intersects the x-axis at 0.1 [s]. With an average velocity at the here considered point of 1.0 [m/s] it yields that the average vortex has a length of approximately 0.1 [m]. It may very well be so that this is the size of vortices created directly by the propeller (which has a diameter of 0.10 [m]).

### Power density spectrum

Another way of analysing a dataset is to create a power density spectrum. It is a spectrum in which the occurring frequencies of the vortex are plotted against a measure for the energy ' $E\omega$ ' ( $[m^2/s^2/Hz]$ ) the vortices carry<sup>A2</sup>.

In figure (D-5) this is done for the point  $x' = 0.45 [m]$ ,  $y = 0$ ,  $z' = 0.025 [m]$  at the slope.

---

<sup>A2</sup> Here the Fast Fourier Transformation method is used to derive the PDS.



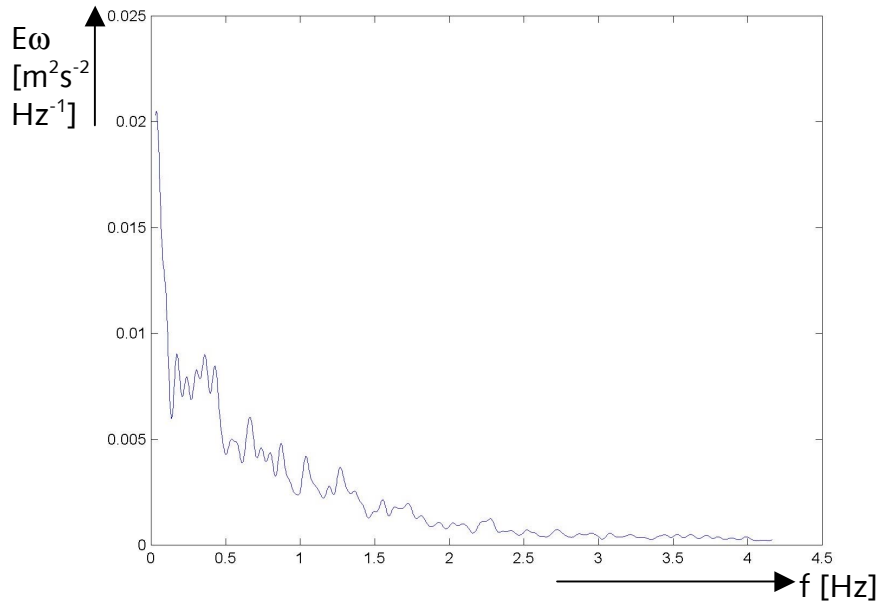


figure D-5 PDS at  $x' = 0.45$ ,  $y = 0$ ,  $z' = 0.025$  [m] at the slope.

It shows that most energy is located in vortices with a small frequency ( $f < 2$  [Hz] or  $T > 0.5$  [s]). After  $f > 4.5$  [Hz] the energy becomes practically zero and is therefore not shown in the plot. The energy peak at a frequency of 0 [Hz] is considered to be the average velocity (with an infinite period) and is not interesting when looking at vortices.

If we compare this point to the previous mentioned point at  $x = 0.10$  [m] from the propeller,  $y = 0$ ,  $z = -0.05$  [m] the following shows in figure (D-6):

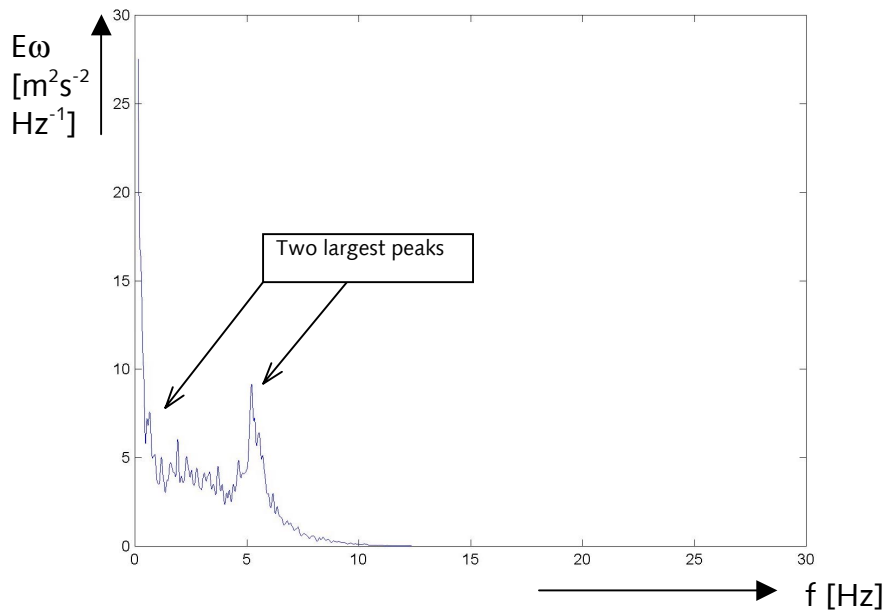


figure D-6 PDS at  $x = 0.10$  [m] from the propeller,  $y = 0$ ,  $z = -0.05$  [m]

First of all, the energy of the vortices in the jet is approximately 1000 times higher than the energy of the vortices at the slope. This is logical since the propeller puts the energy directly into the vortices after which they mix it with the surrounding water, creating smaller vortices which eventually lose their energy by creating heat. Apparently a lot of energy is dissipated when the jet has reached the slope.

Secondly, there appears to be a distinct energy peak at  $f = 5.5$  [Hz] (or  $T = 0.18$  [s]).

The maximum velocity of the fluctuation at the here considered point was found to be  $0.30$  [m/s]. If we consider the rotation velocity at the surface area of the vortex it follows that  $U' = \pi \cdot D \cdot f$ . This means that a vortex with a frequency of  $5.5$  [Hz] and a maximum fluctuation velocity of  $0.30$  [m/s] cannot be larger than approximately  $0.02$  [m].

If looking closely at figure (D-6) it shows that at approximately  $1$  [Hz] there is another peak, slightly lower than the one at  $5.5$  [Hz]. The maximum vortex size here ends up to be  $0.10$  [m], the size of a governing vortex already found in the corresponding autocorrelation plot.

We can not perform a similar calculation for values at the slope since there are no real peaks that can be distinguished. It is however clear that a lot of the energy is found around  $f = 0.5$  [Hz]. The maximum found fluctuation at this point equals  $0.58$  [m]. This leads to a maximum vortex at  $0.5$  [Hz] of  $0.35$  [m]. When the same is done for even lower frequencies the size increases. It is therefore concluded that most energy at the slope is found in relatively large vortices (which according to Booij (1992) is always the case).

Also, according to Booij (1992) the turbulence loses its energy through the smallest vortices ( $d = 10^{-10}$  [m]), creating heat. Since there is hardly any energy in the vortices left at the slope (compared to the energy just behind the propeller) this indicates that these vortices are present in the water. Since smaller vortices develop from larger vortices it is considered that the entire range of vortices from  $0.14$  [m] (found in the autocorrelation plot) to  $10^{-10}$  [m] is present in the water. However, it does not become clear how much energy the vortices with a size of approximately the stone diameter have, which is believed to be important to the stability of the stones.

### Conclusions

From the above two sections, autocorrelation and power density spectrum, the following is clear:

- The average governing vortex at the slope has a diameter of approximately  $0.14$  [m]. The smaller governing vortices could not be detected with this method.
- From the power density spectrum follows that the energy in the vortices at the slope is considerably less than the energy in the vortices just behind the propeller.
- From the power density spectrum it is also concluded that at the slope the energy is found in the relatively large vortices, with no

distinct energy peaks at any frequencies. Just behind the propeller however there is a distinct increase of energy in vortices with a frequency of 1 [Hz] and 5 [Hz]. The size of these vortices is believed to be at most 0.10 [m] respectively 0.02 [m].

## **E. PASCAL program 'diameter of opening in board'**

```

program gatgrootte;
uses wincrt;
var
y:real;
b:real;
r:real;
x:real;
t:integer;
opp:real;
opptot:real;
dt:real;
e:real;
total:real;
W:real;
xtotal:real;
uitvoer:text;
a:real;
wtotaal:real;
begin
assign (uitvoer, 'c:\uitvoer.txt');
rewrite (uitvoer);
dt:=0.001;
e:=0;
w:=0;
r:=0;
b:=1;
wtotaal:=0;
opp:=0;
opptot:=0;
xtotal:=0;
total:=0;
while e<10 do
begin
if e>=0.5 then begin }
w:=dt*exp(-0.5*((e-1.68)/0.36)*((e-1.68)/0.36));
wtotaal:=wtotaal+w;
A:=exp(-0.693*2.53*2.53)/(sqrt(2*pi)*0.36)*wtotaal;
{end; }
x:= (exp(-0.693*(e)*(e))- A)*2;
{writeln (wtotaal);
writeln(A); }
xtotal:=x*(pi*(e+dt)*b*(e+dt)*b-pi*e*e*b*b);
total:=total+xtotal;
opp:= (pi*(e+dt)*b*(e+dt)*b-pi*e*e*b*b);
opptot:=opp+opptot;
if e >=1.6 then begin
writeln('y ',e*b:4:3);
e:=100;
end;
if x <0 then begin
writeln('eta ',e:3:2);
e:=100;
end;
writeln ('Totaal Debiet/Um ',total:5:4);
writeln (uitvoer,e:3:2,', ', x:8:7);
e:=e+dt;

end;
writeln ('oppervlakte ',opptot:3:2);
close (uitvoer);
end.

```

**F. PASCAL program 'dataset analysis'**

```

program dataset (uitvoer);

uses wincrt;
var {aanroepen en definiëren van variabelen}
a,x,y,L,xrgem,w,yrgem,xtotaal,ytotaal,ry,rx,ygem,xgem,xfluc,yfluc,xrsqrt,yrsqrt:real;
t,d,xw,yw: integer;
invoer,uit1,uitvoer,uitv,inv:text;
filenaam: string;

begin
w:=3.4;
assign (uitv, 'uit.txt');
  rewrite (uitv);
assign (uit1, 'uit1.txt');
  rewrite (uit1);

while t<200000 do
begin
a:=1;
while a=1 do
begin
t:=0;
xtotaal:=0 ;
ytotaal:=0;

{$I-}
writeln ('x');
readln (xw);
writeln ('y');
readln (yw);
writeln ('d');
readln (d);

if xw=1 then
begin
writeln ('a');
close (uitv);
close (uit1);
end;
  assign (uitvoer, 'uitvoer.txt');
  rewrite (uitvoer);
writeln (uitvoer, 'y',yw,'x',xw,'.ASC');
close (uitvoer);
assign (inv, 'uitvoer.txt');
reset (inv);
read (inv, filenaam);
writeln (filenaam);
writeln (uitv, filenaam);
close (inv);
  assign (invoer, filenaam);
  reset (invoer);

if ioresult=0 then a:=0 else writeln ('bestaat niet');;
{$I+}
end;
readln (invoer); readln (invoer);readln (invoer);readln (invoer);readln (invoer);readln (invoer);readln (invoer);
readln (invoer);

  while t<18000 do
begin
read (invoer, L);read (invoer, y);read (invoer, x);readln (invoer);
ytotaal:=ytotaal+y;
xtotaal:=xtotaal+x;
t:=t+1;

```

```

end;
xgem:=xtotaal/18000;
ygem:=ytotaal/18000;
writeln ('xgem,ygem ',xgem:6:5,' ',-ygem:6:5);
writeln (uitv,'xgem,ygem ',xgem:6:5,' ',-ygem:6:5);
t:=0;
xtotaal:=0;
ytotaal:=0;
reset (invoer);
readln (invoer);readln (invoer);readln (invoer);readln (invoer);readln (invoer);readln (invoer);readln
(invoer);
readln (invoer);
while t<18000 do
begin
read (invoer, L);read (invoer, y);read (invoer, x);readln (invoer);
xfluc:=x-(xgem);
yfluc:=y-(ygem);
xtotaal:=xtotaal+(xfluc*xfluc);
ytotaal:=ytotaal+(yfluc*yfluc);
t:=t+1;
end;
xrgem:=xtotaal/18000;
yrgem:=ytotaal/18000;
xrsqrt:=sqrt(xrgem);
yrsqrt:=sqrt(yrgem);
writeln ('sqrtx, sqrty ',xrsqrt:4:3,' ',yrsqrt:4:3);
writeln ('piek x, piek y ',((abs(xgem))+w*xrsqrt):4:3,' ',((abs(ygem))+w*yrsqrt):4:3);
writeln ('piektotaal ',(sqrt(((abs(xgem))+w*xrsqrt)*((abs(xgem))+w*xrsqrt))+((abs(ygem))+w*yrsqrt)*
((abs(ygem))+w*yrsqrt))):4:3);
writeln ('hoek ',(arctan(ygem/xgem)*180/pi):4:3);

writeln (uitv,'sqrtx, sqrty ',xrsqrt:4:3,' ',yrsqrt:4:3);
writeln (uitv,'piek x, piek y ',((abs(xgem))+w*xrsqrt):4:3,' ',((abs(ygem))+w*yrsqrt):4:3);
writeln (uitv,'piektotaal ',
(sqrt(((abs(xgem))+w*xrsqrt)*((abs(xgem))+w*xrsqrt))+((abs(ygem))+w*yrsqrt)*
((abs(ygem))+w*yrsqrt))):4:3);
writeln (uitv,'hoek ',(arctan(ygem/xgem)*180/pi):4:3);
ry:=yrsqrt/abs(ygem);
rx:=xrsqrt/abs(xgem);
if ry < 0 then ry:=ry*-1;
if rx < 0 then rx:=rx*-1;
writeln ('rx,ry ',rx:4:3,' ',ry:4:3);
writeln (uitv,'rx,ry ',rx:4:3,' ',ry:4:3);
writeln (uit1,xw,' ',yw,' ',(sqrt((abs(xgem)*abs(xgem))+((abs(ygem))*
(abs(ygem))))):4:3,' ',(sqrt(((abs(xgem))+w*xrsqrt)*((abs(xgem))+w*xrsqrt))+((abs(ygem))+w*yrsqrt)*
((abs(ygem))+w*yrsqrt))):4:3,' ',(arctan(ygem/xgem)*180/pi):4:3);

end;
close (uitv);
end.

```





## **G. Velocities and turbulences in the free propeller jet**

x [m]	z [m]	Ux [m/s]	Uy [m/s]	x [m]	z [m]	Ux [m/s]	Uy [m/s]	x [m]	z [m]	Ux [m/s]	Uy [m/s]
0.05	0.1	-0.026	-0.039	0.2	0.2	0.088	-0.003	0.5	0.2	0.195	0.028
	0.08	-0.014	-0.031		0.16	0.096	-0.001		0.16	0.250	0.038
	0.06	0.203	0.368		0.12	0.114	0.028		0.12	0.330	0.105
	0.05	0.495	0.912		0.1	0.191	0.000		0.1	0.390	0.124
	0.045	0.775	1.128		0.08	0.342	0.183		0.08	0.462	0.118
	0.04	1.087	1.277		0.06	0.552	0.332		0.06	0.549	0.138
	0.035	1.364	1.292		0.04	0.949	0.444		0.04	0.579	0.136
	0.03	1.559	1.120		0.02	0.985	0.443		0.02	0.613	0.104
	0.025	1.524	0.961		0	0.881	0.150		0	0.686	0.074
	0.02	1.469	0.849		-0.02	1.056	-0.114		-0.02	0.644	0.052
	0.015	1.403	0.718		-0.04	0.889	-0.147		-0.04	0.609	0.029
	0.01	1.351	0.620		-0.06	0.574	-0.167		-0.06	0.505	0.007
	0.005	1.286	0.481		-0.08	0.348	-0.180		-0.08	0.482	-0.027
	0	1.229	0.249		-0.1	0.154	-0.066		-0.1	0.423	-0.045
	-0.005	1.351	-0.041		-0.12	0.108	-0.013		-0.12	0.332	-0.044
	-0.01	1.473	-0.140		-0.14	0.098	-0.045		-0.14	0.258	-0.025
	-0.015	1.572	-0.196						-0.16	0.245	-0.077
	-0.02	1.678	-0.298								
	-0.025	1.735	-0.403	0.3	0.2	0.140	-0.001				
	-0.03	1.701	-0.478		0.16	0.147	0.021	0.6	0.2	0.217	0.036
	-0.035	1.447	-0.555		0.12	0.193	0.080		0.16	0.264	0.051
	-0.04	1.101	-0.552		0.1	0.304	0.068		0.12	0.336	0.083
	-0.045	0.755	-0.467		0.08	0.412	0.145		0.1	0.399	0.110
	-0.05	0.444	-0.393		0.06	0.591	0.231		0.08	0.461	0.107
	-0.055	0.207	-0.242		0.04	0.792	0.280		0.06	0.505	0.104
	-0.06	0.065	-0.134		0.02	0.768	0.241		0.04	0.555	0.101
	-0.07	-0.010	-0.075		0	0.797	0.122		0.02	0.562	0.082
					-0.02	0.865	-0.037		0	0.586	0.066
					-0.04	0.748	-0.060		-0.02	0.559	0.037
					-0.06	0.622	-0.085		-0.04	0.548	0.041
					-0.08	0.420	-0.093		-0.06	0.489	0.013
					-0.1	0.281	-0.085		-0.08	0.426	-0.016
					-0.12	0.188	-0.014		-0.1	0.381	-0.007
					-0.14	0.151	-0.024		-0.12	0.318	0.005
					-0.16	0.122	-0.014		-0.14	0.276	-0.007
									-0.16	0.215	-0.019
0.1	0.11	0.020	-0.043								
	0.1	0.048	-0.121								
	0.09	0.052	-0.048								
	0.08	0.125	0.049								
	0.07	0.251	0.241								
	0.06	0.436	0.419								
	0.05	0.749	0.661								
	0.04	1.059	0.872								
	0.03	1.294	0.886	0.4	0.2	0.164	0.022				
	0.02	1.338	0.746		0.16	0.205	0.039	0.7	0.2	0.057	0.220
	0.01	1.221	0.520		0.12	0.293	0.128		0.16	0.065	0.281
	0	1.106	0.147		0.1	0.377	0.091		0.12	0.087	0.341
	-0.01	1.330	-0.089		0.08	0.472	0.139		0.1	0.106	0.391
	-0.02	1.527	-0.277		0.06	0.600	0.181		0.08	0.121	0.448
	-0.03	1.453	-0.369		0.04	0.657	0.186		0.06	0.094	0.498
	-0.04	1.126	-0.394		0.02	0.717	0.154		0.04	0.127	0.569
	-0.05	0.703	-0.303		0	0.716	0.095		0.02	0.119	0.555
	-0.06	0.368	-0.277		-0.02	0.740	0.019		0	0.073	0.551
	-0.07	0.121	-0.089		-0.04	0.680	-0.010		-0.02	0.057	0.533
	-0.09	0.035	-0.014		-0.06	0.574	-0.052		-0.04	0.034	0.487
	-0.11	0.025	0.036		-0.08	0.471	-0.053		-0.06	0.018	0.434
	-0.13	-0.004	-0.016		-0.1	0.381	-0.086		-0.08	0.016	0.371
					-0.12	0.306	-0.077		-0.1	0.008	0.362
					-0.14	0.202	-0.022		-0.12	0.017	0.300
					-0.16	0.196	-0.064		-0.14	-0.014	0.215

table G-1 Average velocities at different heights from x-axis and different distances from the free propeller.

x [m]	z [m]	axial turb.int. [m/s]	tang. turb. int. [m/s]	x [m]	z [m]	axial turb.int. [m/s]	tang. turb. int. [m/s]
0.1	0.08	0.104385	0.148029	0.5	0.12	0.130452	0.115633
	0.06	0.171178	0.198015		0.08	0.164903	0.125912
	0.04	0.179728	0.136694		0.06	0.160637	0.122675
	0.02	0.106427	0.099013		0.04	0.165836	0.123361
	0	0.144722	0.096483		0.02	0.167984	0.125821
	-0.02	0.108108	0.120162		0	0.137179	0.116646
	-0.04	0.213441	0.148485		-0.02	0.147634	0.111656
	-0.06	0.177551	0.14224		-0.04	0.16024	0.114804
				-0.06	0.159034	0.112207	
0.2	0.12	0.065702	0.089324	0.6	0.12	0.158034	0.10897
	0.08	0.170605	0.181661		0.08	0.145292	0.104979
	0.06	0.222359	0.184198		0.06	0.145157	0.104039
	0.04	0.220083	0.166146		0.04	0.147126	0.104535
	0.02	0.179828	0.148839		0.02	0.160148	0.105266
	0	0.183384	0.160895		0	0.160306	0.10823
	-0.02	0.218944	0.139849		-0.02	0.218944	0.139849
	-0.04	0.234628	0.157123		-0.04	0.234628	0.157123
-0.06	0.226845	0.141372	-0.06	0.226845	0.141372		
0.3	0.12	0.100558	0.110026	0.7	0.12	0.171727	0.103474
	0.08	0.184914	0.155977		0.08	0.146045	0.096758
	0.06	0.206633	0.161845		0.06	0.13344	0.098436
	0.04	0.2081	0.152129		0.04	0.136931	0.094414
	0.02	0.19304	0.155552		0.02	0.136946	0.098877
	0	0.184684	0.156559		0	0.131292	0.095774
	-0.02	0.188022	0.135297		-0.02	0.131272	0.095383
	-0.04	0.200305	0.137941		-0.04	0.135378	0.098088
-0.06	0.207698	0.141208	-0.06	0.13758	0.088578		
0.4	0.12	0.138126	0.125029				
	0.08	0.173224	0.146597				
	0.06	0.176977	0.147743				
	0.04	0.194934	0.149283				
	0.02	0.16346	0.133637				
	0	0.158886	0.13531				
	-0.02	0.218944	0.139849				
	-0.04	0.234628	0.157123				
-0.06	0.226845	0.141372					

table G-2 Turbulence intensities at different heights from x-axis and different distances from the free propeller.



## H. Depth profile of the Amsterdam-Rijnkanaal at Houten

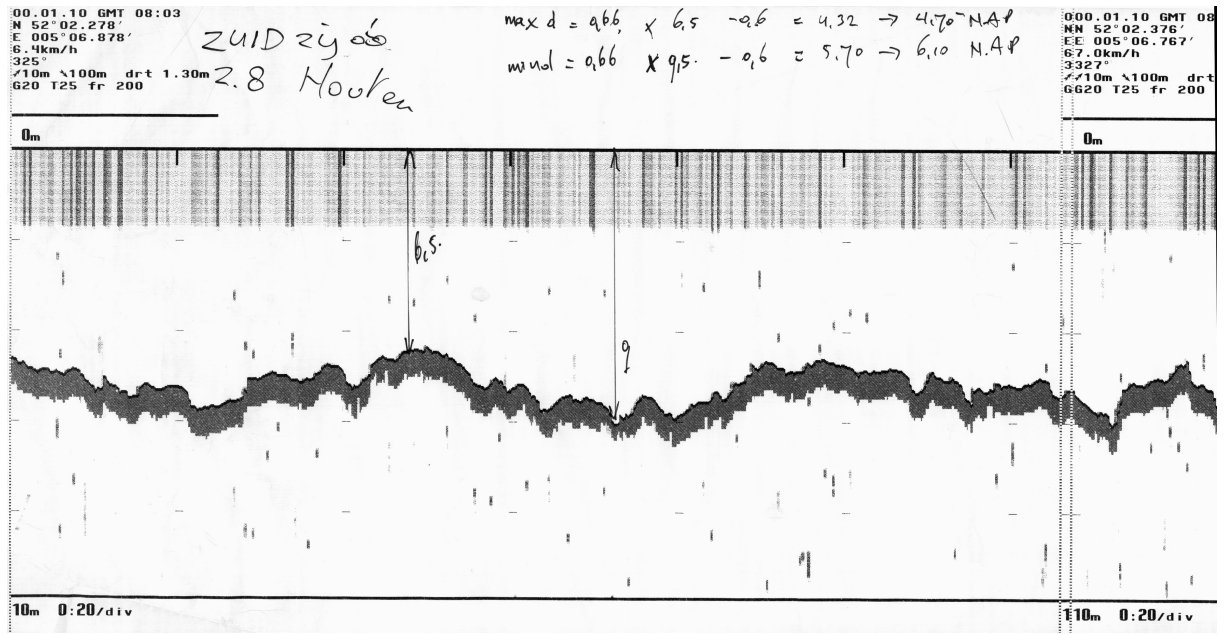


figure H-1 An example of one of the initial depth profiles. This one was taken at Houten, approximately 5 [m] outside the quay.

## **I. Principle of operation of the EMS**



From the manual of the EMS, Chapter 2, *Principle of operation*:

The EMS is in fact the inside-out version of the well-known pipe flowmeter employing Faraday's Induction Law through a magnetic field.

This field is generated by a pulsed current through a small coil inside the body of the sensor. Two pairs of diametrically opposed platinum electrodes sense the voltages produced by the flow past the sensor.

The sensor has been designed in such a way that these voltages are proportional to the sine ( $V_y$ ) en cosine ( $V_x$ ) of the magnitude of the liquid-velocity ( $V_e$ ) parallel to the plane of the electrodes.



*figure I-1 Close up of the probe of the EMS.*

For flow passing this reference plane at an angle  $\beta$  the magnitude of  $V_e$  shall equal  $V \cos \beta$ . In order to meet the different tilt response requirements for various applications, sensors of ellipsoidal and spherical geometry were designed.

By means of advanced electronics the low-level output signals are converted to high-level output signals from which the magnitude of the velocity and its direction (referred to a reference) can be derived by application of common goniometry.

The induced magnetic field is relatively powerful, although the coil consumes small power. This is achieved by a duty cycle of 25 [%] for the coil. Together with a synchronised detection-system this will result in a minimum interference sensitivity.